INVESTIGATION OF LITHIUM SALTS-NONIONIC SURFACTANT LYOTROPIC LIQUID CRYSTALLINE MESOPHASES IN A DYE SENSITIZED SOLAR CELL AS GEL ELECTROLYTES

A THESIS SUBMITTED TO
THE GRADUATE SCHOOL OF ENGINEERING AND SCIENCE
OF BILKENT UNIVERSITY
IN PARTIAL FULFILLMENT OF THE REQUIREMENTS FOR
THE DEGREE OF
MASTER OF SCIENCE
IN
CHEMISTRY

By
EZGİ YILMAZ
September, 2015

INVESTIGATION OF LITHIUM SALTS-NONIONIC SURFACTANT LYOTROPIC LIQUID CRYSTALLINE MESOPHASES IN A DYE SENSITIZED SOLAR CELL AS GEL ELECTROLYTE

By Ezgi Yılmaz,

September, 2015

We certify that we have read this thesis and have found that it is fully adequate, in scope and in quality, as a thesis for the degree of Master of Science.

Prof. Dr. Ömer Dağ (Advisor)

Asst. Prof. Dr. Ferdi Karadaş

Asst. Prof. Dr. Coşkun Kocabaş

Approved for the Graduate School of Engineering and Science:

Prof. Dr. Levent Onural

Director of the Graduate School

ABSTRACT

INVESTIGATION OF LITHIUM SALTS-NONIONIC SURFACTANT LYOTROPIC LIQUID CRYSTALLINE MESOPHASES IN A DYE SENSITIZED SOLAR CELL AS GEL ELECTROLYTE

Ezgi Yılmaz
M.S. in Chemistry
Supervisor: Prof. Dr. Ömer Dağ
September, 2015

Liquid crystals are one of the most widely studied and used materials in chemistry. The properties of liquid crystals make them interesting to research also for various electrochemical applications. In this context, lithium salts such as LiI, LiCl, LiBr, and $LiNO_3$ can be assembled using non-ionic surfactants into lyotropic liquid crystalline (LLC) mesophases[1], [2] and used as gel electrolytes in various applications.

In this work, the LLC mesophases of LiI with and without other lithium salts (such as LiCl, LiBr, and $LiNO_3$) were prepared using 10-lauryl ether ($C_{12}H_{25}(CH_2CH_2O)_{10}OH$, denoted as $C_{12}EO_{10}$) and characterized using the FT-IR (Fourier Transform Infrared Spectroscopy), Raman spectroscopy, XRD (X-Ray Diffraction), POM (Polarized Optical Microscopy), and AC conductivity measurements. Beside from single salt-surfactant mesophases, we also prepared LiI/I_2 redox couple in an LLC phase with the help of a non-ionic surfactant and they were also characterized using the same techniques. We found out that the mesophases can be prepared as gels by directly mixing salt and surfactant with certain amounts of water or as solutions using excess solvent (such as water, ethanol, or acetonitrile) that can be evaporated to form the LLC mesophases. The water content of both sets of samples is the same upon exposing to the atmosphere

for a certain time and it only depends on the salt amount and humidity under the ambient conditions (around room temperature and 20-25 % RH). The required water/salt ratio for a stable mesophase is around 3.0 which, it is much lower than the water needed to dissolve those salts in an aqueous media. The water/salt mole ratio closely follows the Hofmeister series of anions, where the water amount order is as follows; LiCl>LiBr>LiI>$LiNO_3$, however, the AC ionic conductivity follows a different order; $LiNO_3$>LiCl>LiBr>LiI. Adding I_2 by 1/10 mole ratio of the LiI into the media does not change the properties of the mesophases. The AC conductivity increases with increasing salt and water content of the mesophases with a typical conductivity of around 0.1 to 1.0 mS/cm^{-1}. The mesophases are also stable in a very broad temperature (below 0 $^{\circ}C$ to 60-130 $^{\circ}C$) and salt concentration (2-10 salt/surfactant mole ratio) ranges.

Finally, the LiI/I_2 mesophases were used as gel-electrolytes in dye sensitized solar cells (DSSCs) as gel-electrolytes and redox couples. A set of samples were prepared with different ratios of the LiI:I_2 redox couple (such as, 1:0.1, 1:0.2, 2:0.2, 2:0.3, 3:0.2, 3:0.3, 4:0.4, and 5:0.5) and the solar performances were tested in a DSSC, which contains N719 dye sensitized TiO_2 anode and Pt cathode using a solar simulator. However, the LLC phases have gel like structure and it is hard to infiltrate the gel into the pores of dye modified nano-TiO_2 films. To overcome the diffusion problem, the gel-electrolytes were also prepared as a solution in excess water, ethanol or acetonitrile that evaporates upon infiltration over time. In addition to this, by changing the procedure of preparing the TiO_2 paste, improvement on results was also obtained.

The DSSC provides 0.2 % efficiencies with 0.50 fill factors when gel-electrolytes are used. Since water is used for preparing the LLC phases, we had always lower V_{oc} values. However, when it is prepared as a solution with excess ethanol, it provides up to 3.33 % efficiencies with 9.58 mA/cm^2 short circuit current and 0.6 V open circuit voltage. Also, new procedure for preparing the TiO_2 paste provides us even higher V_{oc} values such as 0.76 V, which is unusual for the water based LLC electrolytes in this area.

Key Words: Lyotropic Liquid Crystal, Mesophase, Solar Cell, Gel Electrolyte, Redox Couple, Lithium Salts

ÖZET

LİTYUM TUZLARI VE İYONİK OLMAYAN YÜZEYAKTİF LİYOTROPİK SIVI KRİSTAL FAZLARIN BOYA DUYARLI GÜNEŞ HÜCRELERİNDE JEL ELEKTROLİT OLARAK KULLANILMASI

Ezgi Yılmaz
Kimya Bölümü, Yüksek Lisans
Tez Yöneticisi: Prof. Dr. Ömer Dağ
Eylül, 2015

Sıvı kristaller, kimyada en çok araştırılan ve kullanılan maddelerden bir tanesidir. Sıvı kristallerin özellikleri bu maddeleri araştırmayı ve çeşitli elektrokimyasal uygulamalarda kullanmayı da ilginç kılmaktadır. Bu amaçla, LiI, LiCl, LiBr, ve $LiNO_3$ gibi lityum tuzları iyonik olmayan yüzey aktif maddeler yardımıyla liyotropik sıvı kristal (LSK) mezofazları oluşturmak için birleştirilebilir, ve çeşitli uygulamalarda jel elektrolit olarak kullanılabilir.

Bu çalışmada, diğer lityum tuzlarının (LiCl, LiBr, ve $LiNO_3$) ekli olduğu ve olmadığı, lityum iyodürün LSK mezofazları 10-lauril eter ($C_{12}H_{25}(CH_2CH_2O)_{10}OH$; $C_{12}EO_{10}$ olarak da ifade edilebilir) kullanılarak hazırlandı. Bu numuneler, FT-IR (Fourier dönüşümlü infrared spektroskopisi), Raman spektroskopisi, XRD (X-ışını kırınımı), POM (polarize optik mikroskopisi), ve alternatif akım iletkenlik ölçümleri kullanılarak karakterize edildi. Ayrıca, LiI/I_2 redoks çifti iyonik olmayan yüzey aktif maddeler yardımıyla LSK mezofazında hazırlandı, ve yine yukarıda bahsedilen teknikler kullanılarak karakterize edildi. Bu mezofazlar hem belirli oranlarda tuz ve yüzey aktif maddeyi karıştırıp, az miktarda su eklenerek jel olarak; hem de fazla miktarda çözücü (su, etanol, ya da asetonitril) eklenerek çözelti olarak hazırlanabilir. Çözelti olarak hazırlanan numunelerin fazla miktarda olan çözücüleri buharlaştıktan sonra LSK mezofazlarını oluşturdukları görüldü. Numunelerin jel ya da çözelti olarak hazırlanmaları farketmeksizin, havayla etkileşime girdiklerinde son kalan su miktarlarının aynı olduğu görüldü.

Numunelerin içinde bulunan su miktarlarının; tuz miktarına ve ortamdaki neme bağlı olduğu görüldü; ve yapılan ölçümler sonucunda su/tuz stokiyometrik oranı 3.0 olarak hesaplandı. Bu su miktarı, kullanılan lityum tuzlarını sulu ortamda çözmek için gerekli olan su miktarından çok daha azdır; ve anyonların Hofmeister serisini izler. Kullanılan tuzlar içinde en çok su tutanı LiCl olmakla birlikte, yapının içindeki su miktarının sıralaması LiCl > LiBr > LiI > $LiNO_3$ şeklinde olmasına rağmen iletkenlik sonuçlarının $LiNO_3$ > LiCl > LiBr > LiI sıralamasını izlediği görüldü.

Numunelere lityum iyodür tuz miktarının onda biri kadar I_2 eklemek oluşturulan mezofazların özelliklerini değiştirmemektedir. Ayrıca, tuz ve su miktarları arttıkça iletkenliğin de arttığı gözlemlenmiştir. Bunun dışında, oluşturulan mezofazların geniş bir sıcaklık aralığında ve çok uzun süre kararlı olduğu söylenebilir.

Son olarak, oluşturulan LiI/I_2 mezofazlar boya duyarlı güneş hücrelerinde jel elektrolik olarak kullanıldı. Farklı oranlarda birçok numune hazırlandı, ve en iyi sonuç verenin LiI/I_2 oranının 10 olduğu numuneler olduğu gözlemlendi. 1:0.1, 2:0.2, 3:0.3, 4:0.4, ve 5:0.5 şeklinde hazırlanan numuneler içinde de en iyi verimin 2:0.2 numunesine ait olduğu görüldü. Bu numuneler boya duyarlı güneş hücrelerinde test edildi. Bu güneş hücreleri yapılırken N719 kodlu boya, TiO_2 kaplanmış anot, ve Pt kaplanmış katot kullanıldı. Fakat, jel elektrolit olarak hazırlanan numunelerin, titanyum dioksitin yapısında bulunan gözeneklerin içine girmesi çok zor olduğundan verimlerin de düşük olduğu görüldü. Bu sorunu çözmek için, bu numuneler çözelti olarak hazırlanıp o şekilde test edildi. Çözücü olarak su, etanol, ve asetonitril denendi, ve en iyi sonucun etanol ile olduğu görüldü. Ayrıca başta kullanılan TiO_2 prosedürü değiştirilerek optimal hale getirildi.

Boya duyarlı güneş hücrelerinde jel elektrolitler kullanıldığında alınan verim 0.2 %, ve doluluk oranı 0.50 olarak hesaplandı. Su bazlı sistemde çalışıldığı için voltaj değerleri diğer çalışmalara göre daha düşük çıkmaktadır. Fakat, jel elektrolitteki bazı problemleri çözmek amacıyla fazla miktarda etanol kullanılarak çözelti şeklinde hazırlanan elektrolitlerle 3.33% verim, 0.6 V voltaj, ve 9.58 mA/cm^2 akım elde edilmiştir.

Anahtar Kelimeler: Liyotropik Sıvı Kristal, Mezofaz, Güneş Hücresi, Jel Elektrolit, Redoks Çifti, Lityum Tuzları

ACKNOWLEDGEMENTS

First of all I would like to thank my supervisor, Professor Ömer Dağ, for sharing his ideas with me for 3 years. Every day I learned a lot from him, about chemistry disciplines, scientific methods, life and working principles in all parts of life. I cannot thank him enough for his patience during my research and his kind and encouraging advices. Thanks to him, I learned to study and research systematically and this is the thing that will always help me throughout my life. Without him, I could not finish this program, I could not learn this much and I could not have gone this far; and because all of these, I will be always grateful to him.

I also would like to thank my examining committee members, Ferdi Karadaş and Coşkun Kocabaş for their very valuable time and feedbacks on my thesis.

I also would like to thank Professor Jayasundera Bandara for 3 months of working with me. He taught me lots of things and his works and thoughts became really important and useful for this project in terms of efficiency improvements. Without his help, I could not make this much progress.

I am grateful to all my group members, too, for all of these years. Even after the former group members left, they were still by my side with their guidance. I would like to thank Elif Berna Olutaş, specially, for her time and help on my research topic.

For being successful, it is important to have kind and loving people around, to overcome the all kinds of difficulties with them. I am really lucky in this term, to have lots of people who care for me and try to do their best to help me during this hard period. This is why, I cannot thank enough to Doğa Derman, Sezin Bal, Ethem Barış Öztürk, and Fırat Çimenli for their beautiful and unrequited friendships throughout the 7 years; Tuğçe Esra Uslu, Ersin Altın, Gökçen Sakıncı and my all other lovely friends in my club who have been second family to me, and many other people who were there for me. Most importantly and specifically, I would like to thank to Arda Topuzlu for his patience, his help and his caring in every little time of this period.

Lastly but most importantly, I would like to thank to my mother, father, and my sister. They live far away from me for past 7 years but they were always by my side at the same time. They believed in me for everything and without their beliefs I could not do anything.

To my lovely parents and my beautiful sister…

CONTENTS

LIST OF FIGURES

LIST OF TABLES

LIST OF ABBREVIATIONS

LC	Liquid Crystal
LLC	Lyotropic Liquid Crystal
TLC	Thermotropic Liquid Crystal
CTAB	Cetyl Trimethyl Ammonium Bromide
SDS	Sodium Dodecyl Sulfate
$C_{12}EO_{10}$	Decaethylene glycol monododecyl ether
CMC	Critical Micelle Concentration
Lα, Lβ	Lamellar Phase
I_1, I_2	Cubic Phase
V_1, V_2	Bicontinuous Cubic Phase
H_1, H_2	Hexagonal Phase
L_1	Micellar Phase
CPP	Critical Packing Parameter
TMS	Transition Metal Salts
DSSC	Dye Sensitized Solar Cell
HOMO	Highest Occupied Molecular Orbital
LUMO	Lowest Unoccupied Molecular Orbital
VB	Valence Band
CB	Conduction Band
FTO	Fluorine doped Tin Oxide
ITO	Indium doped Tin Oxide
FF	Fill Factor
V_{oc}	Open Circuit Voltage
I_{sc}	Short Circuit Current
J_{sc}	Short Circuit Current Density
R_{sh}	Shunt Resistance
R_s	Series Resistance
WE	Working Electrode
CE	Counter Electrode
N719	Di-tetrabutylammonium cis-bis(isothiocyanato)bis(2,2’-bipyridyl-4,4’dicarboxylato) Ruthenium(II)

AN	Acetonitrile
EtOH	Ethanol
IL	Ionic Liquid
POM	Polarized Optical Microscope
XRD	X-Ray Diffraction
FT-IR	Fourier Transform-Infra Red
ATR	Attenuated Total Reflectance
UV-VIS	Ultra Violet-Visible
RT	Room Temperature

CHAPTER 1

1. INTRODUCTION

Between solid and liquid phases of materials, there is also one more phase, which is called liquid crystalline phase. In liquid crystalline phase, material shows the properties of both solid and liquid phases. A material which is in liquid crystalline phase can be liquid-like in terms of viscosity but it can show oriented crystalline structure, which can be observed under a microscope or diffracts x-rays at small angles, like solids.

These oriented crystalline structures can be birefringent or non-refringent. Birefringent materials are also called anisotropic (properties change with direction) materials and non-refringent means isotropic (properties of them are uniform in all directions). Birefringence was first mentioned in 1669, but the explanation of it came later, in the 19^{th} century. Augustin-Jean Fresnel used polarization to explain this effect. When it is inspected between two crossed polarizing filters, the crystals display colorful futures; this is called birefringence due to double refractive index.

First liquid crystalline state of a material was discovered accidentally by Friedrich Reinitzer, in 1888, when he saw the material that he studied had two different melting points[3]. The name liquid crystal was given by Otto Lehmann.

There are two major types of liquid crystalline phases that are thermotropic (TLC), lyotropic (LLC) mesophases. Thermotropic phases of liquid crystals go into phase transformation by temperature changes. Lyotropic liquid crystalline phases exhibit phase transformation with the change in concentration of solvent, which is usually water.

Also there are many mesostructures in the categories of liquid crystals. These are nematic, smectic, chiral nematic, chiral smectic, columnar phases for rod-like thermotropic liquid crystals; discotic nematic and discotic columnar phases for disc-like thermotropic liquid crystals; and cubic, bicontinuous cubic, hexagonal, lamellar phases for lyotropic liquid crystals.

Liquid crystals are used in many areas due to their unique properties. For instance, they have really high ionic conductivity in some cases and because of that they are used as electrolytes. Their advantages can be listed as ionic mobility, high

conductivity and so on. Thanks to these properties and easiness of preparation they are really useful for solar cell applications.

People are still investigating the liquid crystals because of the unique and useful properties of them mentioned above.

CHAPTER 2

2. BACKGROUND

2.1. Liquid Crystals

Liquid crystal (LC) is the phase between solid and liquid. This is why, liquid crystalline materials exhibit the properties of both solid and liquid. They have organized and oriented structures like solids and they flow like liquids, **Figure 2.1**.

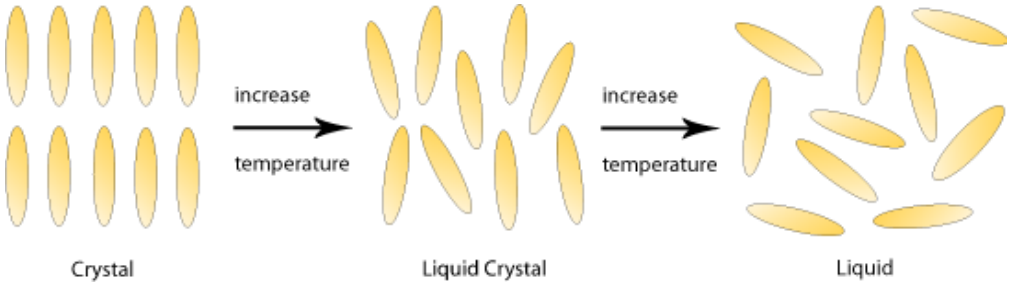

Figure 2.1. The phase transformation from solid to liquid and an illustration of them in terms of orientation of molecules.

Solids have intermolecular forces for keeping their molecules oriented together. Liquids are isotropic materials since they do not show long-range orientational order, which means that they show same optical, mechanical and magnetic properties independent of directions in space, they have single refractive index. From liquid to liquid crystal phase, there is a change in orientation; they show anistropic behavior by becoming more oriented than molecules in a liquid substance. In liquid crystal phase, some molecules have ordered arrangement due to intermolecular forces but some of them are random.[4] If solids are considered to have layers, and the molecules show very well-ordered orientation in these layers; then it can be said that liquid crystals have still layers but the molecules show random orientation in these layers.

Some phases of liquid crystals are anisotropic unlike liquids as mentioned. This is why they are birefringent under a polarizing optical microscope. Birefringent means that they exhibit two refractive index. When light travels faster or slower in one direction than the other, due to the difference in refractive indices,

the birefringence is observed. This phenomena was first explained by Erasmus Bartholin with his work with calcite crystals.[5]

Liquid crystals have many phases in terms of mesostructures or orientations and properties. If the molecular weight is low, these phases of LCs can be categorized as thermotropic and lyotropic phases. In some liquid crystal phases, when the temperature is too high or too low, this phase is lost. It means that phase transition depends on temperature. This kind of liquid crystals are called thermotropic LCs and they do not need solvent.[6] However, in addition to the function of temperature, lyotropic LCs depend also on concentration of the ingredients forming the LLCs. In LLCs, concentration and type of solvent molecules are important parameters.

To explain the TLCs, it is needed to look at the shapes of molecules. For instance, calamitic liquid crystals are one group of TLCs and their molecules are rod-shaped. The other group of TLC is discotic and in this case, their molecules are disc-shaped, **Figure 2.2**.[7]

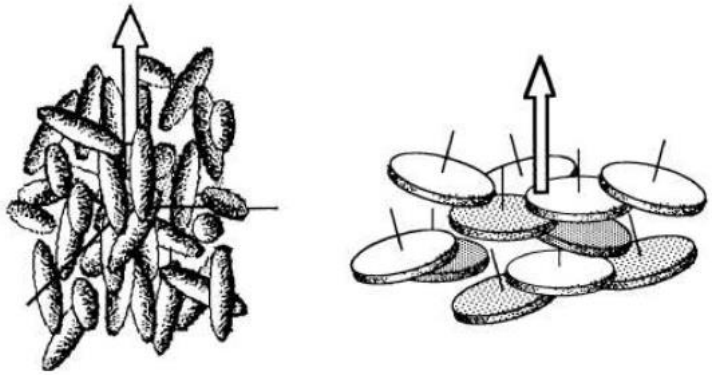

Figure 2.2. The representation of molecules in calamitic (left) and discotic (right) LCs.

Calamitic liquid crystals have molecules in which one molecular axis is longer than the others. Since they have rod-like shapes they can arrange along different axes. This varying orientation produces different subphases such as nematic (N) and smectic (Sm).[8] If molecules are aligned along their long axes but the ends of the molecules are not parallel to each other, this phase is called nematic. However, in smectic phase, molecules are parallel to each other and they form separate layers. There are more than one kind of smectic phase depending on the position of their long axes. Nematic phase is the less ordered than smectic phase.

When temperature is too high, the material shows isotropic property since it is in liquid phase. As temperature decreases, the phase transition is from isotropic to nematic. It is called nematic-isotropic transition temperature and it is different for every material.[9] After further decreasing in temperature, a phase transition from nematic to smectic is observed.

Besides from these, there is also cholesteric phase, which is also called chiral nematic phase (N^*). Only chiral molecules can form this phase. This phase was first discovered in 1888 in cholesterol derivatives and the name was coined because of that.[3] The other phase is called chiral smectic phase (Sm^*) and the liquid crystals which exhibit this phase, have ferroelectric properties, see **Figure 2.3**.

Figure 2.4 shows a representation of discotic liquid crystals. They tend to form either discotic columnar phases by stacking its molecules in one direction; or discotic nematic phase in which disc-like molecules are oriented in layers, similarly.

Figure 2.3. A representation for isotropic, nematic and smectic phases, respectively.

Figure 2.4. Discotic nematic (left) and discotic columnar (right) LC phase.

Besides TLCs, there is a more important type in this category and it is called lyotropic liquid crystal (LLC). In this phase, there is again temperature dependence; however, there is also another parameter which is the concentration of the solvent and surfactant. On the contrary to TLCs, a solvent is needed for lyotropic type. The

molecules of LLCs have both hydrophilic head groups and hydrophobic chains (amphiphilic molecules, see **Figure 2.5**), and they aggregate in the presence of an appropriate solvent (water is generally used). Some amphiphiles are phospholipids, fatty acids and they can be used as detergents. Surfactants are detergent-like amphiphilic materials. They contain both hydrophobic and hydrophilic parts. Hydrophilic part can be ionic or non-ionic and it determines the surfactant's type (anionic, cationic or non-ionic). Sodium dodecyl sulfate (SDS, anionic surfactant)[10]; cetyltrimethylammonium bromide (CTAB, cationic surfactant)[10]; and decaethylene glycol monododecyl ether ($C_{12}EO_{10}$, non-ionic surfactant) are three of the most studied surfactants. The tail part is the hydrophobic part, and it can be hydrocarbon chains (8-10 carbon chain), which do not mix with water, if water is the solvent in the LLC media.

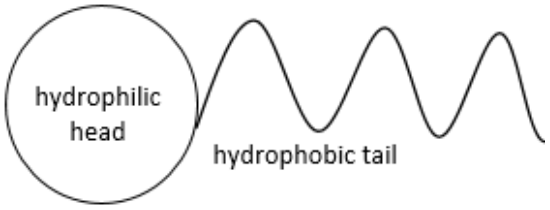

Figure 2.5. Schematic representation of amphiphilic molecule which contains hydrophobic and hydrophilic parts.

Aggregation of these molecules in a solvent is a self-assembly (micellization) process[11] and it happens because of hydrophobic effect. Hydrophilic groups are arranged so that hydrophobic parts do not contact with water. Hydrophilic parts form hydrogen bonding with water by breaking the hydrogen bonding between water molecules, **Figure 2.6**. The self-assembly of these molecules produce micelles and vesicles. The resulting structure differs on an account of the type of surfactant, concentration, and type of solvent. The most influential parameter is the concentration of solvent.

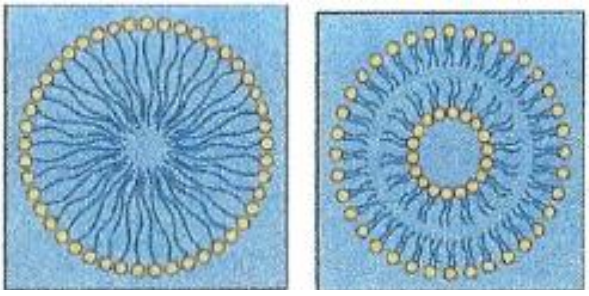

Figure 2.6. Schematic representation of micelle (left) and vesicle (right) structure of a surfactant.

Surfactants are surface active materials. When they are used in very low concentrations, surfactant molecules are aligned in a way that they are at the surface of the solvent. Therefore, they can reduce the surface tension of the solvent (such as water, most common solvent) at the interface between the water and air.[12] The concept of aggregation of surfactants is a subject of an increasing interest, that includes type of solvents and also mixtures of some solvents.[13]–[17]

The aggregate of surfactant molecules is called micelle, as mentioned above, since it is thermodynamically stable[18]. One of the most important parameters in terms of determining the structure of micelles is the length of the hydrophobic non-polar tail of the surfactant molecules. The number of the amphiphilic molecules in them is also important and it is called aggregation number. Besides from these parameters, there is also a critical micelle concentration (CMC), which is important for a micelle to form. If the surfactant concentration is above CMC, the micelle formation starts. At high concentrations of amphiphilic molecules in water, above CMC, the number of formed micelles increases continuously, and therefore viscosity of the material solution increases. This situation causes the formation of the lyotropic liquid crystalline phase.

2.1.1. Lyotropic Liquid Crystalline (LLC) Mesophases

Concentration of the surfactant, temperature, molecular structure are all determinants for resulting phases of lyotropic liquid crystals.[19] These phases of lyotropic liquid crystals are called mesophases[20] and they can be categorized as lamellar phase (L), discontinuous cubic phase (I), bicontinuous cubic phase (V), and hexagonal phase (H).

Lamellar phase (L) is also an anisotropic phase.[7], [21] In this phase, surfactant molecules form bilayers in terms of arrangement. They contain water between these bilayers and this is why a material which is in lamellar phase is less viscous than in hexagonal phase. The subscript of L can take α (due to liquid-like alkyl chains) or β (due to ordered gel-like alkyl chains).[22] The characteristic texture of L_α under polarized optical microscope is mosaic-like texture and it is called streaky texture.[23] For L_β, the characteristic texture is called twisted-ribbons with regular corkscrew-like structures, see **Figure 2.7**.[21], [24], [25]

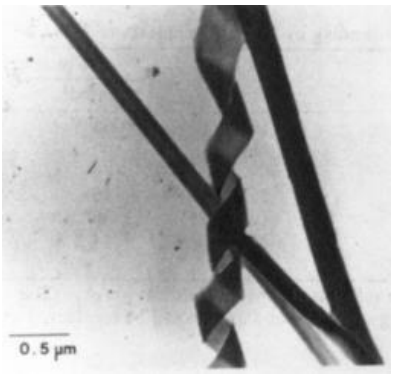

[1]**Figure 2.7.** The POM image of a sample with corkscrew structure.[25]

Cubic phase (I) is optically isotropic and there is no texture to be observed under POM in this phase. In the cubic phase, the concentration of micelles is high, therefore they tend to pack together. A material, which is in a cubic LLC phase is extremely viscous, compared to a hexagonal LLC phase. The micelles are usually packed in a body-centered cubic (bcc) arrangement, however, face-centered cubic (fcc) and clathrate (both type 1 and type 2) packing are also possible.[21] If molecules in the micelles are aligned normal (hydrophilic parts are facing to the solvent molecules), I takes 1 as a subscript (I_1) and if they are reversed it takes 2 as the subscript (I_2). There is also bicontinuous cubic phase[26] (V) which does not exhibit any optical isotropy, same as all other cubic phases.

Hexagonal phase (H) is optically anisotropic on the contrary to cubic phase. This is why they exhibit birefringent texture under polarized optical microscope.[7], [21] This phase can be categorized into two, hexagonal phase (H_1) and reversed hexagonal phase (H_2), depends on whether micelles are normal or reversed. For normal arrangement, non-polar tails of surfactant molecules are directed inwards, whereas for reversed arrangement non-polar tails of surfactant molecules are directed outwards.[23] 2D hexagonal phase gives specific texture, which is called fan texture. Besides from 2D, there is also 3D hexagonal phase of LLCs, where the shape of the micelles are cylindrical and spherical, respectively.

In terms of viscosity, lamellar phase is less viscous than hexagonal phase, and hexagonal phase is less viscous than cubic phases.

[1] Reprinted with permission from (Frankel DA, O'Brien DF. Supramolecular Assemblies of Diacetylenic Aldonamides. *J Am Chem Soc*. 1991;113:7436-7437.) Copyright (1991) American Chemical Society.

To explain phase transition between those mesophases, it can be said that; $I_1 \rightarrow H_1 \rightarrow V_1 \rightarrow L_\alpha$; and this order of phase transition occurs with an increasing in the surfactant concentration. Also with increasing concentration, for some systems, inverted phases can be also be obtained (see **Figure 2.9**[27]).

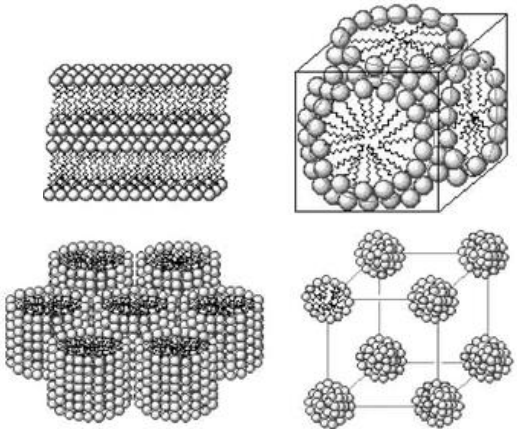

[2]**Figure 2.8.** A schematic representation for mesophases of LLCs, on top lamellar (left) and bicontinuous cubic (right), at bottom hexagonal (left) and cubic (right) phases.[23]

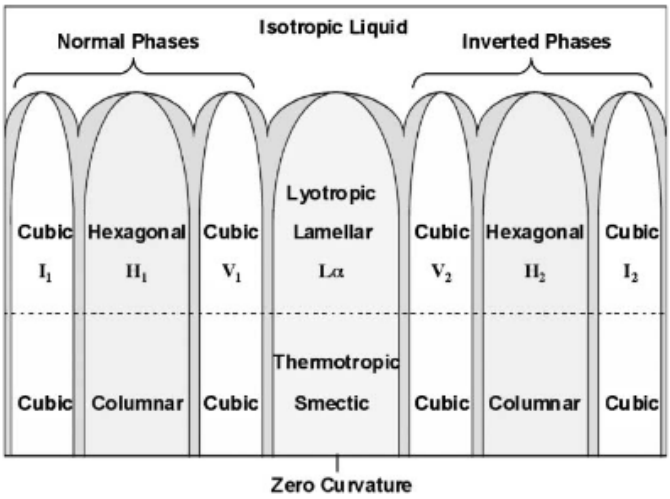

[3]**Figure 2.9.** An illustration for phase transition between LLC mesophases as concentration of surfactant increased.

Since there are more than one factor (temperature, hydrocarbon unsaturation, hydration etc.) for LLC phases to prefer a structure, it is useful to predict the shape of them by using a shape parameter. This shape parameter is called critical packing parameter (CPP). It is defined as;

---

[2] Reprinted with permission from Forrest BJ, Reeves LW. New lyotropic liquid crystals composed of finite nonspherical micelles. *Chem Rev*. 1981;81(1):1-14. doi:10.1021/cr00041a001 .Copyright (1981) American Chemical Society.

[3] [Goodby JW, Görtz V, Cowling SJ, et al. Thermotropic liquid crystalline glycolipids. Chem Soc Rev. 2007;36(12):1971-2032. doi:10.1039/b708458g] - Reproduced by permission of The Royal Society of Chemistry.

$$s = \frac{v_c}{a_0 l_c}$$

where v_c is the volume of the hydrophobic chain, a_0 is the area of the hydrophilic core and l_c is the length of the hydrophobic chain.[28] If s < 1/3 it is spherical micellar unit, if s is 1/2 it can be said as hexagonal (cylindrical), and if it is around 1, lamellar structure can be predicted.[29]

2.1.2. Poly(ethylene oxide) Type Surfactant Systems ($C_mEO_n + H_2O$)

C_mEO_n type non-ionic surfactants include both hydrophobic (alkyl) and hydrophilic (ethylene oxide) parts in a single molecule. m is the number of carbon atoms in alkyl chain, and n is the number of ethylene oxide of the surfactant molecule. Ethylene oxide part is hydrophilic head and the alkyl chain is hydrophobic tail part. When the number m is increased, the efficiency of packing surfactant molecules into micelles is also increased.[30] Besides from the number m, also the temperature has an effect. When the temperature is increased, the hydrophilicity of the surfactant molecules is also increased and hydrophobicity is decreased.[31]

In these systems, when the water content in the mixture is increased (when surfactant concentration is decreased), the phase transformation occurs from I_2 → H_2 → V_2 → L_α → V_1 → H_1 → I_1, **see Figure 2.10**.[32], [33]

In these phase diagrams, phase behavior of all C_mEO_n type surfactants is similar. However, when the number n is increased, i.e. the number of the ethoxy groups is increased; it means that surfactant molecule becomes more hydrophilic. Therefore, the phase diagram can shift to the left, since it becomes more likely to form normal micelle liquid crystals.[34]

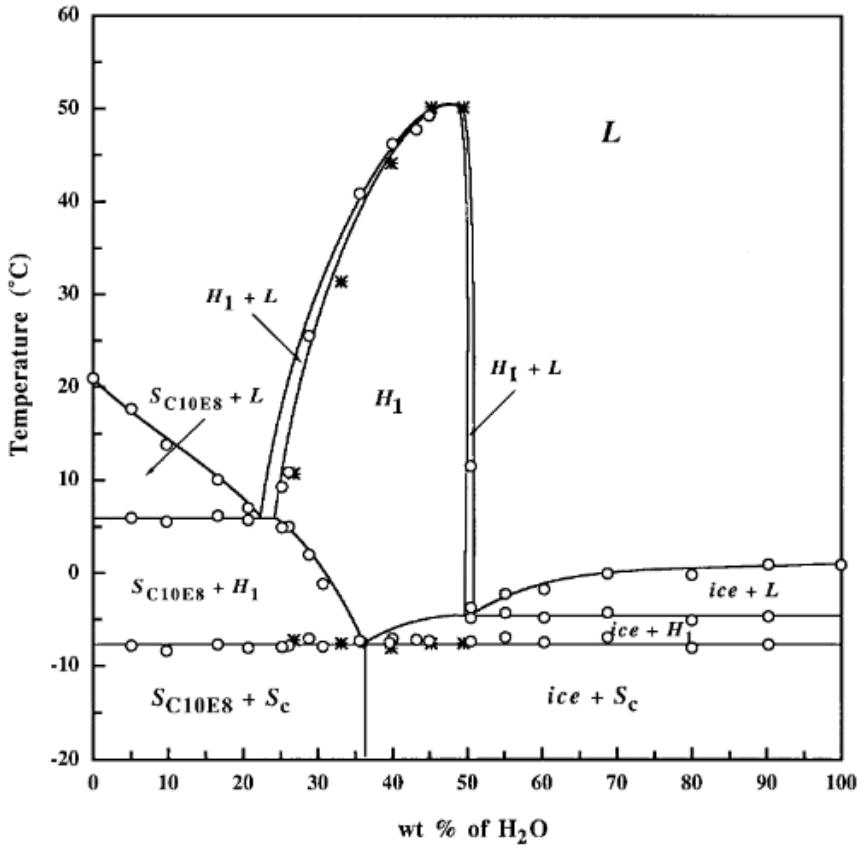

[4]**Figure 2.10.** Phase behavior of $C_{10}EO_8$ with the change in the content of water.[32]

2.1.3. Additives in $C_mEO_n + H_2O$ Type Surfactant Systems

Salts as additives can change the shape parameter(s) of LCs. If salts are added to this system, phase behavior is affected dramatically, not by the cations but by the anions.[35] According to the work of Hofmeister and Lewith; $SO_4^{2-} > HPO_4^{2-} > CrO_4^{2-} > CO_3^{2-} > F^- > Cl^- > Br^- > NO_3^- > I^- > ClO_4^- > SCN^-$ is the series of anions for salting out or salting in processes. Also there is another series for the cations, which is; $NH_4^+ > K^+ > Na^+ > Li^+ > Mg^{2+} > Ca^{2+}$ > guanidinium. These ions can be categorized into two separate groups. One of them is kosmotropic, the other one is chaotropic ions. This categorization can be done by depending on their abilities to interact with water, and to change its structure. Kosmotropic ions, with high charge density, can interact with water strongly; and chaotropic ions, with low charge density, cannot.[36]

[4] Reprinted from Nibu Y, Inoue T. Phase Behavior of Aqueous Mixtures of Some Polyethylene Glycol Decyl Ethers Revealed by DSC and FT-IR Measurements. *J Colloid Interface Sci*. 1998;205(2):305-315., Copyright (1998), with permission from Elsevier

Kosmotropic (structure-maker or lyotropic) ions are the ones on the left side of the series. From right to left, surface tension of the solvent is increased. Thus, solubility of organic compounds in water is decreased, and hydrophobic interaction is strengthened. This leads to a process, which is called salting out. Aggregations can occur because of salting out process. On the other hand, chaotropic (structure-breaker or hydrotropic) ions are the ones on the right-hand side of the Hofmeister series. Just as the opposite of kosmotropes; from left to right, surface tension of the solvent is decreased. Therefore, solubility of nonpolar molecules in water is increased, causing to the process, which is called salting in. This gives result to the increase in solubility of salt.[35]–[37]

As it is mentioned above, the solubility of organic compounds can be greatly changed by these ions. Surfactants are also considered as organic compounds. In this context, it can be said that, these additives can change the solubility of C_mEO_n type surfactants in water. From left of the Hofmeister series to the right side, cloud point and critical micelle concentration of surfactant molecules decreases. For instance, from the phase diagram in **Figure 2.11**, it can be said that adding different cations gives the effect as CsCl < NaCl < LiCl in terms of expanding the L_α phase region. Smaller the cation which is added, the bigger the expansion is, due to the fact that Li^+ has the strongest hydration. Strongest hydration requires larger amount of water. That is why, L_α region is expanded the most in the case of smaller cation.[38]

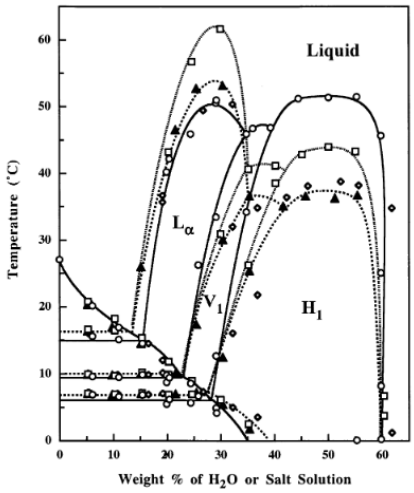

[5]**Figure 2.11.** Phase diagrams of $C_{12}EO_7$ + H_2O system with the addition of LiCl (squares), NaCl (triangles), CsCl (diamonds) and none (circles)[38]

For another example, Sharma et al. studied cloud points of surfactants. Cloud point is that the temperature above which the surfactant is no longer soluble in water. According to **Figure 2.12**, the cloud points of surfactants decrease with F^- > Cl^- > Br^- > I^- anions.[39] The reason is that, water molecules which are close enough to each other, do not form hydrogen bonds with ethylene oxide parts. Therefore, kosmotropic ions cause dehydration of ethylene oxide units; this is why cloud point drops in the case of kosmotropic ions (from right to left in Hofmeister series).

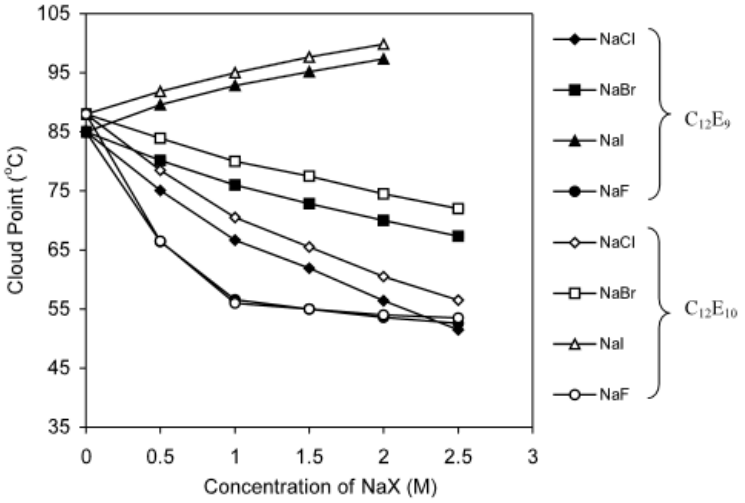

[6]**Figure 2.12.** The effects of NaX salts on the cloud points of different surfactants.[39]

Also, besides from these studies, Inoue et al. investigate the anion effect in this series with $C_{12}EO_7$ + H_2O systems. They used NaCl, NaI, $NaClO_4$ salts as additives with different concentrations of surfactants. As a result, they found that, since Cl^- anion is in a border between kosmotropes and chaotropes, its influence is weak. In this case, Na^+ (as a kosmotrope) takes the role for shrinking the H_1 region while it expands the L_α region. In other two cases, ClO_4^- anion is located on the right side of I^-, so it has more chaotropic effect on the surfactant. Thus, hydration of ethylene oxide unit is more in the case of ClO_4^- addition. That is why, L_α region is became smaller and H_1 region is became larger, see **Figure 2.13**.[40]

---

[5] Reprinted with permission from LQ, Minamikawa H, Harada K, Inoue T, Chernik GG. Effect of inorganic salts on the phase behavior of an aqueous mixture of heptaethylene glycol dodecyl ether. Langmuir. 2003;19(25):10487-10494. doi:10.1021/la030182l. Copyright (2003) American Chemical Society.

[6] Reprinted from Sharma KS, Patil SR, Rakshit AK. Study of the cloud point of C12En nonionic surfactants: Effect of additives. *Colloids Surfaces A Physicochem Eng Asp*. 2003;219(1-3):67-74., Copyright (2003), with permission from Elsevier.

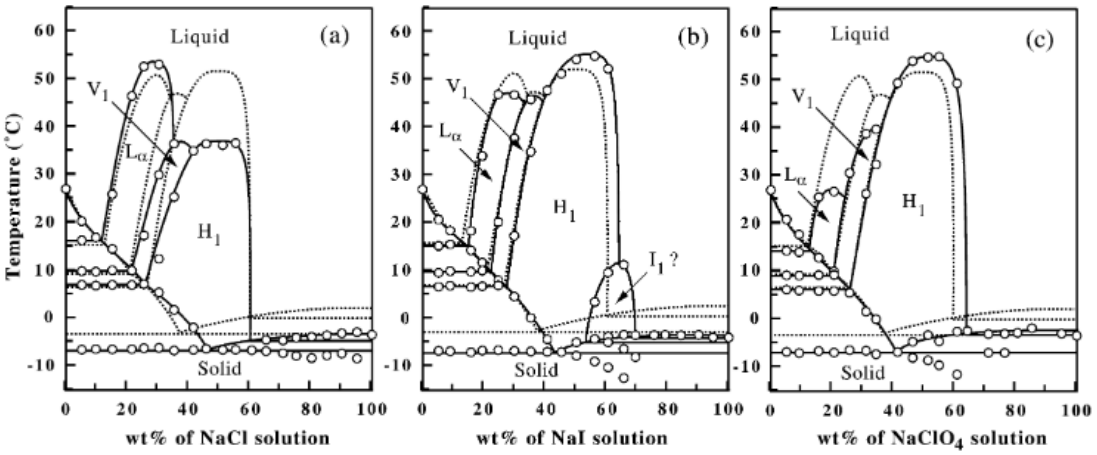

[7]**Figure 2.13.** The effects of NaX salts addition on the phase diagrams of $C_{12}EO_7$.[40]

2.2. Salt-Surfactant System

The salt addition to the liquid crystalline systems has been investigated over the years. In these studies, it was found that the structure of liquid crystalline mesophases (hexagonal, cubic or lamellar depending on the type of salts, counter ions and concentrations) depend on the interactions of water molecules with surfactant molecules. Consequently, the added salts were dissolved in this hydrophilic environment and influence those interactions.[41]–[44]

In 2001, Dag group discovered a new liquid crystalline system with transition metal salts and non-ionic surfactants. In this study, non-ionic surfactants are oligo (ethylene oxide) type surfactants (such as $C_{12}EO_{10}$) and transition metal (Co^{2+}, Ni^{2+}, Zn^{2+}, and Cd^{2+}) nitrate salts (TMS). Here, the transition metal aqua complexes undergo self-assembly process with the addition of non-ionic surfactants, and they form liquid crystalline phases, see **Figure 2.14**. For Cd^{2+} salts, all ratios up to 3.5/1 mole ratio of salt/surfactant give hexagonal LLC phase with characteristic fan texture. Above that ratio, the phase is cubic up to 4.5 and becomes disordered liquid above 4.5 mole ratio. The case for Ni^{2+} and Co^{2+} salts, this ratio is 3.2/1 mole ratio.[45] The interesting point in here is that, when the metal ions are in the system the ratio for forming stable LC phases is four times higher than that of surfactant-water systems.

[7] Reprinted from Inoue T, Yokoyama Y, Zheng LQ. Hofmeister anion effect on aqueous phase behavior of heptaethylene glycol dodecyl ether. *J Colloid Interface Sci*. 2004;274(1):349-353., Copyright (2004), with permission from Elsevier.

In 2004 and 2005, they expanded their investigation, and they found out that just like oligo (ethylene oxides), pluronics (P65, P85, P103, and P123) with TMS also form LLC phase. This time not only nitrates were tried, but also chlorides and perchlorates were investigated. They all form lyotropic liquid crystalline phases with the help of oligo (ethylene oxides) and pluronics. However, in the pluronic systems, lamellar and tetragonal mesophases of LLCs are also observed in addition the more common mesophases such as hexagonal and cubic.[45]–[47] The salt-surfactant LLC phase formation is sensitive to Hofmeister series in terms of solubility of the TMS. Also, temperature has an impact on phase formation. At high temperatures, the LLC phase of non-ionic surfactant with TMS melt but upon cooling it reforms.[46] The system with two surfactants (charged surfactants in addition to non-ionic 10-lauryl-ether) and the effect of charged surfactant were also investigated in the $[Zn(H_2O)_6](NO_3)_2 + C_{12}EO_{10} + H_2O$ system. In this study, SDS and CTAB were used as anionic and cationic surfactants, respectively. Later the salt-surfactant mesophases were extended to alkali and alkaline metal salts (see latter).[1] The structure of LLC can be changed by changing the concentration of metal salts, temperature, or counter ions. For example, nitrate salts of lithium form hexagonal LLC phases, whereas perchlorate salts form cubic, isotropic LLC phases.[45]–[48]

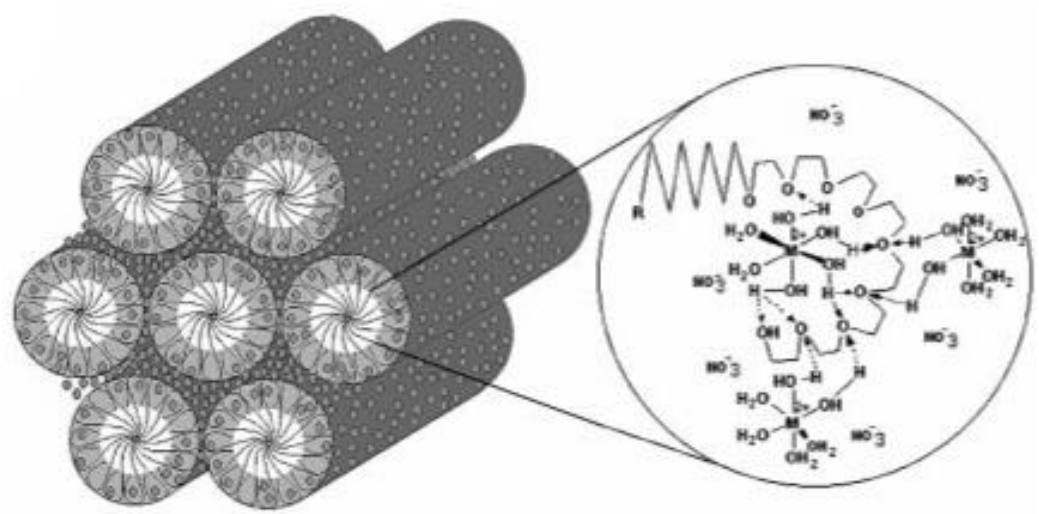

[8]**Figure 2.14.** Hydrogen bonding between coordinated water molecules of TMS and ethylene oxide units of surfactant.[45]

[8] Reprinted from Celik O, Dag Ö. A new lyotropic liquid crystalline system:oligo(ethylene oxide) surfactants with [M(H2O)n]Xm Transition metal complexes. *Angew Chem Int Ed*.;113(20):3915-3919 (2001), with permissions from John Wiley & Sons.

In these systems, ethylene oxide units of the surfactant molecules do not undergo chemical reaction with the metal center. It means, when the metal salts are added, water molecules stay in the coordination sphere. These coordinated water molecules of transition metal salts form hydrogen bonding with the ethylene oxide units of the surfactant. This causes the formation of LLC phase. Due to the fact that the hydrogen bonding of these systems is much stronger than that of surfactant-water systems; thus salt-surfactant systems have higher isotropization points (IPs). The IP or melting point can be as high as 110 ºC in the hexagonal phase.[45]

Besides from structure, there is one more important point, and that is the solubility of TMS in these systems. For instance, the overall charge is decreased in the nitrate salt-surfactant mesophases by coordination of the nitrate ion to the metal ion center that enhances the solubility of TMS in the LLC media.[45] However, when sulfate salts of transition metals are used, the solubility is found to be very small to form LLC mesophase.[45]

In addition to the Co^{2+}, Zn^{2+} is also one of the most commonly and widely studied metal in these systems. According to a work of Dag and his group, salt species are in the molten phase and additionally they act as a solvent in the $[Zn(H_2O)_6](NO_3)_2$-$C_{12}EO_{10}$ LLC mesophases. The first phase diagram of the salt-surfactant has been constructed from the zinc nitrate system, the phase behavior of salt-surfactant is very similar to the water-surfactant systems. The $V_1 \rightarrow H_1 \rightarrow I_1 \rightarrow L_1$ phase transition are observed with increasing the solvent amount (see **Figure 2.15**). However, what is interesting is that these mesophases show unexpected behaviors at low temperatures on the contrary to the rest of the LLC systems. A glass transition temperature is observed around -52 °C and the phase is transformed into a very stable mesostructured solid below that temperature.[49]

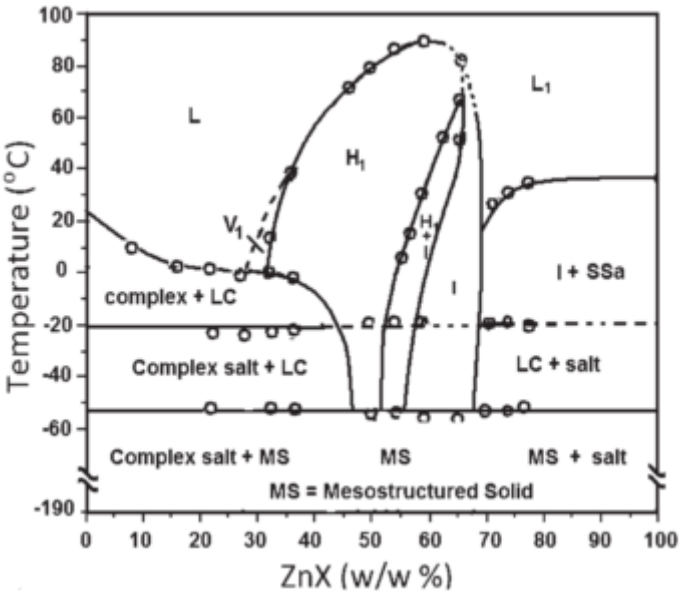

[9]**Figure 2.15.** The phase diagram of ZnX-$C_{12}EO_{10}$ (ZnX is $[Zn(H_2O)_6](NO_3)_2$) system.[49]

After studying transition metal salts with various types of surfactants, Dag and his group started to investigate non-transition metal salts in the same system such as $LiNO_3$, LiCl, and $LiClO_4$. It has been found out that lithium salts also form LLC mesophases with little amount of water and oligo (ethylene oxide) type surfactants (C_mEO_n) over a broad range of compositions.[50] Just like in the case of transition metal salts, alkali metal salts are hydrated and they act like a solvent in this system. One of the most important and useful property of lithium salt-surfactant LLC mesophases is their high ionic conductivity (7.0×10^{-3} S/cm) that gives rise the possibilities for them to be used as gel-electrolytes.[50]

In 2014, the $LiNO_3$ and LiCl salts were investigated using some pluronics to enhance the study of alkali metal salts LLC systems.[51] The lithium salt-pluronic LLC mesophases also form over a broad range of salt concentrations. From 5 to 15 salt/surfactant mole ratio, they form hexagonal and birefringent LLC mesophases and with the increase in salt content they transform first to cubic phase, then to disordered phase and finally to a liquid phase. However, at low concentrations surfactant leaches out and creating two different salt-rich and salt free phases by undergoing a phase separation. Their conductivities are still high and can be used as gel-electrolytes as well.[51]

[9] Reprinted with permission from Albayrak C, Özkan N, Dag Ö. Origin of lyotropic liquid crystalline mesophase formation and liquid crystalline to mesostructured solid transformation in the metal nitrate salt-surfactant systems. Langmuir. 2011;27(3):870-873., Copyright (2011) American Chemical Society.

2.3. Soft Confinement Effect and Origin of Salt-Surfactant Mesophases

The properties of a material are changed enormously, when there is a change in the size of that material. The morphology, chain dynamics, and many other material properties such as glass transition temperature, solubility, and mechanical properties exhibit a change from bulk material to nano-sized material. This can be explained by confinement effect (CE). Confinement effect can be divided into two categories; one of them is hard confinement effect, and the other one is soft confinement effect. Hard confinement effect is about the effect on solid materials, whereas soft confinement effect is about soft materials such as polymers,[52], [53] liquids,[54], [55] and liquid crystals.[56], [57] Here, the soft confinement effect will be explained in detail.

The theory behind this effect is explained by the confinement effect. When the particles are confined in small pores, for instance, their properties can be modified. The important point is the change in the surface area-to-volume ratio. When size is decreased, this ratio increases. This way the amount of surface atoms increases in terms of percentage; thus the properties of the nano-sized particles exhibit difference in compare to the bulk materials, due to the fact that these properties are all size-dependent properties.[58] It is known that freezing and melting point of these confined materials were depressed drastically.[59]–[62] For example, for CdS material, melting temperature varies from 1600 to 400 °C when size of the material changes.[59]–[62] In another study, Awschalom and Warnock stated that not only the confinement itself affects the properties, but also the confining geometry plays a critical role. The confining walls change the confining geometry and it leads to a change in the behavior of liquids.[60] The reason for melting point to decrease is that again high surface area-to-volume ratio (SA/V). High SA/V ratio leads to surface atoms to have less neighboring atoms for the formation of bonds. Thus, they have lower cohesive energy in compared to bulk materials. Cohesive energy is the thermal energy which is needed for a free atom to form a solid. This is why the melting temperature is proportional to the cohesive energy. Thus, when a material has high SA/V ratio, it means that it has a lower cohesive energy, and lower melting temperature. This change in melting temperature can be calculated by Gibbs-Thomson effect with an equation;

$$\Delta T = \frac{2\gamma_{sl} v T_0}{\Delta H_f d}$$

where ΔH_f is the bulk heat of fusion, γ_{sl} is the interface energy between solid and liquid, v is the molar volume, T_0 is the melting temperature of bulk material, and d is the diameter of the particle.[63], [64] With this equation, the change in the melting point of a confined material can be calculated from the melting temperature of its bulk.

Besides from the change in the melting temperature, the electrical and optical properties can also exhibit differences in confined materials, due to quantum size effects. When the size is decreased, the electronic excitations shift to higher energy levels, this can cause a change in the density of electronic energy levels. Thus, optical and electrical properties of materials can be changed by modifying the size of the particles.[58] Because of these changes in terms of the properties of nano-sized materials, salt-surfactant mesophases are started to be investigated and studied widely.

2.4. Dye Sensitized Solar Cells

Dye sensitized solar cells (DSSCs) are widely investigated as photovoltaic devices due to low-cost and their simplicity. DSSCs consist of an anode, electrolyte, and cathode. Anode is usually dye sensitized TiO_2 that is coated over a transparent electrode (usually fluoride doped tin oxide, FTO). The electrolyte is an acetonitrile solution of KI/I_2 (as a redox couple) and the cathode is a Pt nanoparticle coated FTO electrode. In acetonitrile, I^- and I_2 forms I_3^- ion. The working principle of DSSCs (see **Figure 2.16**) is that the incident visible light is absorbed by dye molecules, anchored over TiO_2 particle, the excited dye molecules transfer their electron(s) to the conduction band (CB) of TiO_2 and get oxidized. TiO_2 conducts these electrons to the counter electrode, where a reduction process takes place. The reduced I_3^- (that is $3I^-$) donates the electron back to regenerate the dye molecule and to complete the electrochemical circuit.[65]

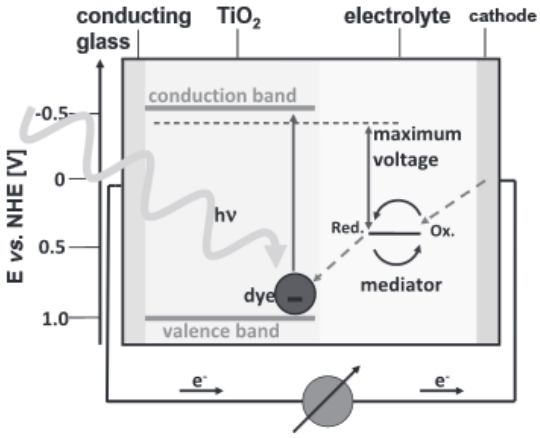

[10]**Figure 2.16.** The schematic representation for working principle of a DSSC.[65]

The process is outlined as following:

$$D + hv \rightarrow D^* \ (dye\ excitation)$$

$$D^* \rightarrow D^+ + e^- \ (electron\ injection)$$

$$D^* \rightarrow D(+hv) \ (dye\ relaxation)$$

$$D^+ + R \rightarrow D + R^+ \ (dye\ regeneration)$$

$$D^+ + e^- \rightarrow D \ (recombination\ to\ oxidized\ dye\ molecules)$$

$$R^+ + e^- \rightarrow R \ (recombination\ to\ oxidized\ redox\ species)$$

The reason for dye coating on TiO_2 nanoparticles is that, TiO_2 is a semiconductor with a very large band gap and cannot absorb visible light. To effectively absorb the sun light, it is necessary to sensitize using dye molecules. In the counter electrode, platinum nanoparticles act as a catalyst for the reduction of I_3^- ion. However, instead of Pt; carbon, graphene, gold can also be used. Finally the electrolyte (it can be in a solid-state, liquid, or liquid crystalline form) provides charge transportation via redox couple.[66]

By completing the circuit, the solar energy is converted into electrical energy. There are two important parameters to define effectiveness of a DSSC; one is a fill factor (FF) and the other one is power conversion efficiency (η). The FF of a cell is defined as maximum power ($P_{max} = I_{max} * V_{max}$, see **Figure 2.17**) divided by open circuit voltage (voltage at I = 0 intercept, V_{oc}) times short circuit current

[10] Reprinted from Nazeeruddin MK, Baranoff E, Grätzel M. Dye-sensitized solar cells: A brief overview. *Sol Energy*. 2011;85(6):1172-1178., Copyright (2011), with permission from Elsevier

(current at V= 0 intercept, I_{sc}). Power conversion efficiency is defined by the multiplication of the short circuit photocurrent density (J_{sc}, I_{sc} per area), open circuit voltage, and fill factor divided by intensity of incident light (P_{in}).

$$FF = \frac{(I_{max} * V_{max})}{(I_{sc} * V_{sc})} = \frac{P_{max}}{(I_{sc} * V_{oc})}$$

$$\eta = \frac{J_{sc} * V_{oc} * FF}{P_{in}}$$

With a solar simulator, I-V curve of the photovoltaic cell can be measured. Here, by looking at the FF, the shape of the I-V curve can be determined. The FF of an ideal cell should be 1 (rectangular shape), however this is impossible in real cells due to resistances of electrolytes or many imperfections in the both electrodes. Therefore, FF can be in a range between 0 and 1.

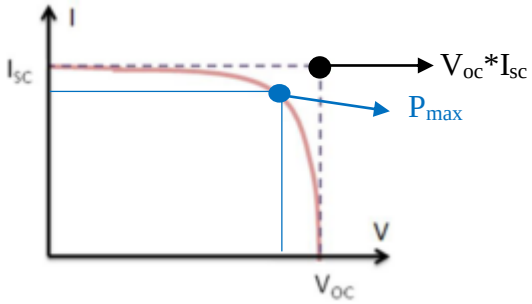

Figure 2.17. I-V curve of a real cell (red line), an ideal one (dashed lines), and P_{max} (with blue line).[67]

To have higher FF, there are two important parameters; one of them is to have high shunt resistance (R_{sh}), and the other one is to have low series resistance (R_s), **Figure 2.18**. Increasing the shunt resistance means that the current flows from the cell, so the current is not split. Also, decreasing the series resistance causes even less losses of the photo generated current, so the open circuit voltage could be higher.[67] Series resistance is a resistance of the electrolyte. So, when a highly conductive electrolytes are used, the series resistance would be lower. Shunt resistance is occurred due to the anode electrode.

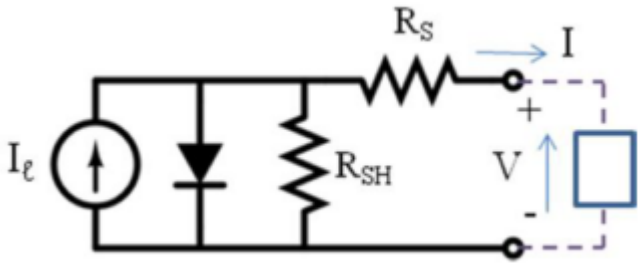

Figure 2.18. Schematic representation of shunt and series resistance in cell.[67]

In the I-V curve, the line, which is parallel to the x-axis changes by changing the shunt resistance, and the one, parallel to the y-axis changes as the series resistance change. If the shunt resistance is maximized and the series resistance is minimized, as much as possible, then the FF will be the highest since the I-V curve gets closer to the ideal shape.[67]

There are some other parameters that affect the efficiency and fill factor of a solar cell, such as the temperature of the cell. When the temperature applied to the crystals, which are used for the formation of photovoltaic cells, is increased, the band gap of semiconductor material (usually TiO_2) is decreased. Therefore, open circuit voltage is decreased. At higher temperatures, a better diffusion of the electrolyte can be achieved. Thus photocurrent is increased a little bit by increasing temperature. Despite the increase in current, this increase is not effective to cancel out the decreasing voltage values. Secondly, the other parameter is the initial light intensity. When light intensity is decreased, solar performance is also decreased.[68]

The working principle seems simple, however, there are many factors that affect the efficiency of a solar cell, such as blocking layer, defects on TiO_2, surface area for both dye and TiO_2 particles, density, viscosity of electrolyte solution, redox couple efficiency for regeneration of the oxidized dye molecules and so on.

TiO_2 is coated on the anode side as a mesoporous semiconductor thin film that has large surface area and no toxicity. These properties make the titania ideal for coating the FTO surface to use as part of the anode in the DSSCs. It is also called working electrode (WE). Some other metal oxides have also been tested, such as ZnO[69], [70], SnO_2[71], Nb_2O_5[72] and etc. due to the fact that they have different Fermi energy. However, the best performance has been achieved from the anatase TiO_2 nanoparticles. Anatase has the highest Fermi energy (E_f), therefore usually

this form is used. Electron mobility of metal oxide is an important parameter for the theory of DSSC, since they are the ones which transport electrons to the counter electrodes; the higher the electron mobility, the more efficient the DSSC is.[73]

One other parameter in DSSCs is the dye. There are many different dyes, tested in DSSCs. So, when choosing the dye; binding ability of dye molecules to the semiconductor surface, ability to absorb visible light, LUMO level of those molecules and stability are important properties that must be checked. The most widely used dyes are ruthenium complexes due to the fact that they are the most efficient ones (mostly N719 and N3 dyes, **Figure 2.19**). However, there are also some studies with Os(II)[74], Re(I)[75], Pt(II)[76], and Cu(I)[77] dye complexes. No matter which dye is used, the lifetime of it should be long enough when it is in its oxidized state and strong anchoring should be accomplished between the dye molecules and semiconductor surface.[73]

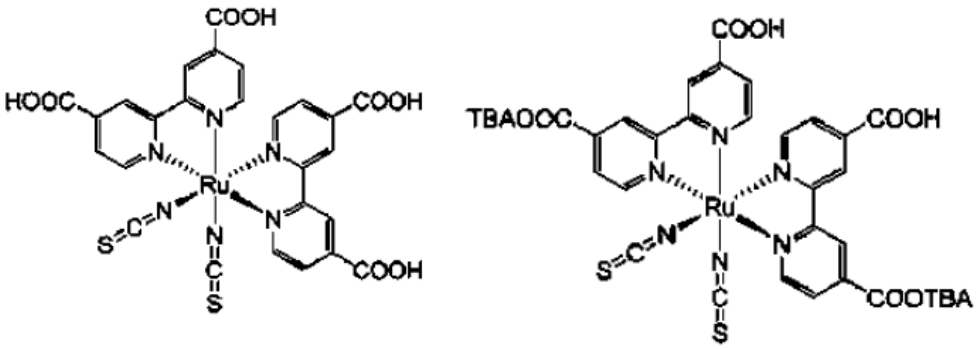

[11]**Figure 2.19.** The molecular structures of N3 (left) and N719 (right) dyes

For completing the circuit, counter electrode is needed as cathode. FTO glasses are used for counter electrodes (CE), however they should be coated with some material which has catalytic properties. Usually Pt-solution is prepared and it is used for coating. When FTO glass is coated with this solution, by spin coating, vapor phase deposition, or electrochemical deposition etc., the resistance of the glass is decreased and conductivity is increased. Besides platinum, there are also some other materials used as counter electrodes, even though they are not that common. Many groups have studied carbon black[78], conducting polymers[79] and cobalt sulfide[80] to increase efficiencies of the DSSC by changing the material used as a counter electrode.[73]

---

[11] Reprinted with permission from Hagfeldt A, Boschloo G, Sun L, Kloo L, Pettersson H. Dye-sensitized solar cells. *Chem Rev*. 2010;110:6595-6663. Copyright (2010) American Chemical Society.

2.5. Electrolytes for Dye Sensitized Solar Cells

Different kinds of electrolytes for these kind of studies, such as solid-state[81]–[84] (see **section 2.4.1**), liquid[85] (see **section 2.4.2**), gel and liquid crystal (see **section 2.4.3**) etc. have been investigated. Also several additives are added into the electrolytes, especially into the liquid and gel electrolytes, to increase the open circuit voltage, photocurrent density, and power conversion efficiency, and/or fill factor. However, the liquid electrolytes are the most investigated due to easy application, availability, and lower-cost, compared to solid electrolytes.

2.5.1. Solid-State Electrolytes for Dye Sensitized Solar Cells

The reason for using solid-state electrolytes for DSSCs is the disadvantages of liquid ones such as volatility and leakage problems. For the first time, in 1995, CuI was used as inorganic hole conductor in solid-state DSSC. In those devices, the dye molecules inject photo generated electrons into n-TiO_2, and the holes into p-CuI when dye molecules were sandwiched between these two semiconductors. In this process, when the dye molecule oxidized, , it is reduced by the valence band electrons of CuI.[86] In 1997, Yanagida and co-workers fabricated solid-state solar cell using an organic hole conductor layer, polypyrrole.[87]

Since then, the solid-state DSSCs have been extensively investigated.[83], [86]–[92] Although, perovskite-sensitized solar cells have high efficiency (14.1% and after a little time 15% efficiency[93]), the solid-state dye sensitized solar cells work with much lower efficiency. This is because of the fact that there is a drawback of a solid-state DSSC, which is inefficient filling of the pores with the solid electrolytes, inhomogeneous electrode-electrolyte conducts, etc.

2.5.2. Liquid Electrolytes for Dye Sensitized Solar Cells

The reason for using liquid electrolytes in these systems is that they are chemically stable, they have low viscosity and thanks to this there is no diffusion problem and etc. As solvents, acetonitrile (AN) and 3-methoxypropionitrile (MPN)[94] are mostly used, and they have usually high power conversion efficiencies, up to 12.3%.[95]

The mostly used liquid electrolytes are I^-/I_3^- redox couple in acetonitrile as solvent. There are also alternative redox couples[96] such as Br^-/Br_3^-, $SCN^-/(SCN)_3^-$ and $SeCN^-/(SeCN)_3^-$ and different solvents also can be used such as THF, DMSO, DMF, propionitrile, benzonitrile, alcohols, DME and so on.[97]–[99] When the solvent is a strongly donating solvent (having large number of donor sites), the V_{oc} is increased but the I_{sc} is decreased according to a study.[100]

Since the Fermi level of the semiconductor TiO_2 is dependent on the cations in electrolytes due to semiconductor/electrolyte interactions, there are various numbers of studies which investigate this effect.[101]–[103] According to Liu et al., the V_{oc} value increases as $Li^+ < Na^+ < K^+ < Rb^+ < Cs^+$ (as cation radius is increasing), due to the fact that the potential of the conduction band of TiO_2 is decreased. However, when the radius of cation is increased, the photocurrent of the cell decreases on the contrary to the voltage values.[98] For example, Li^+ has a small radius in compare to others in the series. Since it has smaller radius, the penetration of Li^+ ion into the pores of TiO_2 is easier than that of larger radius cations. Also, the formation of ambipolar cation-electron couple with the electrons in the conduction band of TiO_2 is easier in the case of smaller cations, thus transport speed of the electrons is increased. So, it is reasonable to say that the I_{sc} is increased when the radius of the cation is decreased. However, when radius is smaller, it also means that ambipolar cation can combine with I_3^- easily. As a result the V_{oc} is decreased when the radius of the cation is decreased.[104]

Besides from these electrolytes, ionic liquid (IL) electrolytes are also widely investigated by solar cell research groups. Since they are ionic, they have better conductivities. Alkylimidazolium (1-alkyl-3-methylimidazolium) is usually added into the electrolytes for increasing the efficiencies by increasing the conductivities of electrolytes.[105], [106] Fill factors and efficiencies are improved up to 5%[105] by using alkylimidazolium since it is believed to cut the contact between the triiodide and TiO_2 layer. Also it is found that alkyl imidazolium cation improves the stability of the dye molecules.[85]

Liquid electrolytes have higher power conversion efficiencies in compare to solid-state electrolytes due to effective diffusion, or high ionic conductivity. However, liquid electrolytes are not good for environment since they may be toxic, flammable, and low long-term stability. The solvent can evaporate due to high volatility and the solar cells based on liquid electrolytes have leakage problems; so

that those electrolytes cannot be stable for long time. Also they can desorb the attached dye molecules from TiO_2 layers overtime and causes a decrease in efficiency. Because of these, ionic liquid electrolytes are considered to be better replacement of liquid and solid-state electrolytes. Also, water-based liquid electrolytes are considered to be better than organic solvent-based liquid electrolytes due to the reasons as mentioned above. Nevertheless, liquid crystal gel electrolytes are even better even though they have to be improved in terms of efficiency of the cells.

2.5.3. Gel Electrolytes for Dye Sensitized Solar Cells

Gel electrolytes are considered to be more environmental-friendly electrolytes for solar cell applications. They can be in liquid crystalline phase. So, they exhibit the properties of both solid and liquid phases. They are viscous, so volatility is not a problem as in liquid electrolytes. They have lower but still comparable conductivity to that of the liquid electrolytes. Since volatility is not a problem here, they have longer life-time than liquid ones in terms of stability. However, there is a major problem that is the diffusion of gels into the pores of both electrodes. Since they have high viscosity, infiltration of electrolyte into the pores of TiO_2 is harder, and the conversion efficiency of the gel- electrolytes is lower.

Solidification of the liquid electrolytes has been accomplished using different methods, in place of using a solid electrolyte, but the efficiency of the cells were quite low.[107]–[112] There are both organic solvent based gel electrolytes and water-based gel electrolytes, tested in DSSCs. Water-based electrolytes have lower efficiency because of the properties of water in the electrolyte medium, however, it can still be improved. Since they have lower efficiency, there is a limited number of work on this kind of electrolyte; therefore it is the motivation for this thesis to study these electrolytes for DSSCs.

2.5.4. Most Widely Used Redox Couple: Iodide/Triiodide

Redox couple is one of the most important part of the DSSCs. As mentioned above, it regenerates the oxidized dye molecules. Because of that, it is important to choose most suitable redox couple to have higher efficiency. Redox potentials of

these couples directly affect the open circuit voltage values. Iodide/triiodide redox couple is the most preferable choice in literature. Electron lifetime of I^-/I_3^- in solar cell is measured as 1-20 ms, which can be considered as long.[73] It also has suitable redox potential (0.35 V versus normal hydrogen electrode, NHE) and good solubility in solvents.

To explain why I^-/I_3^- redox couple is the most preferred one, the energetics of it should be first mentioned. In solution, iodine combines with iodide ion and gives triiodide ion as a result (see the equation below).

$$I_2 + I^- \rightarrow I_3^-$$

When the concentration of iodine is high enough, I_5^-, I_7^- and I_9^- ions can also form in the solution at low concentrations and they are not considered to be a problem.

$$I_3^- + 2e^- \rightarrow 3I^-$$

The Nernst equation can be used to calculate the redox potential of the redox couple using above half reaction; where $E^{0'}$ is the formal potential, R is the ideal gas constant, T is the temperature (in Kelvin), F is the Faraday constant (see the equation below).[113]

$$E_{redox} = E^{0'} + \frac{RT}{2F} ln \frac{[I_3^-]}{[I^-]^3}$$

Oxidization potential of N719 is 1.10 V; so, since 0.35 V is the redox potential of iodide/triiodide redox couple, the driving force for the reduction of oxidized dye molecules is 0.75 V (see **Figure 2.20**).[113]

In the dye sensitized solar cell, this redox couple has the most crucial role; regeneration of oxidized dye molecules. Some other redox couples are also tried and investigated as mentioned, but the time scale of electron injection for LiI-I_2 redox mediator is more suitable for the process (see **Figure 2.21**). This durations depend on the electronic coupling and the energetic overlap between donor and acceptor states. In this redox mediator, electron recombination between TiO_2 and triiodide is extremely slow, regeneration of oxidized dye molecules is very rapid as

needed, and that is why it is very favorable.[113] The possible reaction paths are shown in **Figure 2.21**. The green ones are the paths which correspond to the desired reactions; and the red ones are unwanted ones, belonging to the recombination reactions. When LiI-I_2 redox couple is used, these unwanted reactions are mostly prevented.

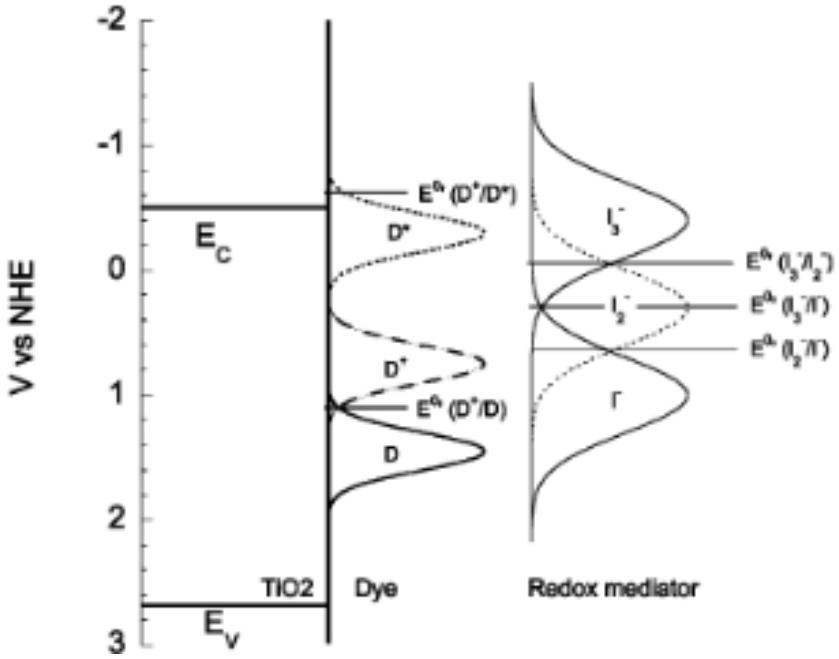

[12]**Figure 2.20.** Energy scheme for DSSC with Ru-based dye, TiO_2 semiconductor and I^-/I_3^- redox couple.[113]

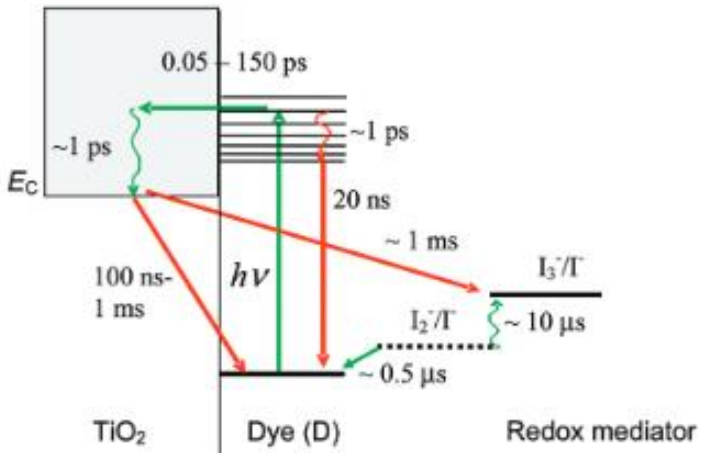

[13]**Figure 2.21.** Kinetics of DSSC with the approximate time constants.[113]

[12, 13] Reprinted (adapted) with permission from Boschloo G, Hagfeldt A. Characteristics of the iodide/triiodide redox mediator in dye-sensitized solar cells. *Acc Chem Res*. 2009;42(11):1819-1826. Copyright (2009) American Chemical Society.

2.5.5. Additives for Electrolytes in Dye Sensitized Solar Cells

There are certain additives, which are investigated and used frequently to increase the open circuit voltage values, and thus efficiency and fill factor of DSSCs.

Those additives serve the purpose of changing the redox potentials, shifting the band gap of semiconductors, or enhancing the interaction between dye molecules and the surface, and minimizing the contact between the TiO_2 surface and I_3^-.[73] Most common additive is 4-tert-butylpyridine (4TBP). The enhancement on the efficiency of the DSSC due to 4TBP was first found by Graetzel and his co-workers in 1993.[114] After that, many groups have worked on this additive to the electrolyte, and it is found that 4-tert-butylpyridine decreases the electron transport time.[115]–[117] Also 4TBP shifts the TiO_2 semiconductor band edge to the higher energies, leading to the passivation of the surface, and this causes the photovoltage to increase.

There are also many other additives that have been studied, such as pyridine derivatives[118], 4-ethoxy-2-methylpyridine[119], 1-methyl-benzimidazole[120], nitrogen donating additives such as pyrimidines, aminotriazoles, quinolines and alkylpyridines.[121]–[123] These are all useful to decrease the recombination reaction rates and therefore increase the photovoltage in the DSSCs.[73] Guanidinium thiocyanate (GuNCS) is also one of the most commonly used additives. It increases the lifetime of the electrons by decreasing the rate of recombination with electrolyte, and it shifts the CB edge of TiO_2 to the lower energies.[124] This causes the electron injection efficiency to increase.[125] This is why, whereas the other additives increase the V_{oc} values only, GuNCS increases both the V_{oc} and the I_{sc} values.[124], [126] However, it should also be noted that, these effects depend on the concentrations of both the components of the electrolyte and the additives.

CHAPTER 3

3. EXPERIMENTAL

3.1. Materials

All chemicals used were obtained from Sigma Aldrich. Distilled water was obtained by purification of tap water using Millipore Synergy 185 water purifier.

3.2. Sample Preparation

3.2.1. Preparation of the LiX-xH_2O-$C_{12}EO_{10}$ Gel Samples

The samples were prepared by mixing the surfactant ($C_{12}EO_{10}$) and lithium salts in determined amounts. The mole ratio of surfactant is always 1, and the rest was calculated according to surfactant ratio. Mix salt, surfactant and distilled water in a vial and put into heating bath to homogenize the mixture by shaking and heating at the same time. After 24 hours of shaking at 80 ºC, they were ready for measurements. For instance, a sample with the mole ratios of 3:3:1 for LiCl-H_2O-$C_{12}EO_{10}$ was prepared using a 0.20 g of LiCl salt, 0.09 g of H_2O and 1.00 g of $C_{12}EO_{10}$. After 24 hours, the samples were ready for further characterizations; see **Table 3.1** and **Table 3.2** for the other compositions.

3.2.2. Preparation of the Gel Samples with Redox Couple

LiI salt and I_2 were used as a redox couple for solar cell measurements. $C_{12}EO_{10}$ was used as a surfactant. 0.46 g of distilled water was used for all gel electrolytes and the ratio of LiI:$C_{12}EO_{10}$ and I_2:$C_{12}EO_{10}$ were 2.0 and 0.2, respectively. Moreover, 1 to 0.1, 3 to 0.3, and 4 to 0.4 (LiI to I_2 mole ratio, respectively) were also prepared using different amounts of water. For instance, to prepare 2LiI and 0.2I_2 gel electrolyte; 0.43 g of LiI, 0.08 g of I_2, 1.0 g of surfactant and 0.46 g of H_2O were put into a vial, and then into a heating bath at 80 ºC for 24 hours for the homogenization, see **Table 3.3** for the other compositions. After that,

the gel samples were ready for further characterization and solar performance measurements.

3.2.3. Preparation of the Solution Phase Samples with Redox Couple

Same mole ratios of LiI, I_2 and surfactant were used for preparing the electrolyte solutions. However this time, excess solvent was added (5 g). Since these samples were not in a gel phase, 24 hours in heating bath was not necessary, 6 hours of stirring on the magnetic stirrer was enough for the homogenization. Different solvents were tried to prepare electrolyte solutions, such as just water, ethanol, acetonitrile and some combinations of two of them, see **Table 3.3** for the composition details.

3.3. Fabrication of the Solar Cells

3.3.1. Preparation of Blocking Layer Solution

After FTO (fluorine doped tin oxide) glasses were cleaned with tap water, detergent and ethanol, these glasses were coated with a protecting layer. A solution of 5 mL of ethanol, 0.25 g of $Ti(BuO)_4$ and 0.5 mL of HNO_3 were prepared and spin coated over a FTO glass electrode at 1000 rpm. The films were then calcined at 450 ºC for 10 minutes. The coating process was repeated just to make sure that there is no uncoated part in the FTO glass.

3.3.2. Preparation of Mesoporous Titania Films and Working Electrodes

Different procedures for preparing the titania films have been tested. First one was 3.5 g of P25 (>25 nm particles) was mixed with 15 mL of ethanol and sonicated for half an hour. After that 0.5 mL of Ti(IV) isopropoxide was added into the suspension and stirred until it became uniform. Second one was with 0.200 g of TiO_2 powder (>21 nm particles), 12 drops of acetic acid, 1 drop of Triton X100, 0.6 mL of distilled water and 0.6 mL of ethanol were put into a mortar and grained until it became a smooth mixture. Both of the titania paste were separately spread over the FTO glass with a blocking layer by doctor blading and then calcined at 450 ºC

for 1 hour. These electrodes were used as working electrodes for solar cell measurements upon sensitizing.

3.3.3. Preparation of Dye Solution

0.024 g of N719 dye powder was added into the 20 mL of ethanol to prepare a 1 mM dye solution. The working electrodes, which were prepared as mentioned in **section 3.3.2** were dipped into these solutions for 24 hours to adsorb dye molecules.

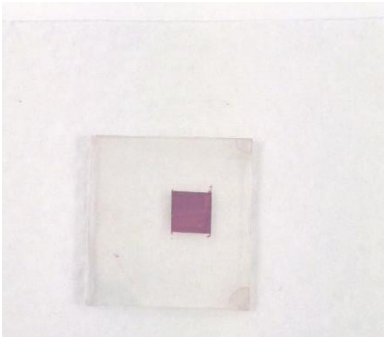

Figure 3.1. A representative working electrode after all the steps.

3.3.4. Preparation of Pt Solution and Counter Electrodes

0.026 g of H_2PtCl_6 was added into 5 mL of 2-propanol to prepare 5 mM Pt(IV) solution. One or two drops of it was spread over cleaned FTO glasses and then calcined at 450 ºC for 1 hour. These Pt-coated electrodes were used as counter electrodes in the DSSCs.

3.3.5. Assembly of Dye Sensitized Solar Cells

The gel electrolytes or the electrolytes which were in solution phase were put onto the dye adsorbed titania covered working electrodes. Then they were rest for some time for an effective diffusion of the electrolyte into the pores of titania working electrode. When the solution phases were used as the electrolyte, they were usually rested for 3-4 hours until the solvent evaporated and solution became gel-like. Then the counter electrode is closed onto the working electrode, like a sandwich; one must be very careful for electrolyte not to spread uncovered parts of the working electrodes.

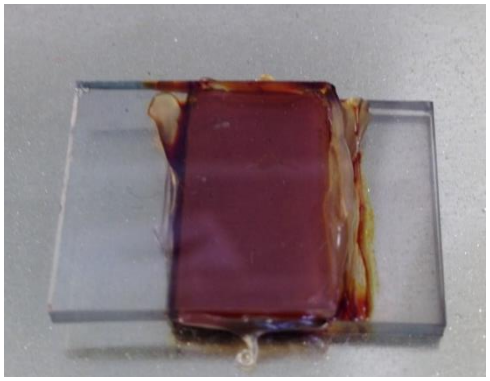

Figure 3.2. Dye sensitized solar cell with working electrode on top and counter electrode at the bottom.

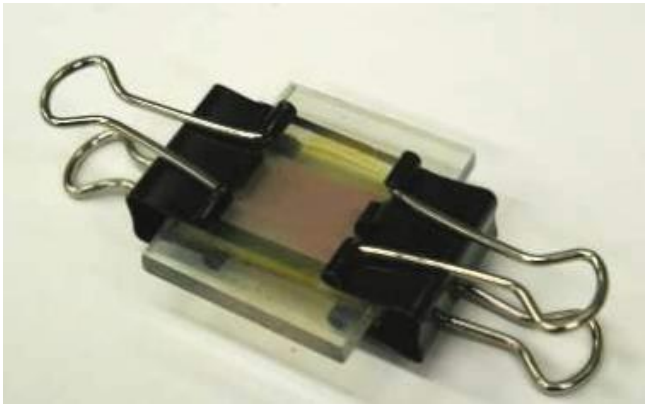

Figure 3.3. Dye sensitized solar cell with clips to hold them together.

	LiCl	**Surfactant**	**Water**
3-1-1.5	0.203 g	1.000 g	0.043 g
3-1-3	0.203 g	1.000 g	0.086 g
3-1-4.5	0.203 g	1.000 g	0.129 g
3-1-6	0.203 g	1.000 g	0.173 g
3-1-7.5	0.203 g	1.000 g	0.216 g
3-1-9	0.203 g	1.000 g	0.259 g
3-1-12	0.203 g	1.000 g	0.345 g
3-1-15	0.203 g	1.000 g	0.431 g
3-1-18	0.203 g	1.000 g	0.518 g
3-1-21	0.203 g	1.000 g	0.604 g

Table 3.1. Preparation of the samples with LiCl-$C_{12}EO_{10}$-H_2O system.

	LiI	Surfactant	Water
3-1-1.5	0.641 g	1.000 g	0.043 g
3-1-3	0.641 g	1.000 g	0.086 g
3-1-4.5	0.641 g	1.000 g	0.129 g
3-1-6	0.641 g	1.000 g	0.173 g
3-1-7.5	0.641 g	1.000 g	0.216 g
3-1-9	0.641 g	1.000 g	0.259 g

Table 3.2. Preparation of the samples with LiI- $C_{12}EO_{10}$-H_2O system.

	LiI	I_2	Surfactant	Water
1-0.1	0.21 g	0.04 g	1.00 g	0.03/0.06/0.09/0.12/1.73 g
2-0.2	0.43 g	0.08 g	1.00 g	0.06/0.12/0.17/0.23/1.73/5.0 g
3-0.3	0.64 g	0.12 g	1.00 g	0.17/0.26/0.36/0.43/1.73/5.0 g
4-0.4	0.86 g	0.16 g	1.00 g	0.23/0.36/0.46/0.56/1.73 g
5-0.5	1.07 g	0.20 g	1.00 g	0.43/0.56/0.72/0.86/1.73 g
1-0.2	0.21 g	0.08 g	1.00 g	0.23/5.00 g
2-0.3	0.43 g	0.12 g	1.00 g	0.23/5.00 g
3-0.2	0.64 g	0.08 g	1.00 g	0.23/5.00 g

Table 3.3. Preparation of gel and solution phase electrolytes with redox couple.

	LiCl	LiI	I_2	Surfactant	Ethanol
0.2-2-0.2	0.014 g	0.43 g	0.08 g	1.00 g	5.00 g
0.4-2-0.2	0.028 g	0.43 g	0.08 g	1.00 g	5.00 g
0.6-2-0.2	0.042 g	0.43 g	0.08 g	1.00 g	5.00 g
0.8-2-0.2	0.056 g	0.43 g	0.08 g	1.00 g	5.00 g
1.0-2-0.2	0.070 g	0.43 g	0.08 g	1.00 g	5.00 g
0.5-5-0.5	0.03 g	1.07 g	0.20 g	1.00 g	5.00 g
1.0-5-0.5	0.07 g	1.07 g	0.20 g	1.00 g	5.00 g
1.5-5-0.5	0.10 g	1.07 g	0.20 g	1.00 g	5.00 g
2.0-5-0.5	0.14 g	1.07 g	0.20 g	1.00 g	5.00 g

Table 3.4. Preparation of the solution phases of LiCl added redox couple samples.

	LiBr	LiI	I_2	Surfactant	Ethanol
0.2-2-0.2	0.03 g	0.43 g	0.08 g	1.00 g	5.00 g
0.4-2-0.2	0.06 g	0.43 g	0.08 g	1.00 g	5.00 g
0.6-2-0.2	0.08 g	0.43 g	0.08 g	1.00 g	5.00 g
0.8-2-0.2	0.11 g	0.43 g	0.08 g	1.00 g	5.00 g
1.0-2-0.2	0.14 g	0.43 g	0.08 g	1.00 g	5.00 g

Table 3.5. Preparation of the solution phases of LiBr added redox couple samples.

	$LiNO_3$	LiI	I_2	Surfactant	Ethanol
0.2-2-0.2	0.11 g	0.43 g	0.08 g	1.00 g	5.00 g
0.4-2-0.2	0.09 g	0.43 g	0.08 g	1.00 g	5.00 g
0.6-2-0.2	0.07 g	0.43 g	0.08 g	1.00 g	5.00 g
0.8-2-0.2	0.04 g	0.43 g	0.08 g	1.00 g	5.00 g
1.0-2-0.2	0.02 g	0.43 g	0.08 g	1.00 g	5.00 g

Table 3.6. Preparation of the solution phases of $LiNO_3$ added redox couple samples.

3.4. Instrumentation

3.4.1. The Polarized Optical Microscope (POM)

The POM images of all samples were obtained in transmittance mode by using a ZEISS Axio Scope A1 polarizing optical microscope with a Linkam LTS350 temperature controlling stage attached to the microscope. The temperature control was performed by using a LinkamT95-LinkPad temperature programmer attached to the stage. The imagings of the samples were done after solvent is evaporated.

3.4.2. The X-Ray Diffraction (XRD)

Rigaku Miniflex diffractrometer, which uses a high power Cu-K_α source operating at 30 kV/15 mA and a wavelength of 1.5405 Å, was used to characterize all of the samples. The measurements were carried out by spreading the samples on

clean glass slides by either spin-coating or drop casting methods. The measurements were done at different scan rates at 0.01 data intervals.

3.4.3. The Fourier Transform–Infrared Spectroscopy (FT-IR) and Attenuated Total Reflectance (ATR)

The Bruker Tensor 27 model Fourier Transform - Infrared Spectrometer (FT-IR) or the Bruker ALPHA-P FT-IR spectrometer, which includes a diamond ATR attachment were used to characterize all of the samples. A Digi Tect TM DLATGS detector was used with a resolution of 4.0 cm^{-1} in the 400-4000 cm^{-1} range in the Bruker Tensor 27. The FT-IR measurements were carried using the samples either by spreading them onto silicon wafers or by sandwiching them between two silicon wafers in order to prevent solvent evaporation, to check water amount. The ATR measurements were carried by just dropping the samples onto the diamond part of the ATR and to prevent solvent evaporation they were covered with small glasses.

3.4.4. The Raman Spectroscopy

Raman spectrometer by Jobin Yvon Horiba Scientific was used to characterize all of the samples. LabRam confocal Raman microscope with a 300 mm focal length was attached to the spectrometer. A Ventus LP 532, 50 mW, diode pumped solid state laser operator is equipped in the spectrometer. The spectrometer has 1024x256 element CCD camera. The detector collects the signals by a fiber optic cable with 600 g/mm grating.

3.4.5. The AC Impedance Spectroscopy

The conductivity measurements of all samples were done by using Gamry G750 potentiostat/galvanostat with a homemade conductivity cell. The cells were made up of a FTO glass, which was scratched with diamond cutter to break the contact between each side of the FTO. Then the scratched line was filled with 0.01 M KCl to determine the cell constant; and after that the samples were put into the

same cell to determine the conductivity of the samples by using the predetermined cell constant.

3.4.6. UV-VIS Spectroscopy

A Varian Carry 5 double beam spectrophotometer is used. The spectra were collected with 600 nm/min speed and 0.2 nm resolution over a wavelength range from 190 nm to 900 nm using the samples that were spin coated on quartz windows at different rpm rates depending on the purpose.

3.4.7. The Solar Performance Measurements

The photovoltaic measurements were done with an AM 1.5 solar simulator with a 300 W xenon lamp, model no. 81172, Oriel. The intensity of the incoming light was adjusted to 100 $mW \cdot cm^{-2}$ by using a reference silicone photodiode. After that, the photocurrent of the cells, were measured for the solar performances by applying external bias to them with a Keithley model 2400 digital source meter.

CHAPTER 4

4. RESULTS AND DISCUSSION

Due to the unique properties and various possible applications, the lyotropic liquid crystalline (LLC) mesophases with transition metal salts, non-transition metal salts, water, and many more solvents have been extensively investigated over the years. The key point here is the use of surfactants (amphiphilic materials, as mentioned in **Chapter 2**) with salted-water to form the lyotropic liquid crystalline mesophases.

In this work, C_mEO_n type surfactants (such as $C_{12}EO_{10}$, 10-lauryl ether) and lithium salts have been used to from mesophases that have been employed as gel-electrolytes in DSSC. Usually LiI-I_2-C_mEO_n-water system has been used as the electrolyte; however, mixture of the LiI-I_2 and LiCl, LiBr, or $LiNO_3$ have also been tested as the gel-electrolyte to increase the conductivity of the gels and also instead of water, ethanol was used as the solvent to form the LLC mesophases to overcome some of the issues in the applications (see latter). These are the subjects, which will be discussed in this chapter.

4.1. Lyotropic Liquid Crystalline (LLC) Mesophases of 10-Lauryl Ether and LiCl and LiI

LiCl and LiI salts were used to prepare the lyotropic liquid crystalline mesophase in the presence of a very little amount of water. The samples were prepared as gel and solutions by varying the amount of the lithium salts and the solvent.

In the lithium salt-surfactant self-assembly, there is a specific amount of water that is kept by the salt ions; it is known as the hydration water. The hydration water is important in this system to form the mesophases, since it is used to dissolve salt species in the mesophase. The extra water is called free water in the LLC media. The free water can cause problems during the application as gel-electrolytes; however the hydration water is needed to form the stable mesophases.

LiCl was used with a 3 mole ratio to the surfactant that has been well established from Dag's group previous works.[50] When the LiCl/$C_{12}EO_{10}$ mole ratio is 3, the gel is in a hexagonal LLC phase. The amount of water has been changed in the samples to investigate the role of water in the media. Different mole ratio of water was added (from 1.5 to 21) to find out the amount of water that is needed to have a stable LLC mesophase. **Table 3.1** shows the amounts of LiCl, $C_{12}EO_{10}$ and water to form stable LLC phases. The POM images, FT-IR, Raman, XRD and conductivity data were collected using those samples.

The LiI-$C_{12}EO_{10}$ samples were also prepared in the salt/surfactant mole ratio of 2 and 3 by changing the water amounts (from 1.5 to 15) to determine the stable LLC mesophase composition. **Table 3.2** shows the amounts of LiI salts, $C_{12}EO_{10}$, and the water needed for preparation of the LLC phases. It is observed that the sample with 1.5 mole ratio of water cannot be dissolved due to insufficient amount of water. The characterization of these LLC mesophases has also been carried using the POM imaging, FT-IR, Raman spectroscopy, XRD and AC conductivity measurements.

4.1.1. Characterization of LiCl - $C_{12}EO_{10}$ - Water LLC Mesophases

The samples were prepared using a required amount of LiCl salt, 1.0 gram of $C_{12}EO_{10}$ and different amounts of distilled water. The mole ratio of salt/surfactant was always 3 in this study, since it was known that this ratio formed hexagonal LLC mesophase, even though broad range of salt concentration still forms liquid crystalline mesophases. The samples look like gel with high viscosity, see **Figure 4.1.**

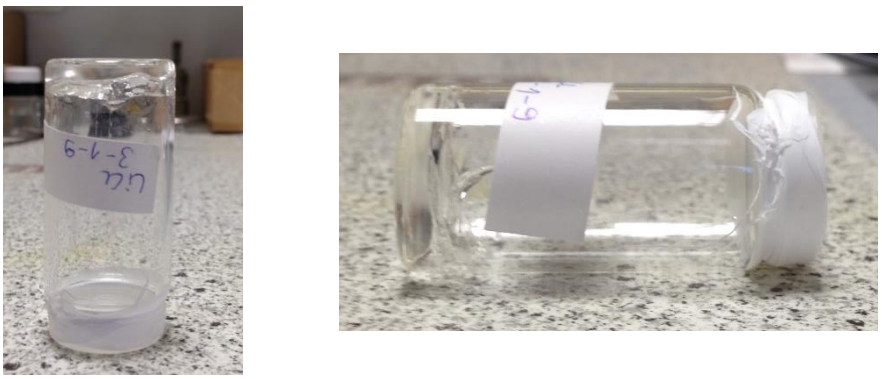

Figure 4.1. Photos of the 3-1-9 ratio of LiCl salt LLC with high viscosity.

The samples were prepared and spread over a clean glass with and without cover glass. This was done to see the differences in the mesostructures, and to determine whether the samples were exposed to the ambient conditions or not. We have found out that only the 3-1-9 (salt-surfactant-water) ratio formed a hexagonal LLC mesophase, when it was prevented to interact with the laboratory atmosphere. However, all other samples prepared with different amount of water than 9, did not form LLC mesophase unless exposed to the ambient laboratory atmosphere, by adsorbing water or releasing extra water.

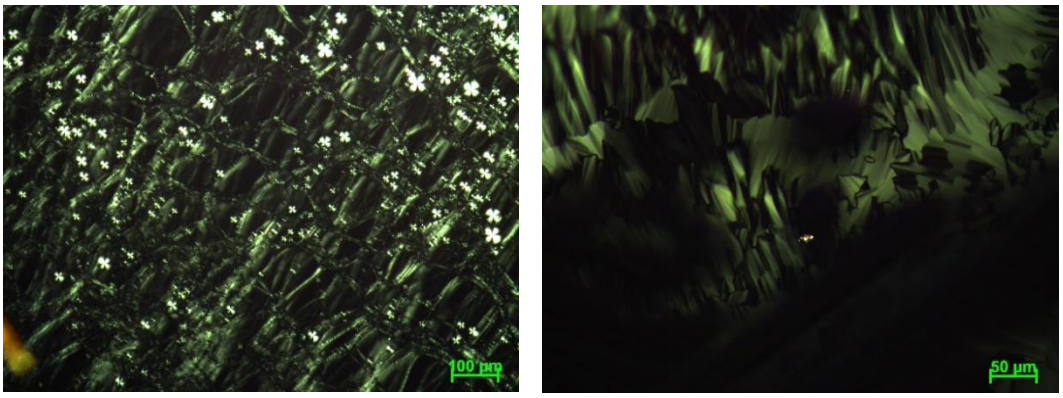

Figure 4.2. The POM images of LiCl-oligo-water systems of 3-1-3 ratios covered with glass (left) and open to air (right)

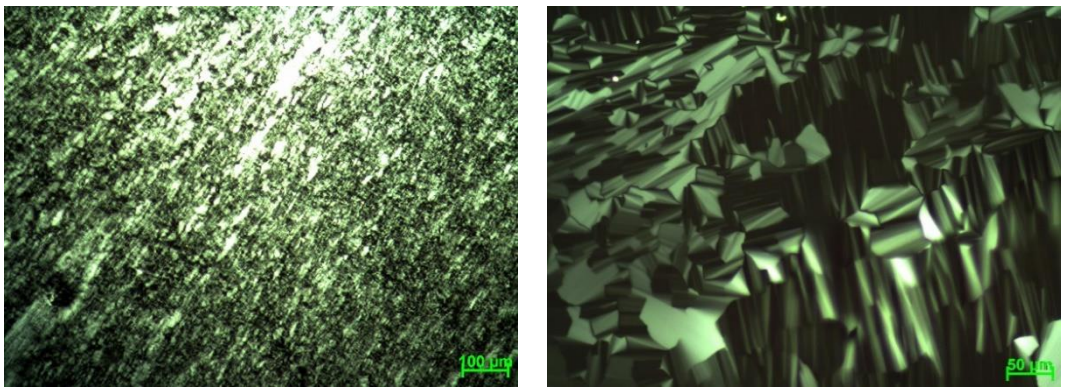

Figure 4.3. The POM images of LiCl-oligo-water systems of 3-1-4.5 ratios covered with glass (left) and open to air (right).

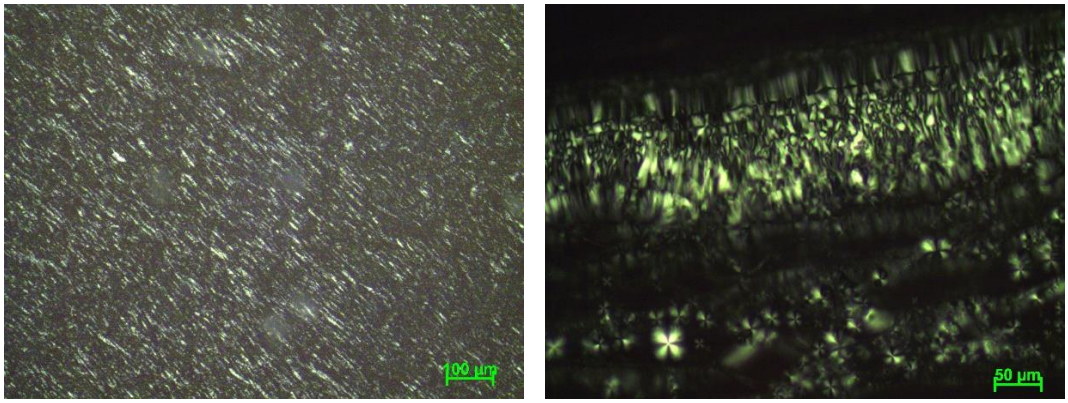

Figure 4.4. The POM images of LiCl-oligo-water systems of 3-1-6 ratios covered with glass (left) and open to air (right).

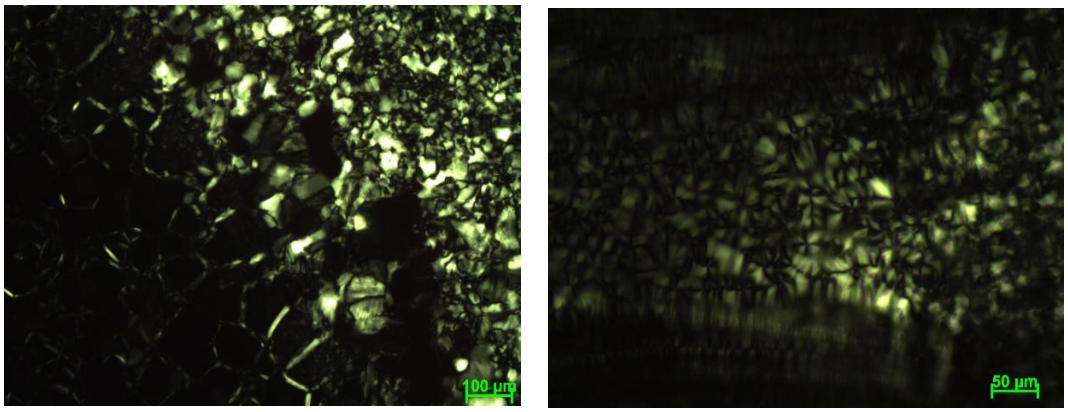

Figure 4.5. The POM images of LiCl-oligo-water systems of 3-1-7.5 ratios covered with glass (left) and open to air (right).

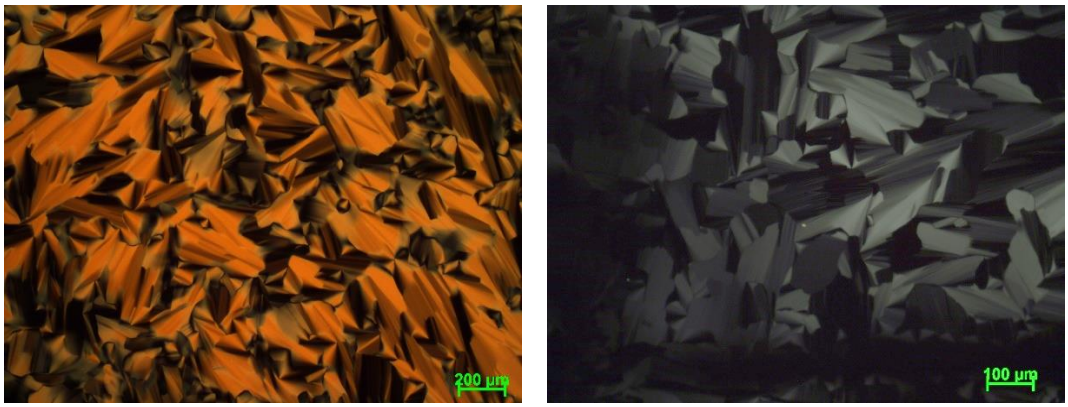

Figure 4.6. The POM images of LiCl-oligo-water systems of 3-1-9 ratios covered with glass (left) and open to air (right).

From the images in **Figure 4.2** to **4.6**, it is clear that the optimum amount of water is 9 waters to a surfactant mole ratio or 3 waters to a lithium salt to form the stable mesophases. When there is more water in the media, the LLC release the excess water until this ratio to become 3; or when there is less than 3 water then the samples adsorbs water from the atmosphere until this ratio is reached. The process of adsorption or desorption of the water takes almost 1 day in terms of water exchange to stabilize the mesophases.

To demonstrate this behavior of the LLC mesophases we also collected time dependent ATR-FTIR spectra. We observed that all samples with the water/surfactant mole ratio, below 9 (3 water per salt), adsorb water from the atmosphere over time and all samples with the ratios above 9 release water to the atmosphere over time as monitored using the bending mode of the water.

Figure 4.7 shows the ATR-FTIR spectra of the sample with a 3 water per 1 LiCl salt. There is no change in the spectra, see **Figure 4.7**, over 4 hours, indicating that the rate of water up take and release are the same at 3 water/LiCl mole ratio. The water content is optimum in the sample, due to the fact that there is no change on the spectra over time; all the spectra are the same with the fresh one. The fresh samples were also measured with a little amount of gel, which was spread over the diamond of ATR and covered with a microscope glass to make sure that there was no change on the water peak intensity. However, there is equilibrium between the water in the gel-phase and the atmosphere. To demonstrate this, we also prepared samples using D_2O and found out that the gel gives water to the atmosphere and absorb the exact amount from the atmosphere. There is a continuous evaporation and absorption when the sample is exposed to open atmosphere. We have proven this by monitoring the D_2O and H_2O (see **Figure 4.8**) by collecting ATR-FTIR spectra over time. **Figure 4.8** clearly shows that there is a continuous exchange of water between the gel and atmosphere, as observed from the spectra; the D_2O peaks goes down in intensity while the H_2O peaks gain intensity over time.

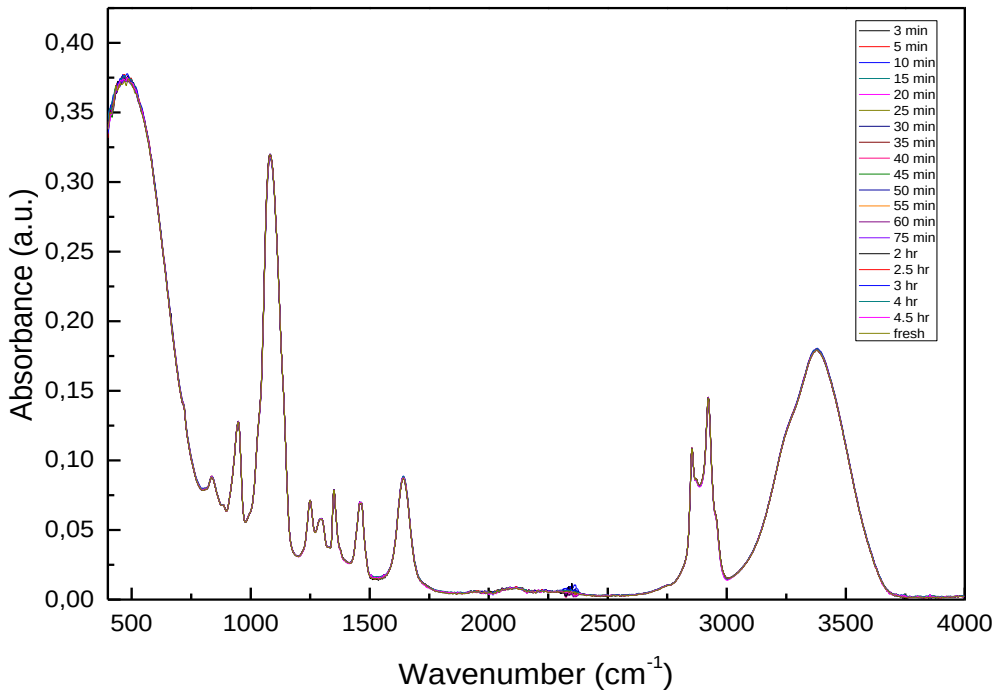

Figure 4.7. The ATR-FTIR measurements for 3-1-9 LLC over time.

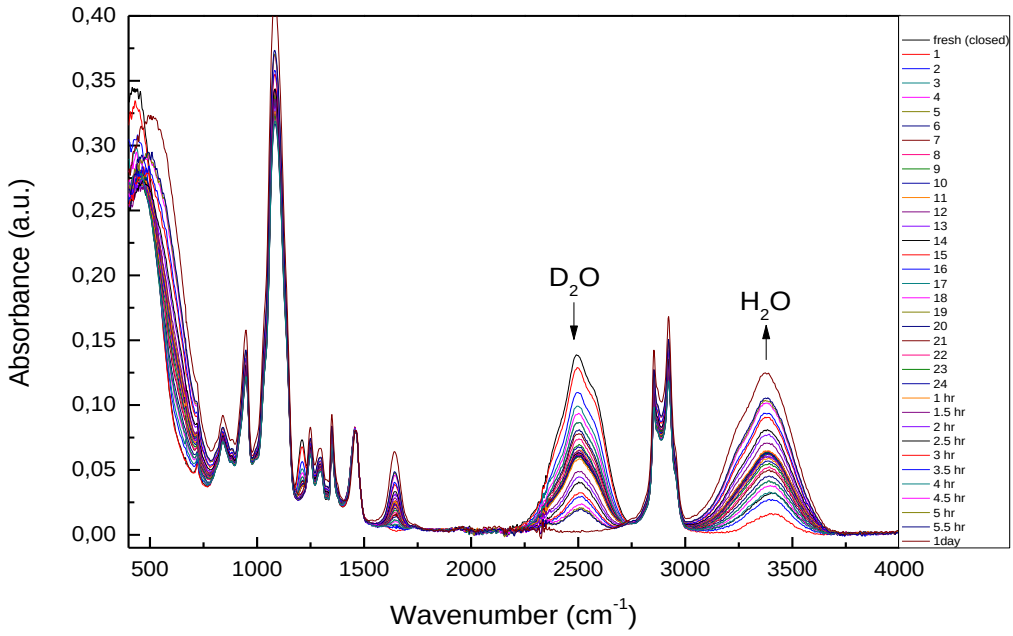

Figure 4.8. The ATR-FTIR spectra of 3-1-9 LiI-$C_{12}EO_{10}$- D_2O instead of H_2O.

To investigate the water absorption/desorption characteristics of these samples, more ATR-FTIR data were collected using the samples with different amount of water and conditions. The samples were first measured using a glass

covered, as fresh samples, and then some samples were exposed to atmosphere and monitored over time, **Figure 4.9.**

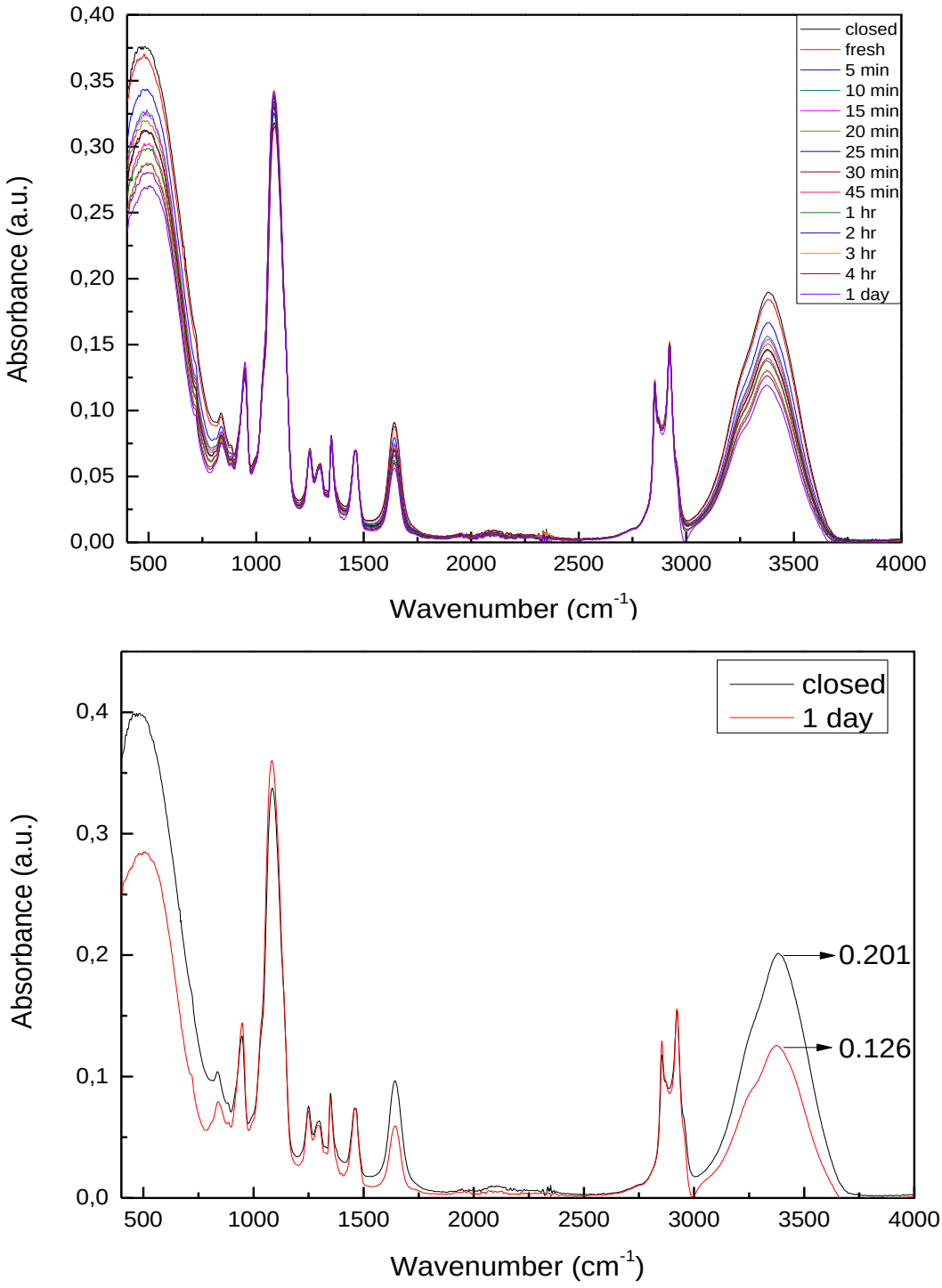

Figure 4.9. The ATR-FTIR spectra for 3-1-12 mole ratio over time (top) and the normalized results to compare fresh one with the 1 day-aged one (bottom).

From the intensities of the normalized data, it is calculated that 3 H_2O/LiCl is truly the optimum amount of water that each mole of LiCl can keep. Calculation

has been performed by comparing the ATR-FTIR spectra of the samples 3-1-9 and 3-1-12. From the intensities of water stretching peak, it is clear that the sample with 12 water mole ratio loses some of its water until the equilibrium is reached, and at the equilibrium the intensity is the same as 3-1-9 sample, which is 0.177 a.u. (see **Figure 4.10**).

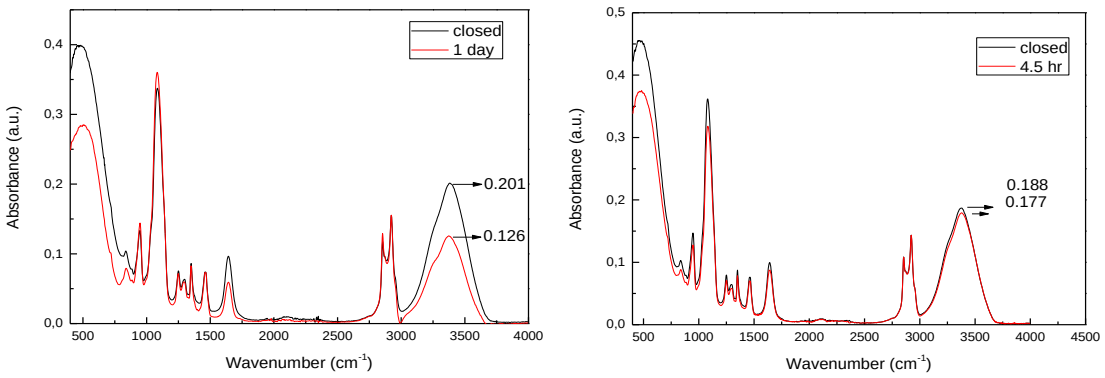

Figure 4.10. Normalized ATR-FTIR spectra of 3-1-12 (left) and 3-1-9 (right) are shown. When calculation is done by using these normalized intensities, 3-1-12 sample is seen to have 0.177 a.u. intensity which is the same with 3-1-9 sample.

We also obtained a calibration curve from a set of samples with known amount of water (see **Figure 4.11**). It is clear from the calibration curve that the high water amounts are problematic. It is likely that these samples lose their extra water too fast that could not be measured and therefore those points negatively deviate from the linearity. The intercept from the calibration curve is calculated to be 0.1046 with a slope of 0.0035, corresponding to an intensity of water for each LiCl. However, we know that the 3 water/LiCl mole ratio can be used as a reference point and almost no water exist for the samples without salt. The reference line is also shown in the plot in **Figure 4.11** that shows both side of this reference point is trying to reach this value. This plot shows that it is very difficult to construct a reliable calibration curve. It is assumed that the sample with 3-1-9 mole ratio can be measured correctly, since the intensity of water peaks does not change over time. Thus, when this information is combined with the calibration curve, it is clear that the samples below 3-1-9 adsorb water, and the ones above 3-1-9 release water (see **Figure 4.11**).

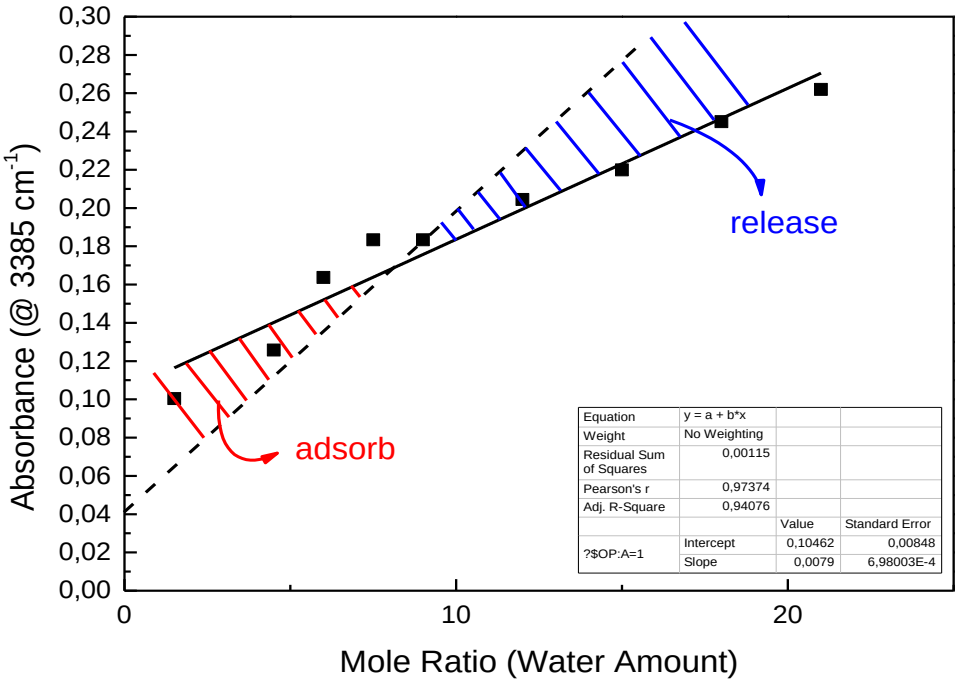

Figure 4.11. The calibration curve for LiCl - $C_{12}EO_{10}$ - water samples.

The Cl^- ion in the Hofmeister series can be considered as structure-maker. It keeps the structure of bulk water in the LLC media. According to the all ATR measurements (see **Figure 4.12**) the peaks can be identified as follows: There are water stretching peaks at around 3380 cm^{-1}, and the water bending peaks are observed at around 1642 cm^{-1}. The peaks at 1248, 1294, 1348 and 1462 cm^{-1} correspond to CH_2 bending modes and there is no shift in those peaks regardless of water content. Also, there is not much change in the surfactant CH_2 stretching modes at around 2854 and 2923 cm^{-1}. From high water content to low, a slight shift is observed in some of the surfactant peaks, such as the peaks at 948 and 1048 cm^{-1} shift to 946 cm^{-1}, and 1082 cm^{-1}, respectively. The shifts are too small, and caused by hydrogen bonding interaction between the hydration sphere of Li^+ and Cl^- ions and the surfactant molecules in LLC media. Otherwise, there is no applicable changes in the surfactants peaks due to variation in the water amount of the mesophases.

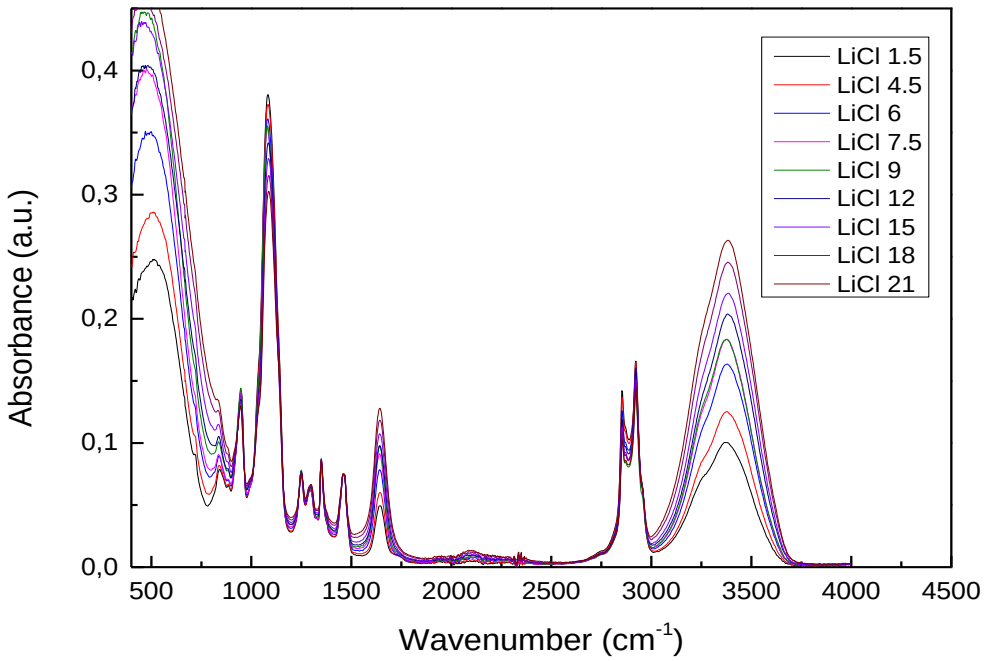

Figure 4.12. The ATR-FTIR results for all the samples with different mole ratios of water.

Besides from these results, if the samples are prepared in gel form, the water amount can be approximately predicted using above data. Roughly speaking from the ATR-FTIR spectra, the calibration curve and calculations, the approximate ratio of water amount per 1 LiCl salt is 3 that can be considered as the hydration water. The rest is free water, and the sample releases this free, excess water when it interacts with the atmosphere. All the excess free water is evaporated; and if the sample is lack of hydration water, it adsorbs water from the atmosphere for the LLC mesophase to form.

An increase in water amount changes the viscosity; however from 1.5 to 21 mole ratios of water, the mixture is in the LLC phase and there is no transformation into liquid phase. The excess water in above range does not change the mesostructure. Nevertheless, it changes the conductivity of the samples as expected. When the amount of water in the samples increases, conductivity also increases. As low as 0.098 mS/cm is the conductivity of 3-1-3 sample, whereas 3.31 mS/cm belongs to 3-1-21, the sample with highest water amount. The conductivity also depends on the concentration of ions. Although when there is more water in the sample, the concentration of ions decreases in total, it is known that at low water content ion pairs are formed; and at high water content ions are free that could be

the reason for increasing the ionic conductivity. However, there is no linear correlation between the conductivity caused and water amount in the samples. This is because the samples with high water amount release water so fast that every measurement gives different results due to different time spent during the measurements. But still the conductivity increases by adding more water to the sample, see **Table 4.1**. However, owing to the fact that the excess water is evaporated when the sample is exposed to the atmosphere, the high conductivity of the samples with excess water decreased over time and all samples displayed the same conductivity around 0.6 mS/cm.

Sample	Conductivity (mS/cm)
3-1-3	0.098
3-1-6	0.570
3-1-9	0.600
3-1-15	1.100
3-1-18	2.670
3-1-21	3.310

Table 4.1. The conductivity results of LiCl-$C_{12}EO_{10}$-H_2O samples

We also were prepared samples of 2-1-60, 3-1-90, 4-1-120, 5-1-150, and 6-1-180 (salt-surfactant-water), and their ATR-FTIR spectra were collected. From these spectra, it is clear that, when the amount of salt is increased, the hydration water amount is also increased (see **Figure 4.13**). A calibration curve is obtained by plotting the intensity at 1645 cm^{-1} versus LiCl mole ratio using these samples. From the plot, it is clear that there is a linear correlation between the hydration water amount and salt amount in the LiCl-$C_{12}EO_{10}$ system.

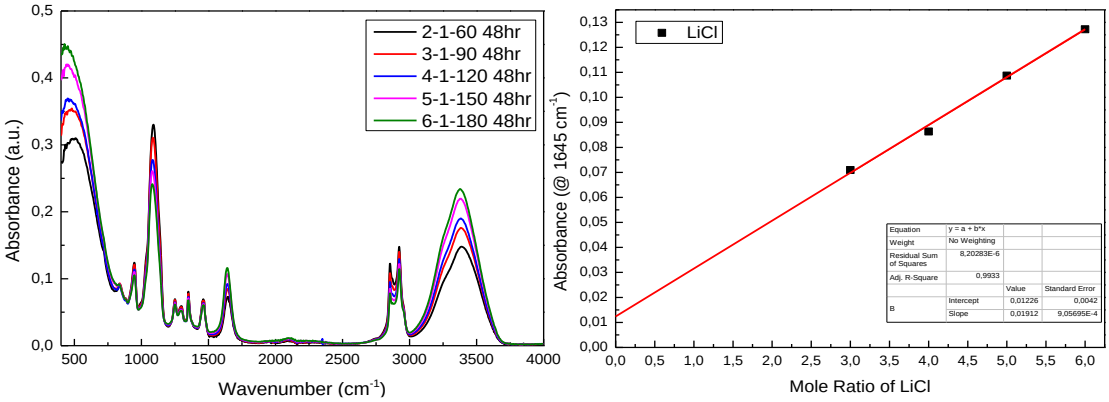

Figure 4.13. The ATR-FTIR spectra of LiCl samples (left) and the calibration curve obtained from it (right).

To support the ATR-FTIR data for the LiCl samples, the samples with excess water were also monitored using a 4 digit balance. The samples were spread onto clean glasses and weighed over time. The plot of weight versus time shows an exponential decay and fitting this data provides the amount of water, left in the mesostructure. However, there are differences in results in terms of the amount of hydration water.

We found out from the weight measurements that the water amount is 2.69 H_2O/LiCl for the sample with 2-1-60 mole ratio, 2.95 H_2O/LiCl for the sample with 3-1-90 mole ratio, and 3.10 H_2O/LiCl for the sample with 4-1-120 mole ratio, **Figure 4.14** and **Figure 4.15** The water amount increases with increasing the salt amount (see **Figure 4.14**). That is why the water amount per salt is different for these samples. Nevertheless, they are all between 2 and 3 mole ratios of water, and this is in good accordance with the ATR-FTIR results. The ATR-FTIR measurements of the fresh samples may not be reliable when they were prepared as gels. The rate of evaporation or release of water is so fast that the water amount is changed even during preparation of the gels. That is why the ATR-FTIR measurements of the gel samples gave slightly different results than weight measurements of the samples with excess water.

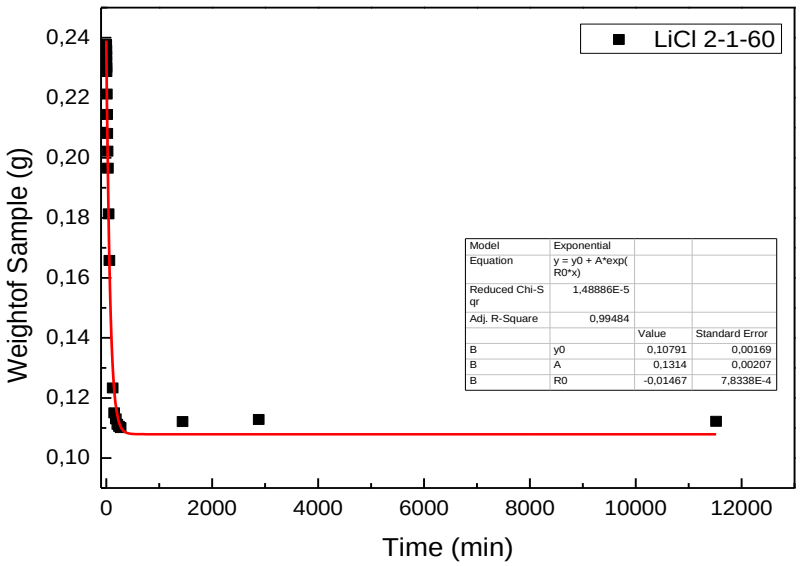

Figure 4.14. Weight measurement for the sample with 2-1-60 mole ratio over time.

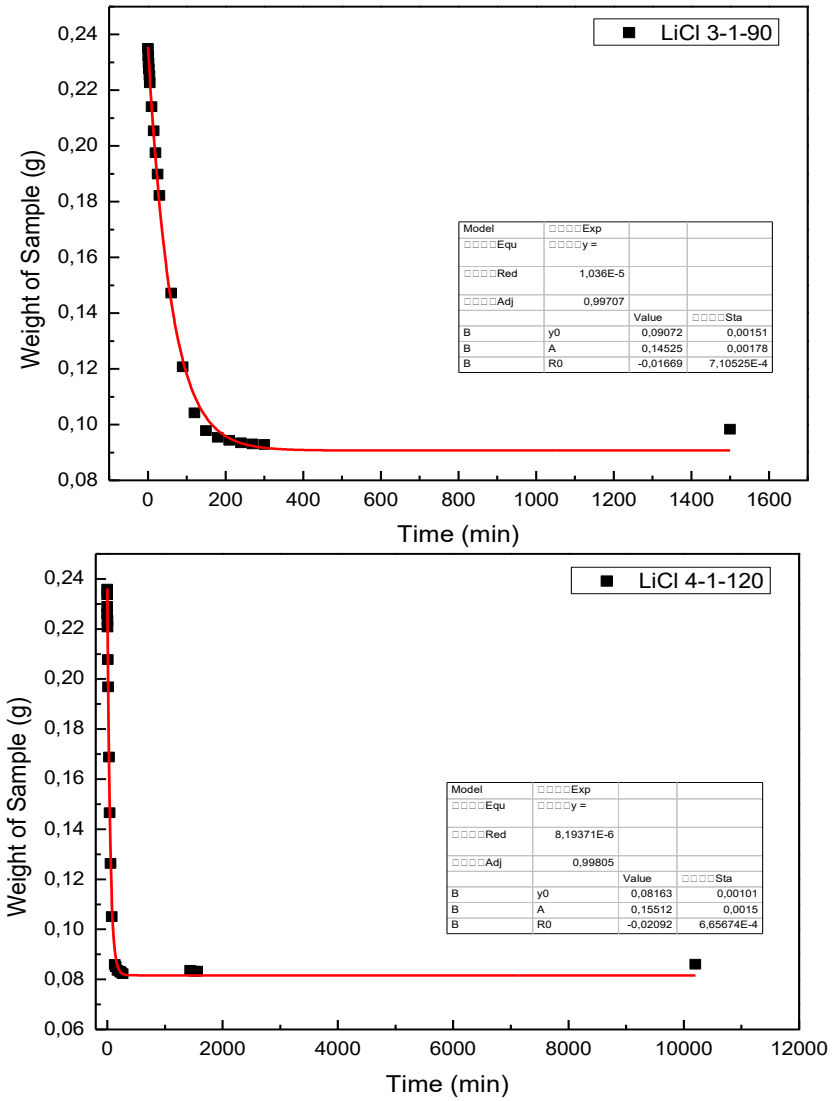

Figure 4.15. Weight measurements for the samples with 3-1-90 (top) and 4-1-120 (bottom) mole ratios.

4.1.2. Characterization of LiI - $C_{12}EO_{10}$ - Water LLC Mesophases

The LiI-$C_{12}EO_{10}$ samples were prepared with the required amount of LiI salts, 1.0 grams of $C_{12}EO_{10}$ and different amounts of distilled water, **see Table 3.2**. The mole ratios of salt/surfactant were always 2 or 3 in this investigation, because of the fact that these ratios form an hexagonal LLC mesophases, and at higher salt content mesocrystallization is unavoidable.[127] The samples had gel-like look with high viscosity, just like LiCl samples, **Figure 4.16**.

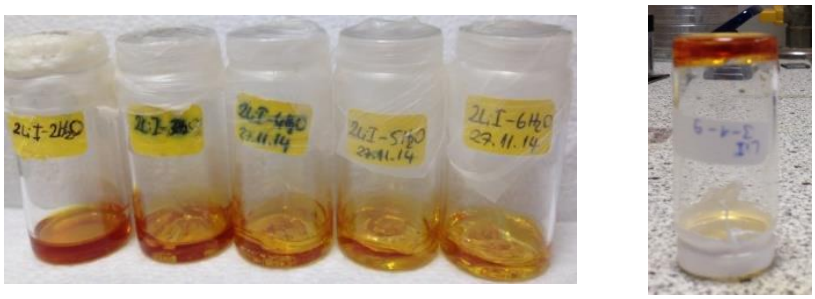

Figure 4.16. The photos of highly viscous liquid crystalline 2 LiI (left) and 3 LiI (right) samples.

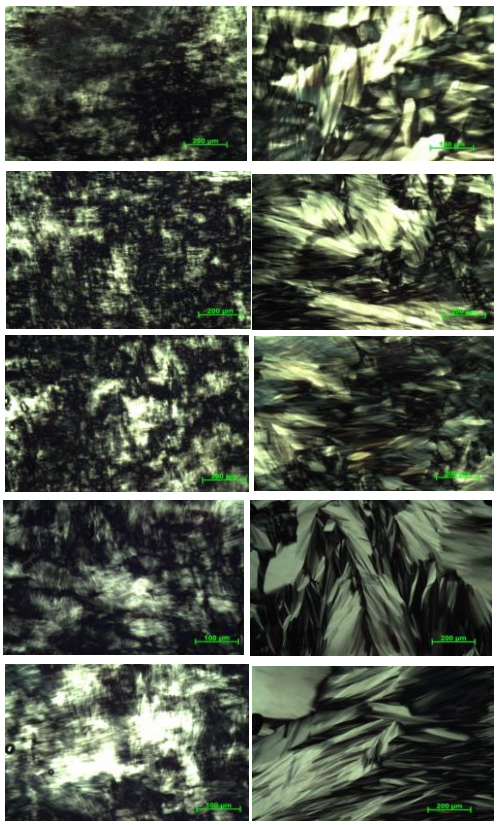

Figure 4.17. The POM images of 2 LiI with 2,3,4,5, and 6 mole ratios of water from top to bottom, respectively. The images on the left side belong to the fresh samples, and the images on the right side belong to the 3 days aged samples.

In the 2 LiI mole ratio, the samples were also prepared using different amounts of water, such as 2, 3, 4, 5, and 6 mole ratios with respect to the surfactant. They all formed the hexagonal LLC mesophases after water adsorption from the atmosphere; however, when the samples were covered with glass slides to prevent water exchange, they seem to be disordered. But over time, the samples became ordered. (see **Figure 4.17**).

From the XRD patterns of the LiI-$C_{12}EO_{10}$-water LLC samples, it can be predicted that they are all in hexagonal mesophases (see **Figure 4.18**). The hexagonal mesophase displays a characteristic line in the XRD pattern at around two theta = 2°, which corresponds to the (100) plane. There is a slight shift to wider angles with increasing water content that the unit cell of the samples decreases with increasing water amount in the samples.

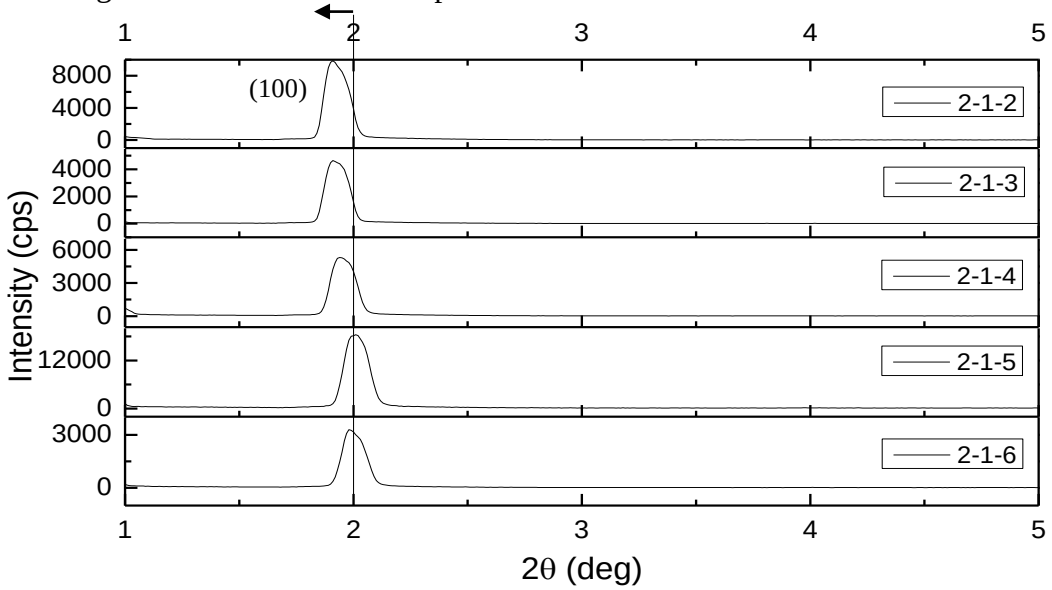

Figure 4.18. The XRD patterns for fresh LiI samples with different amounts of water.

The calculated d spacings are 46.2, 46.2, 45.7, 43.9, and 44.6 Å from top to the bottom in **Figure 4.18**. Also the *a* parameter of the unit cells are calculated to be 53.4, 53.4, 52.8, 50.7, and 51.5 Å again from top to the bottom, respectively.

However the XRD patterns of the aged samples (1 week) were all recorded again and found out that the unit cell parameters became the same. All aged samples adsorbed/desorbed water until some particular amount. Thus, they had all similar unit cell parameters at the end; the unit cell parameter *a* is 52 Å. When they are compared within the same ratio over time, it is clear that the line shifts from higher angle to lower angle, indicating that unit cell of them becomes bigger (see **Figure 4.19**).

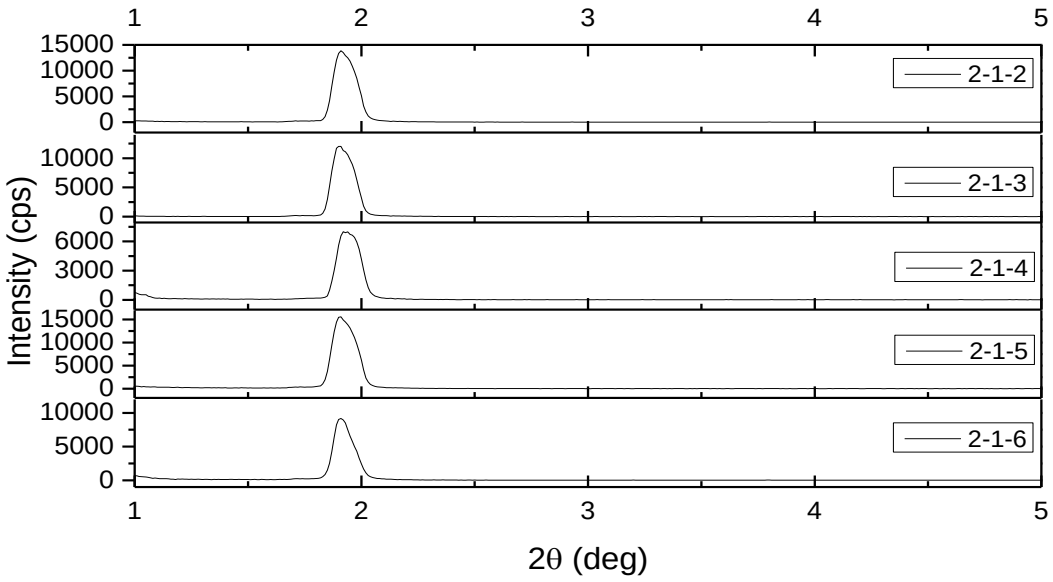

Figure 4.19. The XRD patterns of 2 mole ratio of LiI samples with different water content after 1 week.

From the ATR-FTIR results, it can be concluded that all the samples keep the water when they were measured with a glass cover, as fresh; however if they were exposed to atmosphere, over time, the water amounts reach to a specific mole ratio. This behavior is the same in the LiCl-$C_{12}EO_{10}$ mesophases (see **Figure 4.20** and **Figure 4.21**).

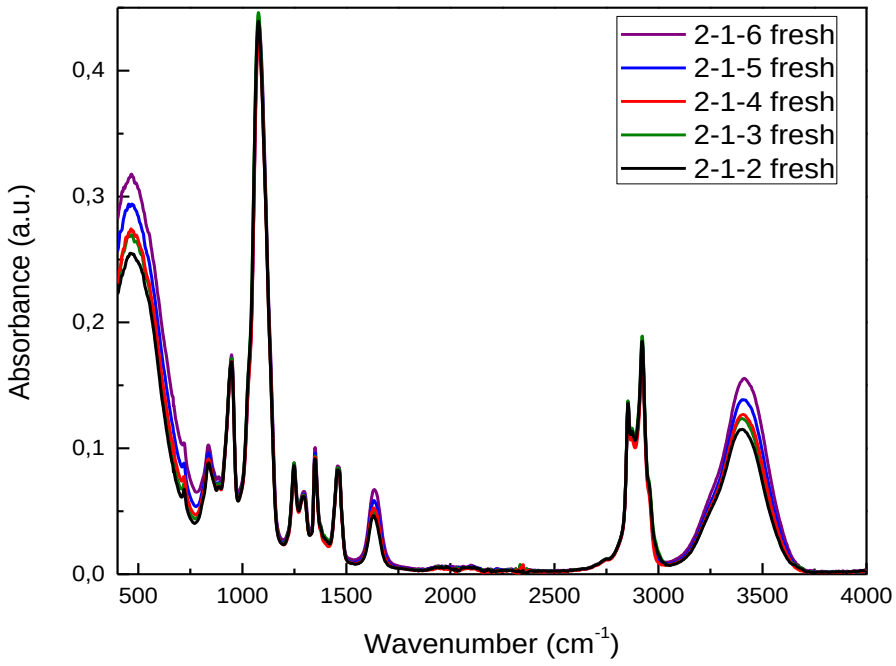

Figure 4.20. The ATR-FTIR spectra of fresh 2 LiI samples with different water content.

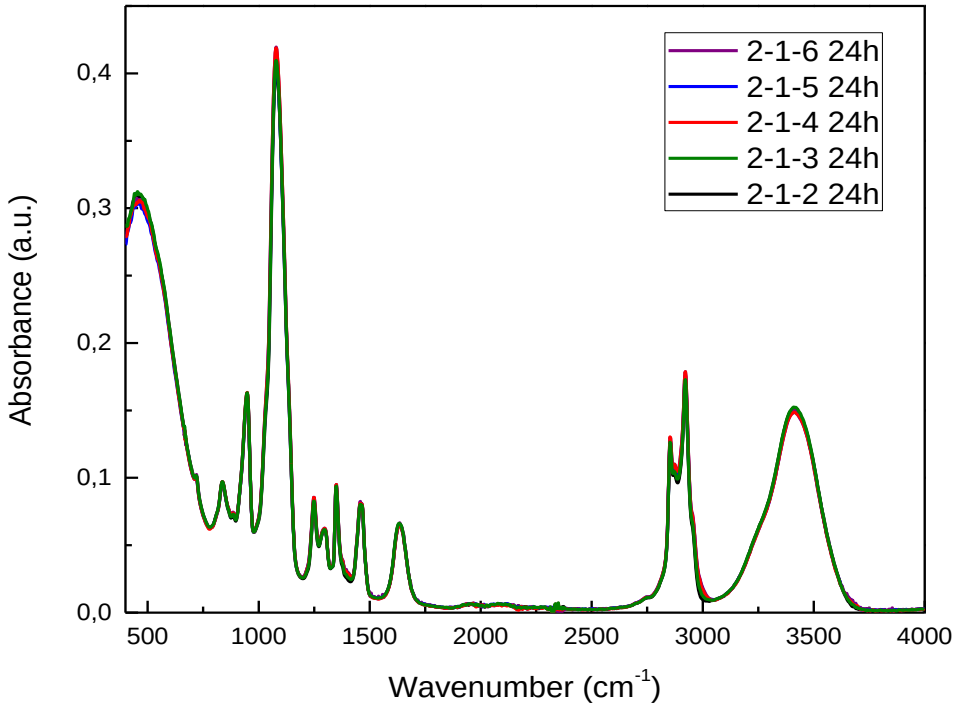

Figure 4.21. The ATR-FTIR spectra for all LiI samples in **Figure 4.20** after 24 hours.

If the ATR-FTIR spectra of 2-1-6 ratio sample are examined as an example, it is found out that the amount of water is not changed over time (**Figure 4.22**); whereas the other samples adsorbed water from the atmosphere. In other words, the equilibrium for the LiI salt is achieved at around 6 water per 2 LiI salt (3 H_2O/LiI) as in the case of LiCl.

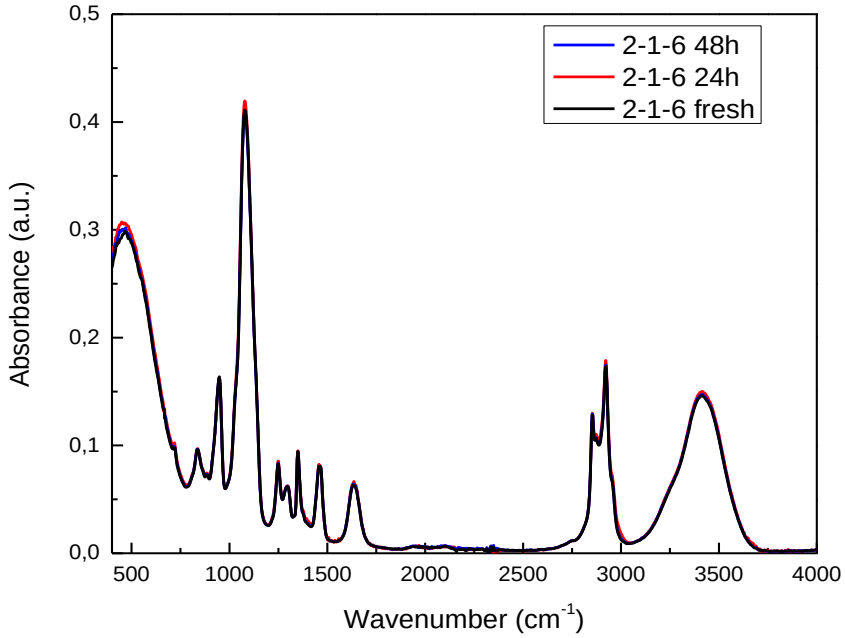

Figure 4.22. The ATR-FTIR spectra of the sample with 2-1-6 ratio over time.

The 3 mole ratio of the salt to surfactant has also been tested. Note also that the 4 and 5 LiI samples undergo mesocrystallization.[127] The 3 mole ratio LiI-$C_{12}EO_{10}$ sample forms highly viscous hexagonal mesophase in the presence of very little amount of water.

The **Figure 4.23** shows the POM images of 3 LiI samples over time. They usually display no texture as they were spread onto the glasses; however when they interact with the atmosphere, by adsorbing or releasing water, the characteristic fan-texture of the 2D hexagonal mesophases appear under the POM. Even the sample with 3-1-3 mole ratio exhibit the fan texture after some time. Moreover, these samples displayed the same fan texture upon examining after almost a year.

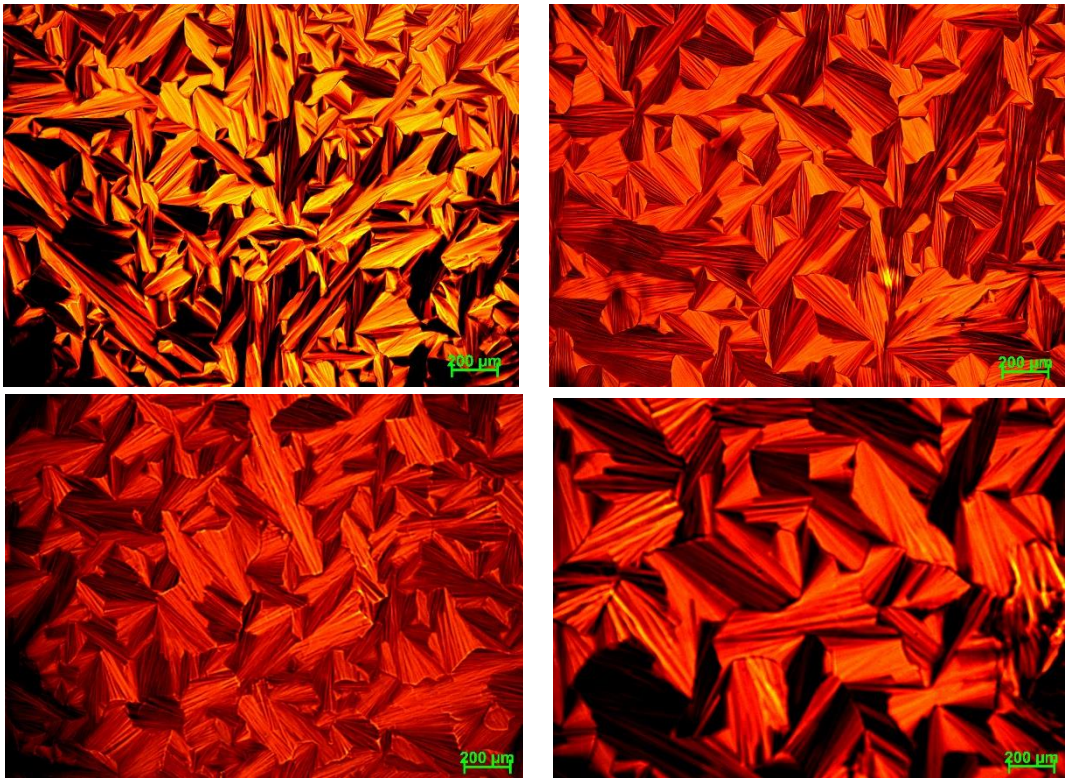

Figure 4.23. The POM images of 3 LiI sample with 3 (top, left), 4.5 (top, right), 6 (bottom, left), and 9 (bottom, right) mole ratios of water closed with a glass (left) and open to the air (right).

The XRD patterns of these gels display slight changes with a characteristic line at around 2°, two theta that can be assigned to (100) plane of 2D hexagonal phase. The unit cell size changes slightly if the water amount is changed. The XRD pattern of fresh sample with more water display the diffraction line at smaller angle than that of the sample with less water. The trend is the opposite of the LiCl-

$C_{12}EO_{10}$ samples. The d-spacing is calculated to be 46 Å. For the higher ratios of water in the same system; the trend seems to be similar. The unit cell of the sample with 18 mole ratio of water is bigger; the samples with 9 and 12 mole ratios of water are almost exactly the same with each other, and are smaller than that of 18 (see **Figure 4.25**).

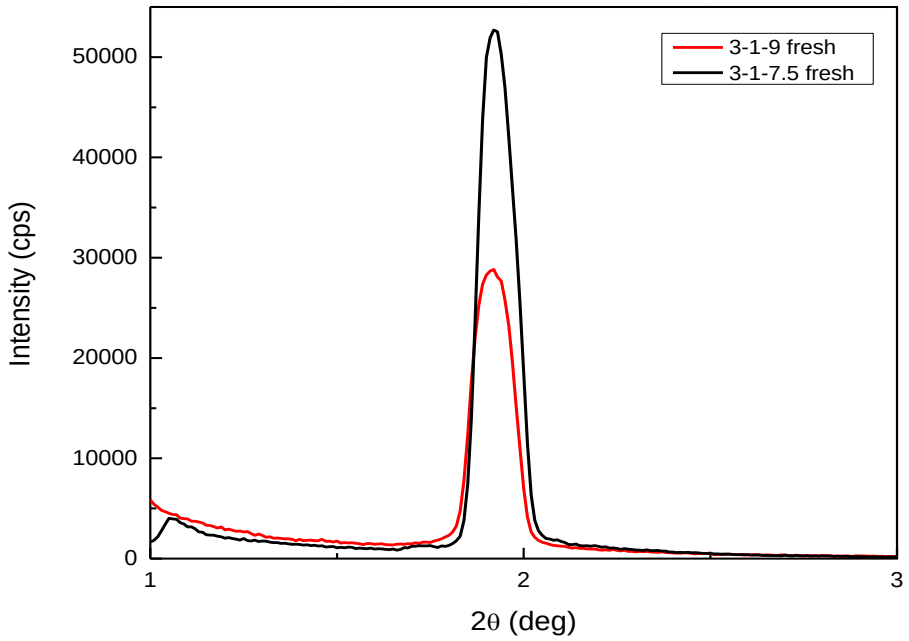

Figure 4.24. The XRD pattern for comparison between 9 and 7.5 mole ratios of water in 3 LiI salt system.

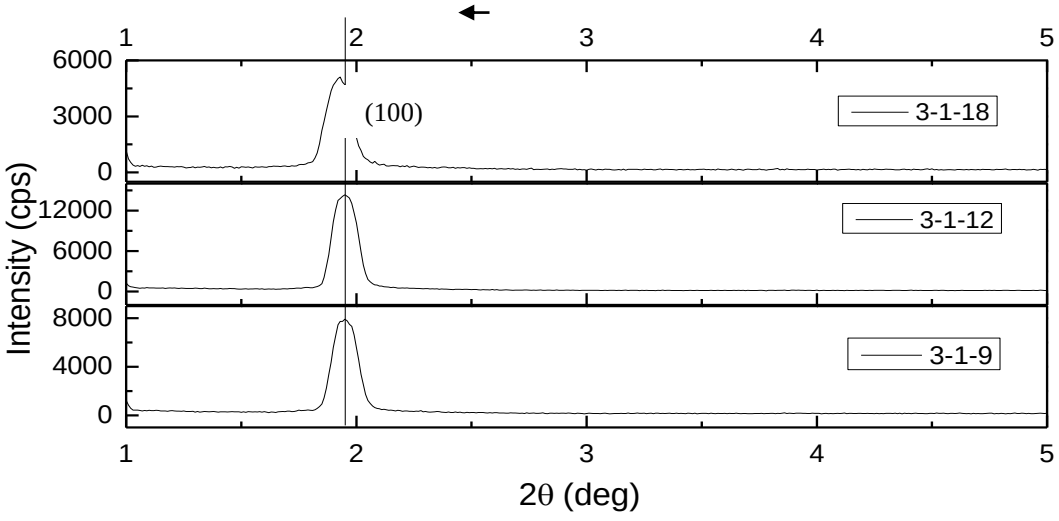

Figure 4.25. The XRD pattern for higher amount of water in 3 LiI salt system.

Also, the ATR-FTIR spectra of the fresh LiI samples were collected by covering them with a glass. Besides from the fresh samples, also 3-1-9 ratio of LiI was measured over time; thus, the stability and hydration water amount of the sample were examined. It is clearly visible from these data that the specific mole ratio of water for the 3 LiI is a little bit less than 9, due to the fact that when 9 mole ratio is examined over time, the sample evaporates some of its water and then it becomes stable.

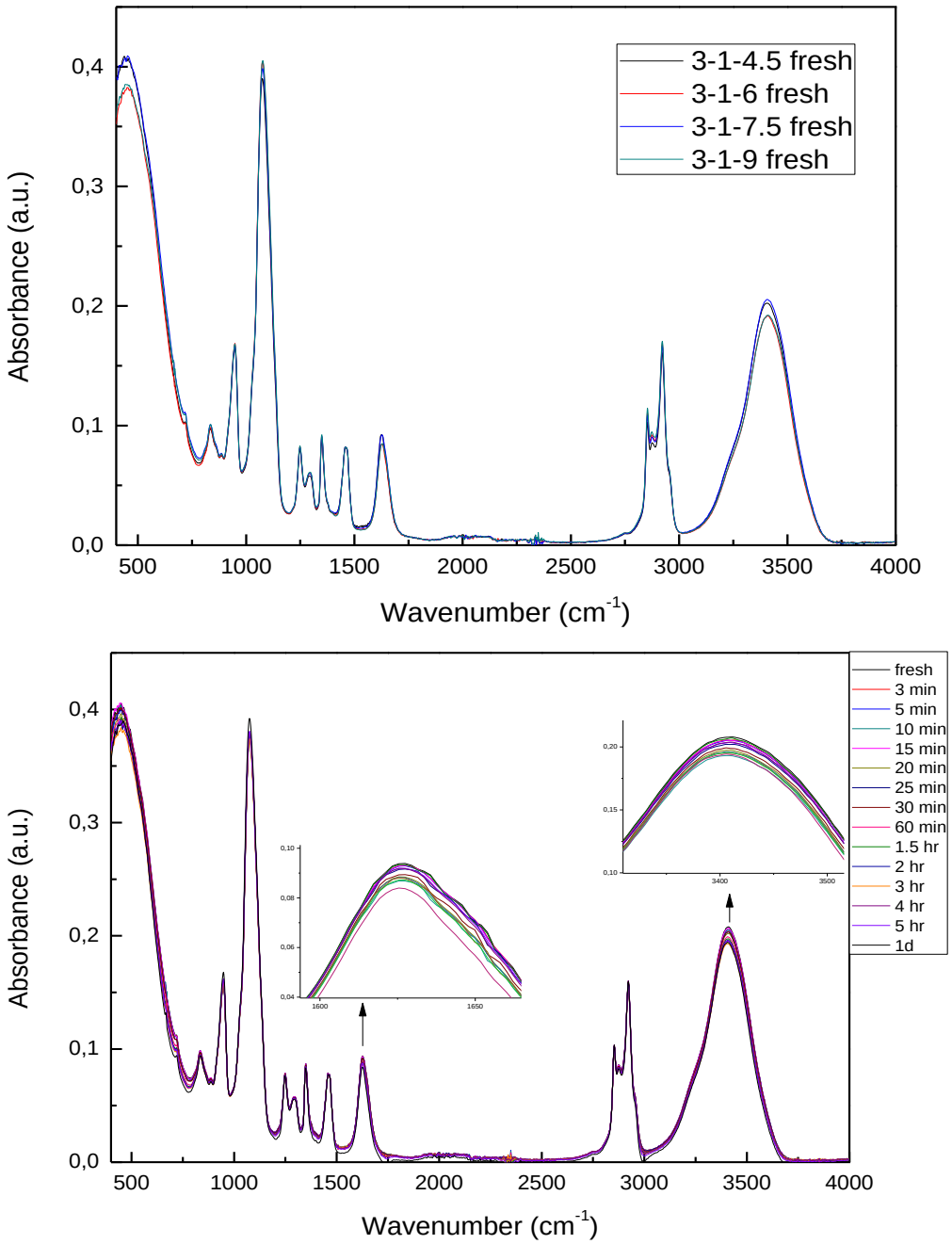

Figure 4.26. The ATR-FTIR spectra for all fresh LiI samples with different water amount (top) and for sample with 3-1-9 mole ratio over time (bottom).

Notice that it is really difficult to determine of the amount of the hydration water, since the samples adsorb or release the water in a very fast manner. Some of samples lose the water faster than others. This situation makes hard to detect the water amount in the 3 LiI system. However, from all these ATR-FTIR results, it can be concluded that, just like 2 LiI system, the hydration water mole ratio per LiI salt is a little bit less than 3, since there are really small changes in the sample with 3-1-9 ratio, as mentioned above.

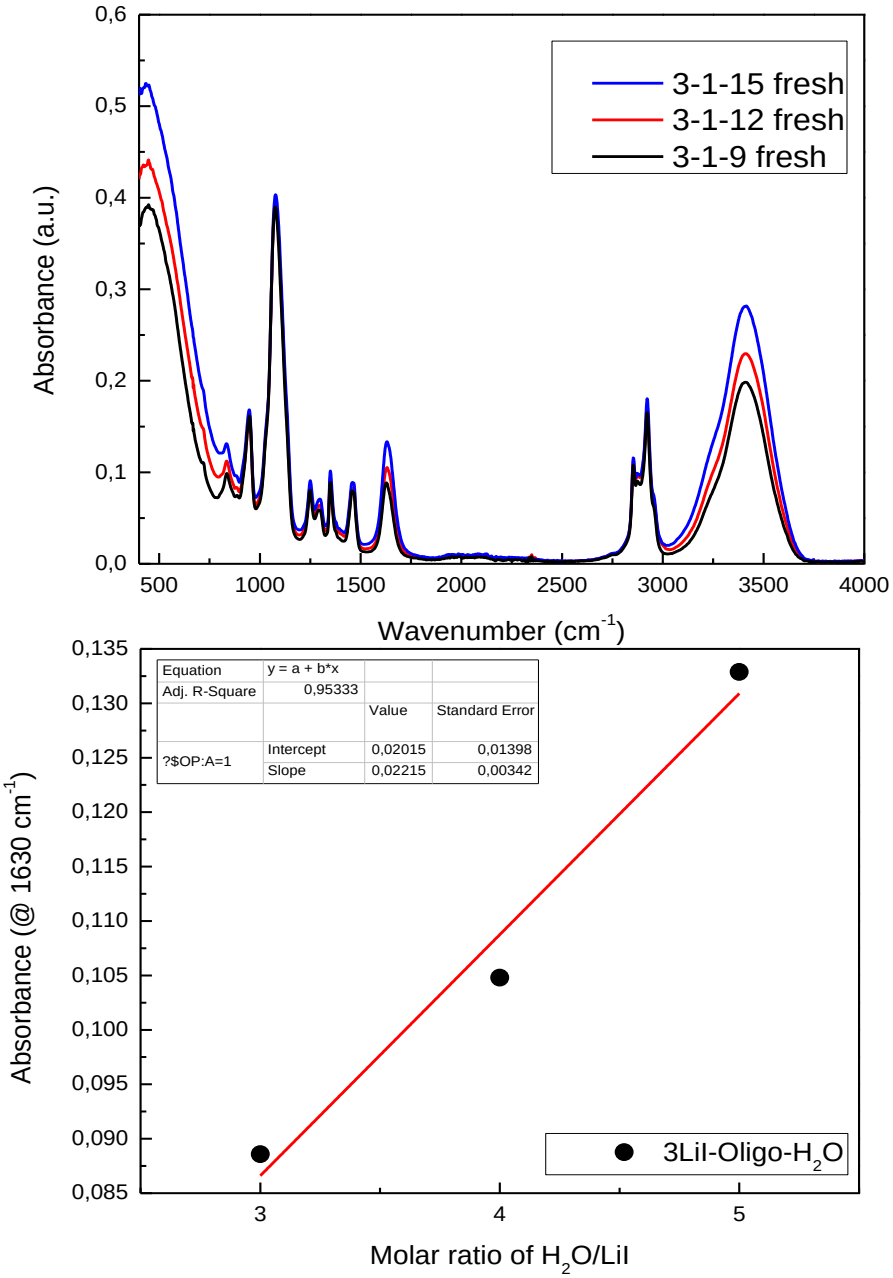

Figure 4.27. The ATR-FTIR spectra for the 3 LiI samples with higher water content (top) and the calibration curve for them (bottom).

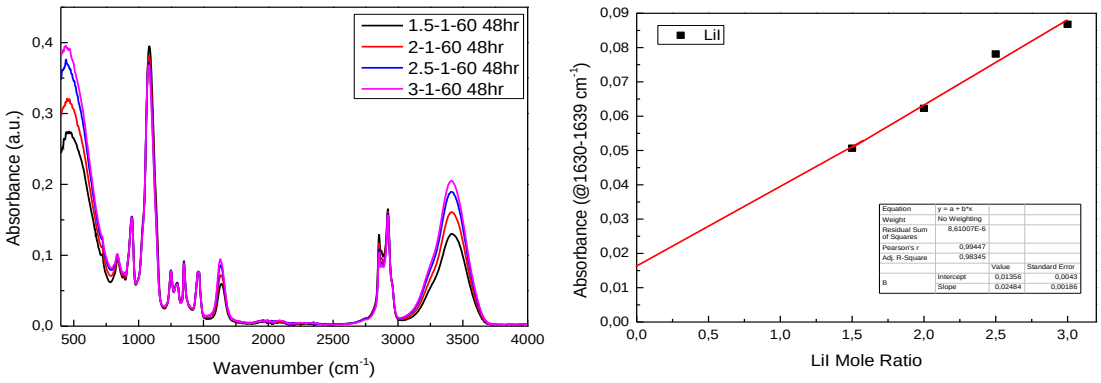

Figure 4.28. The ATR-FTIR spectra with different mole ratios of LiI with 60 mole ratio of water (left), and the calibration curve obtained from it (right).

Both the ATR-FTIR spectra and calibration curve are shown for LiI samples with different mole ratios of LiI salt to evaluate the effect of the LiI salt on the hydration water amount in **Figure 4.28**. It is clear from the spectral data that there is a linear correlation between the amount of LiI and the hydration water. However, it is also noticed that the water bending mode shifts from 1639 to 1630 cm^{-1} when the amount of LiI is increased. To compare it with LiCl, in the case of LiCl the water peaks is observed at around 1645 cm^{-1} that corresponds to the free water; however, in the case of LiI, the water peak is observed between 1639 and 1630 cm^{-1}, which can be considered to be belongs to the hydration water, see **Figure 4.29**.

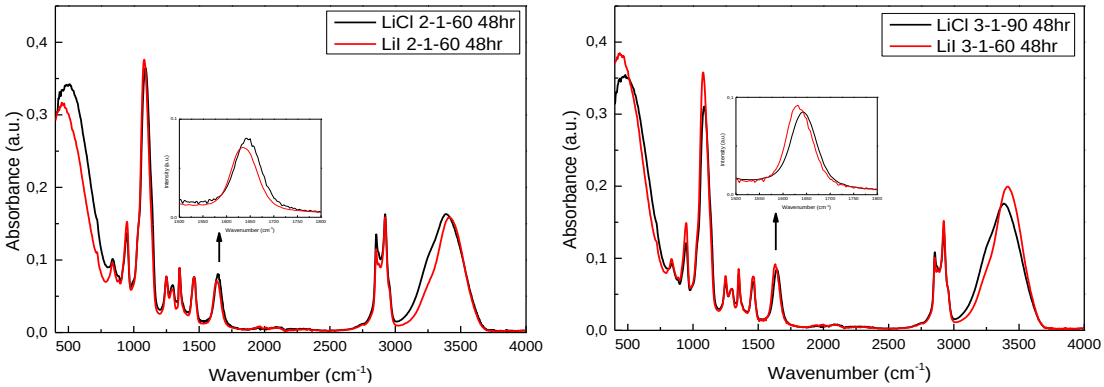

Figure 4.29. The ATR-FTIR spectra for LiCl and LiI samples to see the shifting in water bending mode frequencies.

This shift is probably caused by the difference in the structure of water which is kept by the mesostructure. In the case of LiCl, the water is more likely to be free water, and in the case of the LiI it is more likely to be hydration water.

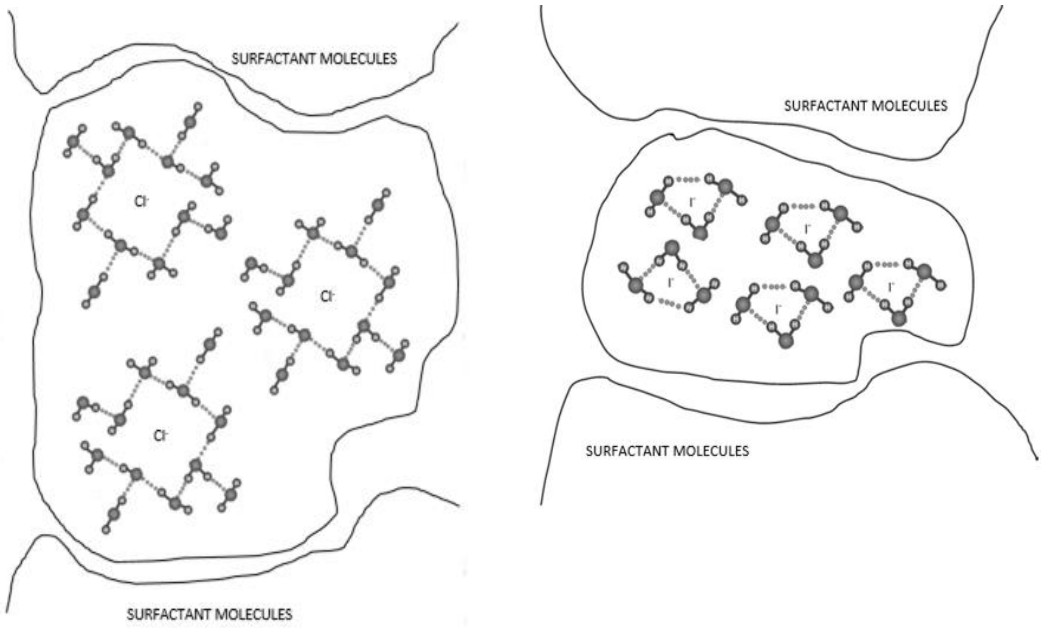

Figure 4.30. A schematic representation of the local structures of water and LiCl (left) and LiI (right) samples.

Due to the fact that the LiI and LiCl have different influences on the structures of water in the mesophase that are schematically shown in **Figure 4.30**. In the case of LiCl, the water molecules keep their structure but in case of LiI, the water molecules are around the Li^+ and I^- ions (see **Figure 4.30**). That is why there is a stronger interaction between the ions and water in the case of LiI, and this is the possible reason for the shift on the bending mode of water in the ATR-FTIR spectra. Another possible reason of the shift could be the mesocrystallization of the LiI-H_2O-$C_{12}EO_{10}$ mesophases. Upon mesocrystal formation, the frequency of the bending mode of water shift from 1630 to 1602 cm^{-1}. For the liquid form, the water peaks is at around 1645 cm^{-1}, and shifts to 1630 cm^{-1} upon mesophase formation. Note that LiI mesophase is known to form mesocrystals when high amount of salt is used; thus, when the amount of LiI is increased the water peak shifts to lower frequencies (see **Figure 4.29**).

To support the ATR-FTIR results, the weight lost measurements were also done for the samples with different mole ratios of LiI with excess water, as in the case of LiCl samples. The weight lost measurements have given somewhat a different result. For the 2-1-60 LiI sample, upon complete evaporation of excess water, the water amount is calculated to be 2.34 H_2O/LiI, whereas in the 3-1-60 LiI sample it is 3.15 H_2O/LiI (see **Figure 4.31**). The hydration water amount correlates

with the ATR-FTIR results, since it was found that the amount of water is between 2 and 3 mole ratio per salt. The slight change from 3 mole ratio of water per salt is caused by the difficulty of measuring the exact amount of water with the ATR-FTIR when gel samples were used. Notice that the previous ATR-FTIR spectra were collected from the gel samples; therefore it can be concluded that during the course of preparation of the gel samples, the evaporation or release of water is unavoidable. That is why, the weight lost measurements may give a more accurate result in terms of determination of hydration water amount in the samples.

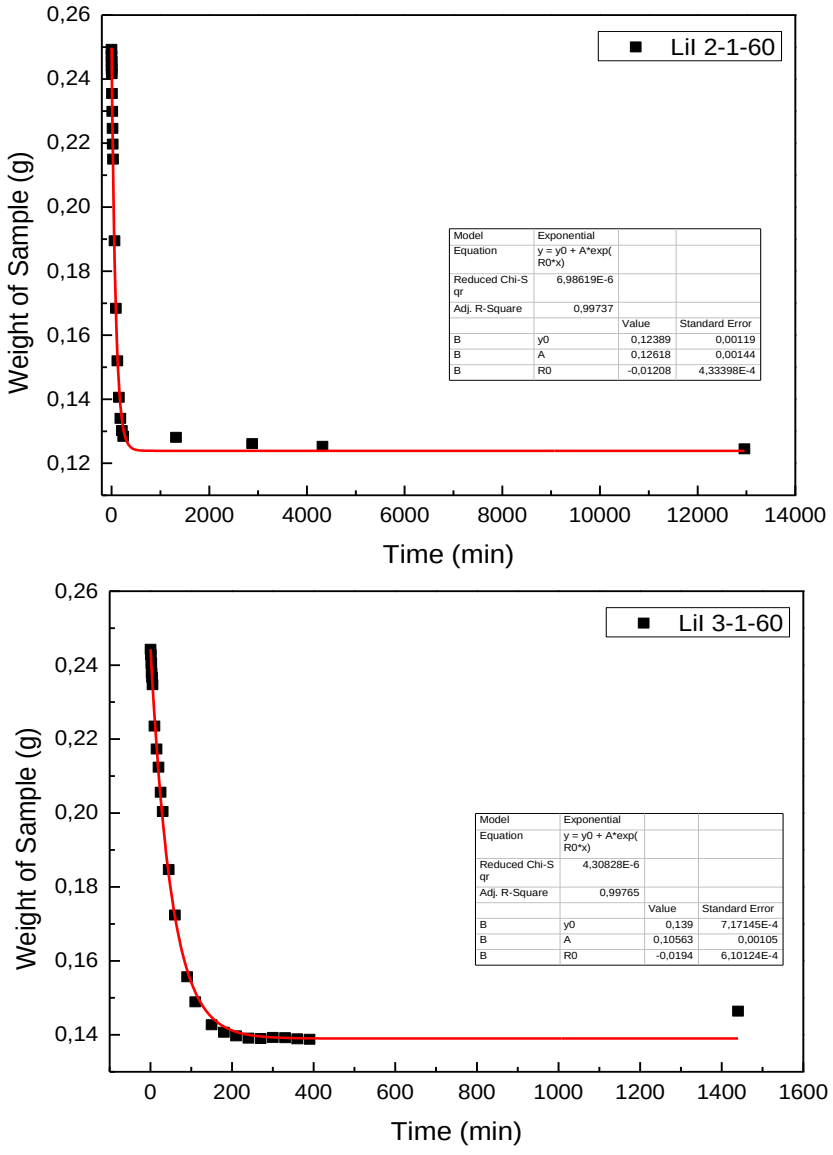

Figure 4.31. Weight measurements for the LiI samples with 2-1-60 (top) and 3-1-90 (bottom) mole ratios.

4.1.3. Summary of Lithium Salts-Surfactant Systems

Aqueous media is always considered to have a negative effect and it is not desired as electrolytes in electrochemical systems. However, here it is demonstrated that the water is needed for the formation of the LLC mesophases and have a positive effect. Unwanted water molecules are free water molecules. As long as the water molecules are part of the mesostructure, they are useful and actually they are needed for the stabilization of the mesostructure. The water molecules in the salt-surfactant mesophases are the hydration water molecules and necessary for the mesophases. Even if there is less or more water than needed for a stable mesostructure, the sample adsorbs or desorbs the water by the interaction with the atmosphere until a constant and fixed amount of water. For the LiCl salt, the hydration water amount is 3 H_2O/salt; for 2 LiI system, it is around 3 H_2O/salt, and for 3 LiI system it is a little bit less than 3 H_2O/salt according to the ATR-FTIR results in the gel samples. However, when the samples were prepared with excess water and followed by weight lost (using a sensitive balance), the amount of hydration water is slightly different than the ATR-FTIR results. This is acceptable, because of the difficulty of the preparation and the measurement of the gel samples. Remember that the gel samples absorb or release the water during the preparation step. That is why; it may not be accurately measured. Also, in the case of the LiCl samples, the water bending peak at around 1645 cm^{-1}, which means that there is a network of water molecules in the LLC media; while in the case of LiI samples, this peak shifts to 1630 cm^{-1}, due to the fact that it has the hydration water molecules rather than a water network. Also the shift can be due to the formation of mesocrystals in the LiI samples. The complex behavior of LiI can be caused by the complex chemistry of I^- ion in the media. The LiCl salt is known to form hexagonal LLC mesophases from 2 to 10 mole ratio of salt/$C_{12}EO_{10}$, over a broad range; however, LiI salts start to form mesocrystals even when they are as low as 4 or 5 salt/surfactant mole ratio. This may also be the reason for the different behavior of the LiI mesophases. These behaviors will be investigated further in the future.

4.2. LLC Mesophases of LiI – I_2 – $C_{12}EO_{10}$ – Water Systems

The LLC mesophases of LiI-I_2 can also be prepared in the presence of very little amount of water. When I_2 is added into the LiI-$C_{12}EO_{10}$-H_2O system, it changes the conductivity, structure and many other properties. The samples were prepared as described in **Table 3.3**. The mixtures were put into a shaking bath at 80 °C for 24 hours, and resulting products are in the gel form. Shaking and heating are required to homogenize the mixture, since these samples were prepared using a very little amount of water. A set of samples with different ratios of LiI:I_2 and one $C_{12}EO_{10}$ were prepared as described above (such as 1-0.1, 1-0.2, 2-0.2, 2-0.3, 3-0.2, 3-0.3, 4-0.4, 5-0.5). Note that the homogenization took longer time with decreasing the water amount in the samples. For instance, in the 2-0.2 ratio of LiI-I_2, if the H_2O/LiI mole ratio is 2, 72 hours in heat bath treatment is needed until it became homogeneous.

The sample with 1-0.2 (LiI-I_2) mole ratio is less viscous than the sample with 2-0.2 ratio, proving that it is the mesophase that determines the viscosity. The sample with 10 H_2O/LiI, and if the LiI/$C_{12}EO_{10}$ mole ratio is 1, it becomes homogeneous in 1 day, but if it is 2 mole ratio of LiI, the homogenization of the sample takes 3 days at 80 °C in heat bath.

Usually, the samples with little amount of water exhibit disordered structures and dark under the polarized optical microscope. However, as in the case of LiCl and LiI systems, the LiI-I_2 samples also interact with the atmosphere, adsorb water and form 2D hexagonal structures. The gels were generally prepared using 0.23 g of water, corresponding to 8 water molecules per surfactant. However; to see the difference, we also prepared samples with even lower amounts of water.

The 1-0.1 ratio of LiI-I_2 samples were prepared with 1, 2, 3, and 4 mole ratios of water. All samples show fluidic behavior instead of showing high viscosity. They exhibit no structure under the POM, however they diffract a broad line at small angles likely due to a bicontinuous cubic phase, which is optically isotropic (see **Figure 4.32**). Those samples display a characteristic line corresponding to the (200) plane at around 1.83^o, two theta, corresponding to a d spacing of 48 Å.

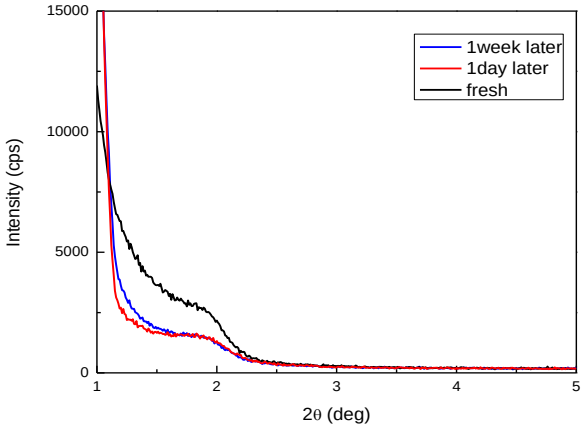

Figure 4.32. The XRD pattern of the sample with 1-0.1 ratio LiI-I_2 with a 2 mole ratio of water.

Bicontinuous cubic phase of 1-0.1 gel samples were also examined using the ATR-FTIR spectroscopy. Also a sample with 60 mole ratio of water was prepared. After 24 hours of evaporation of the excess water, in other words when the sample became stable, we found out that the mole ratio of water in the 1-0.1 gel sample lies between 2 and 3 per LiI salt (see **Figure 4.33**). However, the intensity trend could be misleading and cannot be directly translated into the amount of water, because sample with 1 and 2 water already absorbed some water and sample 3 lost some water, see inset in **Figure 4.33**.

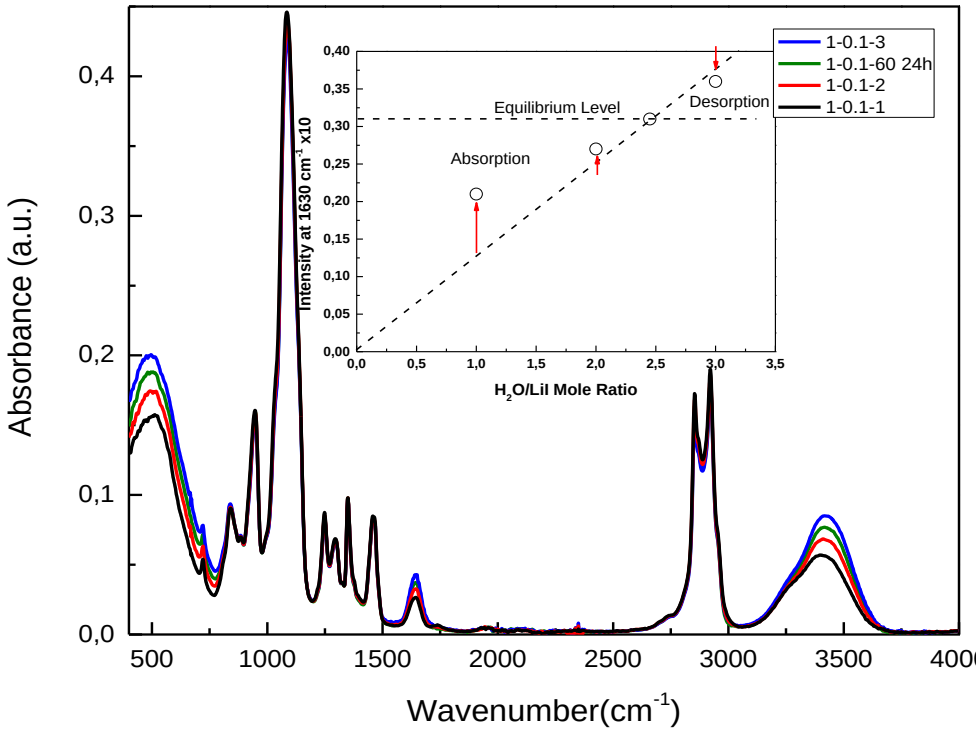

Figure 4.33. The ATR-FTIR spectra for 1-0.1 gel samples with the mole ratio of water 1, 2, 3, and 60.

The 2-0.2 LiI-I_2 samples were also prepared using 2, 4, 6, 8, and 60 water/surfactant. The one with 2 mole ratio of water became homogeneous after 72 hours in heat bath, all the other samples were homogeneous after 24 hours. It is because 2 mole ratio of water is really low for dissolving the 2 LiI salt. Also, all samples were highly viscous on the contrary to 1-0.1 gels (see **Figure 4.34**).

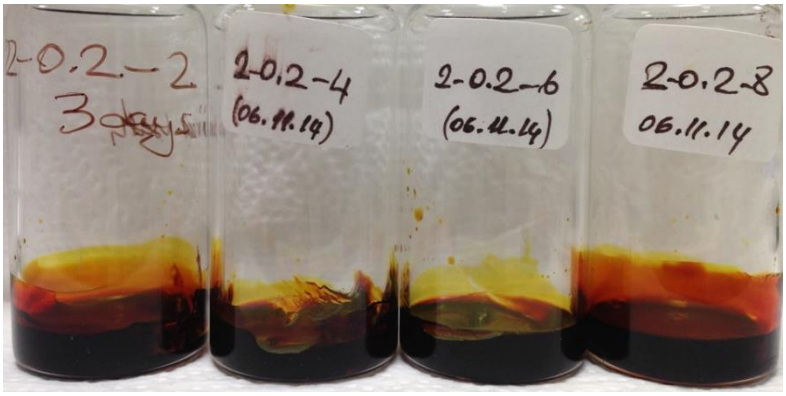

Figure 4.34. The photos of the 2-0.2 gel samples with different amount of water (left to right 2, 4, 6, and 8).

The 2-0.2 LiI-I_2 gel samples form 2D hexagonal mesophases. All of them exhibits a fan-texture under the POM. They have disordered structure at first, however upon exposing the sample to atmospheric water; the 2D hexagonal structure forms after some time (see **Figure 4.35**). Also the XRD pattern displays a characteristic line corresponding to the (100) plane at around 2 degrees, indicating that they form 2D hexagonal structure. After 1 week, the samples still diffract the characteristic lines at small angles, indicating that they are very stable (see **Figure 4.36**).

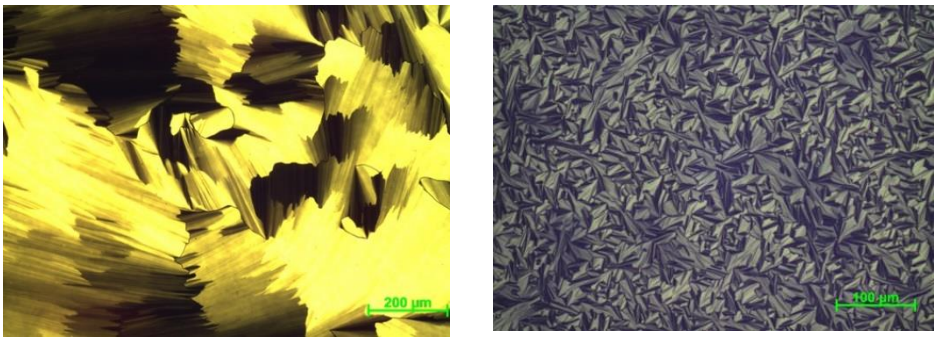

Figure 4.35. The POM images of the 2-0.2 gel with 4 mole ratio of water after 2 days (left), and 2-0.2-60 sample after spin coating and evaporating all excess water (right).

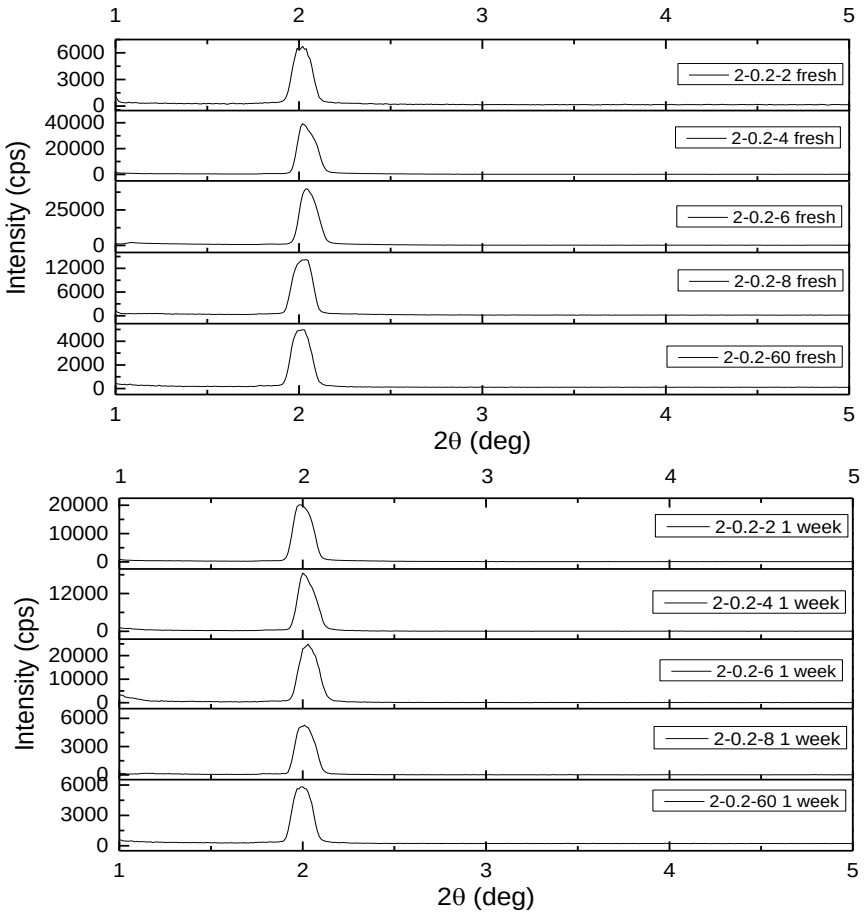

Figure 4.36. The XRD patterns of fresh (top) and 1 week aged (bottom) 2-0.2 samples with different mole ratios of water.

A sample with 2-0.2-60 (LiI-I_2-H_2O) mole ratios was also prepared to determine the water amount that this sample can keep. The ATR-FTIR spectrum after 24 hours shows that the mole ratio of water for the 2-0.2 gel lies between 4 and 6. In other words, the hydration water for 2-0.2 gels is between 2 and 3 mole ratio per 1 LiI salt and correlates with the previous results (see **Figure 4.37**).

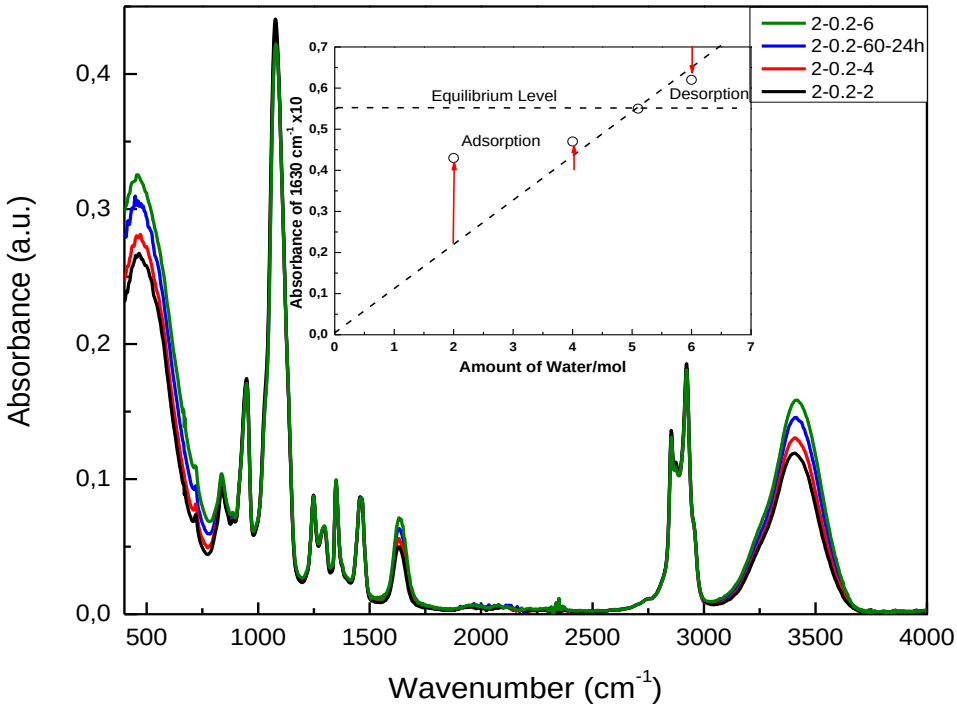

Figure 4.37. The ATR-FTIR spectra for the examination of hydration water amount for 2-0.2 gels.

To determine the amount of hydration water in the 2-0.2 samples, the sample with mole ratios of 2-0.2-60 was also followed using a sensitive 4 digit balance over time. Using the weight lost data, a calibration curve was constructed by plotting the weight of the sample versus time. In this context, it is seen that when the sample is fresh there is 60 mole ratio of water, however after 7 days there is about 5.2 water left per 2 LiI salts; it lost about 90 % of its water content. In other words it is 2.6 mole ratio of water per one LiI salt, which verifies the ATR-FTIR results (see **Figure 4.38**).

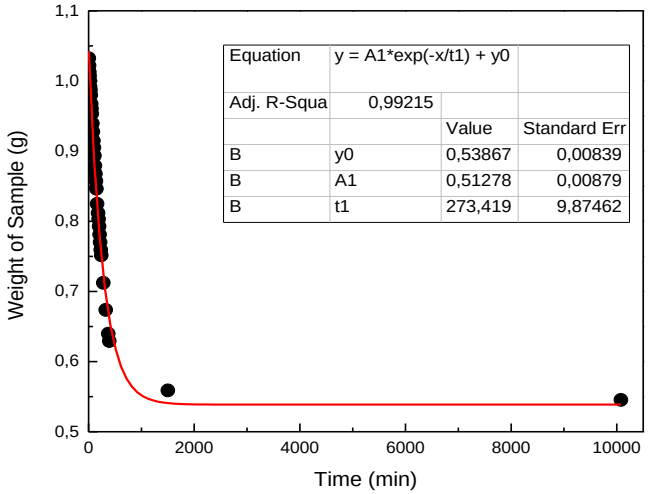

Figure 4.38. The change in water amount in the 2-0.2-60 sample over time, determined using a 4 digit balance.

To further understand the water release process, a sample with 2-0.2-60 mole ratio was prepared using D_2O, instead of H_2O. The main purpose here is to determine how much water is absorbed by the sample. The stretching modes of D_2O and H_2O are observed at around 2500 and 3500 cm^{-1}, respectively. The ATR-FTIR spectrum of the fresh sample shows no water stretching or bending peaks. The peak at 3500 cm^{-1} is due to OH groups of the surfactant molecules. Over time, the intensity of D_2O peaks decrease while the intensity of H_2O peaks increase proportionally due to the exchange of D_2O with H_2O (see **Figure 4.39**). The process seems to take place simultaneously, while the D_2O is evaporating some amount of H_2O is being absorbed until all D_2O is desorbed from the media and H_2O reached to equilibrium value.

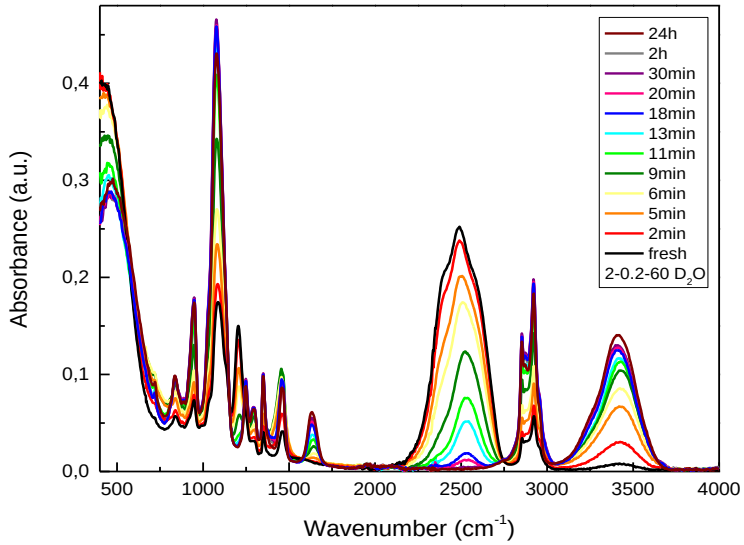

Figure 4.39. The ATR-FTIR spectra for the sample 2-0.2-60 mole ratio prepared using D_2O instead of H_2O.

The sample with 2-0.3 mole ratio is less viscous than 2-0.2 one, proving that I_2 amount is important for the viscosity of the samples. If the I_2 amount is more than 0.1 times of LiI, the gel becomes less viscous and it is fluidic. However, if the LiI/I_2 ratio is 10, or even higher, the sample exhibits always high viscosity.

To the samples of 3-0.3 $LiI-I_2$ mole ratio; 6, 9, 12, 15, and 90 mole ratios of water were added to prepare a set of samples to test the role of water. The one with 6 mole ratio of water does not form any fan-texture. All the other samples form 2D hexagonal mesophases with the characteristic fan-texture (see **Figure 4.40**). Also, they all give the characteristic line in their XRD patterns; both the fresh and 1 week old samples (see **Figure 4.41**) and the samples are stable for very long time.

Figure 4.40. The POM images of the samples with 3-0.3-9 (LiI-I_2-H_2O) mole ratios (left) and 3-0.3-90 mole ratios after spin coating and evaporating of all water (right).

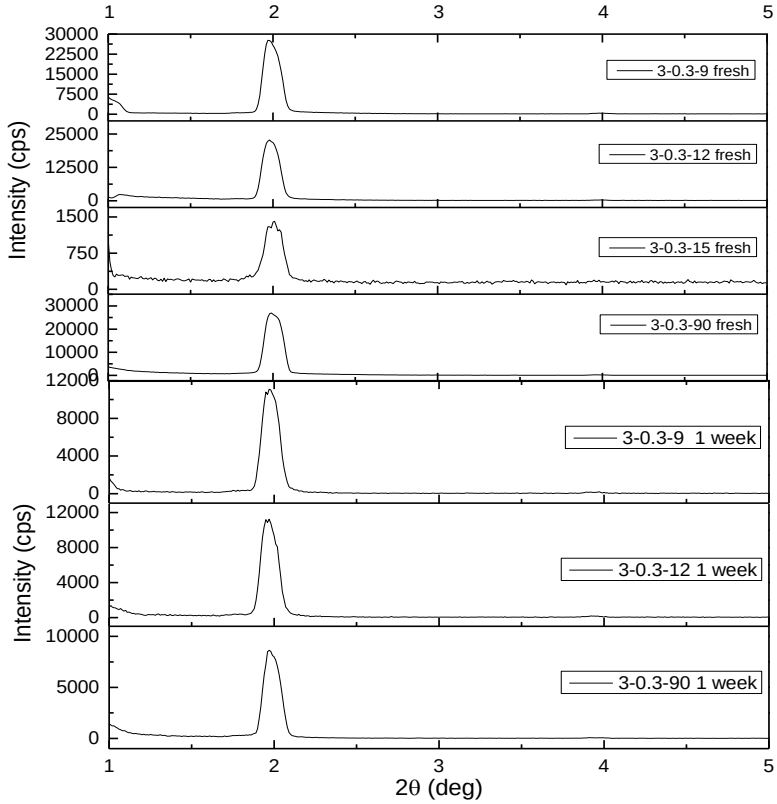

Figure 4.41. The XRD patterns for fresh 3-0.3 samples (top), and 1 week aged 3-0.3 samples (bottom) with different water content.

The ATR-FTIR spectral changes show that the 3-0.3-90 sample after 24 hours becomes stable in terms of exchange of water. In the stable sample, the water ratio drops to between 6 and 9 per 3 LiI. It means that the hydration water mole ratio is between 2 and 3 per one LiI salt. Thus, the water amount in the LiI-I_2 samples is the same as in the I_2 free samples (see **Figure 4.42**). In addition to the ATR-FTIR results, we also monitored the water release process using a 4 digit balance. The weight of the sample versus time plot is shown in **Figure 4.43**. The calculation using this plot shows that the water amount drops from 90 mole ratio

(in the fresh sample) to 9.3 by the end of fourth day; it corresponds to 3.1 water per LiI salt. The sample lost almost 90 % of its water content and became stable with only 10 % water, which is the hydration water in the structure (see **Figure 4.43**). These findings are also consistent with that obtained from the spectral data.

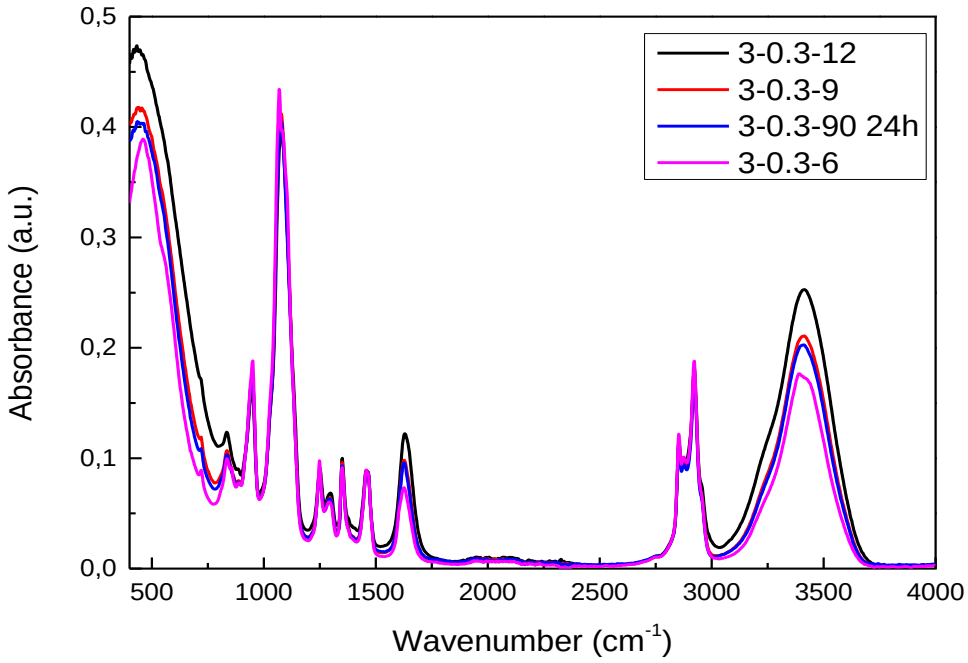

Figure 4.42. The ATR-FTIR spectra for the examination of hydration water amount for the 3-0.3 gels with various amount of water.

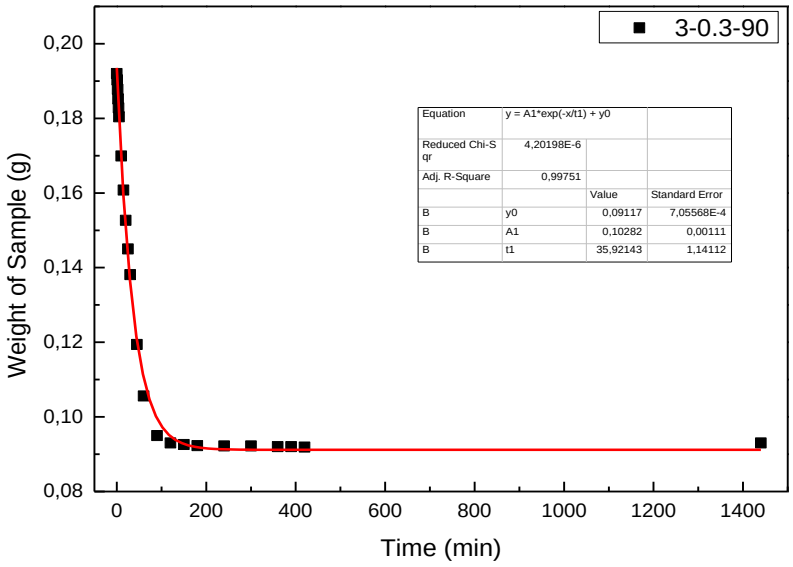

Figure 4.43. The change in the water amount in the 3-0.3-90 sample over time, determined using a 4 digit balance.

The 3LiI-0.2 I_2 sample is also highly viscous, and it is disordered for very long time, however it forms eventually a 2D hexagonal mesophase by absorbing ambient water. Here the important point is the amount of I_2, or the ratio between LiI and I_2. If the LiI/I_2 ratio is 10, the mesophase form sooner than the case of higher ratios.

The samples of 4-0.4 LiI-I_2 mole ratios to surfactant and 8, 12, 16, 20, and 60 mole ratios of water were also prepared. The ones with 8 and 12 mole ratios of water do not form the 2D hexagonal structure even after long time. However, from 16 and more water, the samples form the mesostructure upon exposing them to the atmosphere (see **Figure 4.44**). In the case of 8 and 12 waters, the samples also diffract at higher angles, which mean that they form mesocrystals (see **Figure 4.45**); however all other compositions give the characteristic diffraction line at around 2 degrees in their XRD patterns (see **Figure 4.46**).

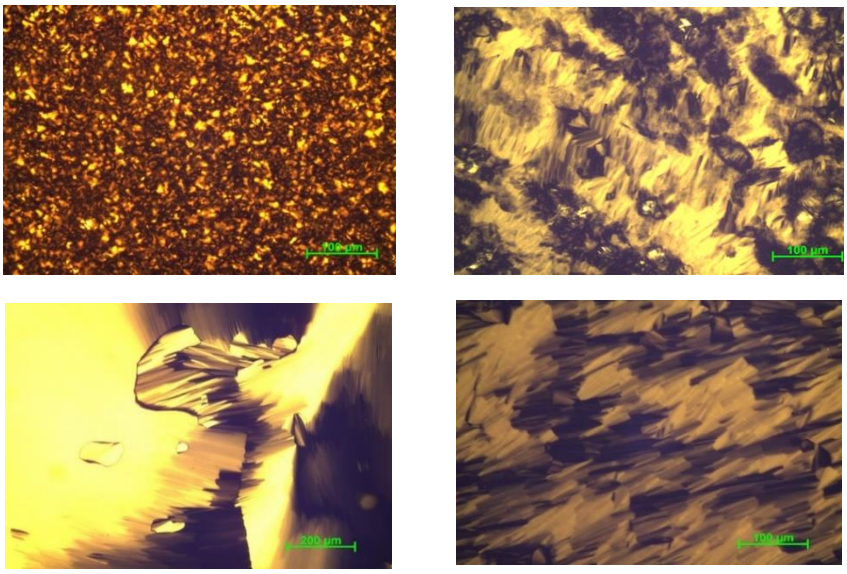

Figure 4.44. The POM images of 4-0.4-8 (top, left), 4-0.4-12 (top, right), 4-0.4-16 (bottom, left), and 4-0.4-24 samples.

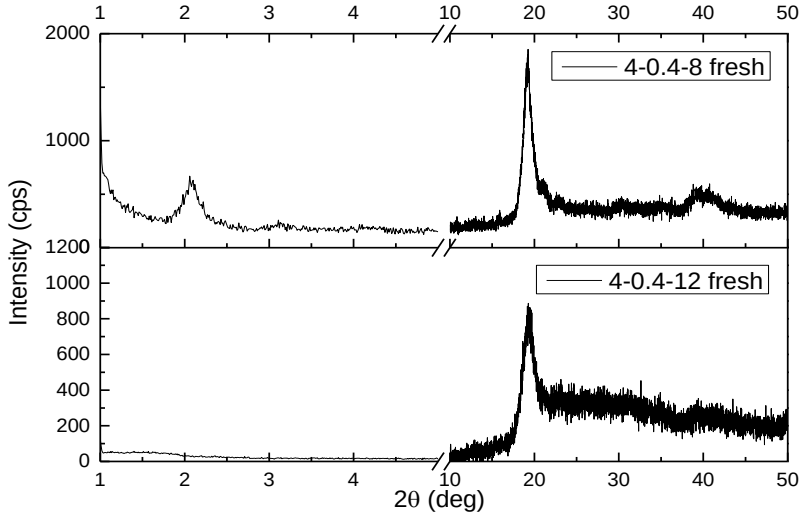

Figure 4.45. The XRD patterns of the fresh samples with 4-0.4-8 and 4-0.4-12 mole ratios.

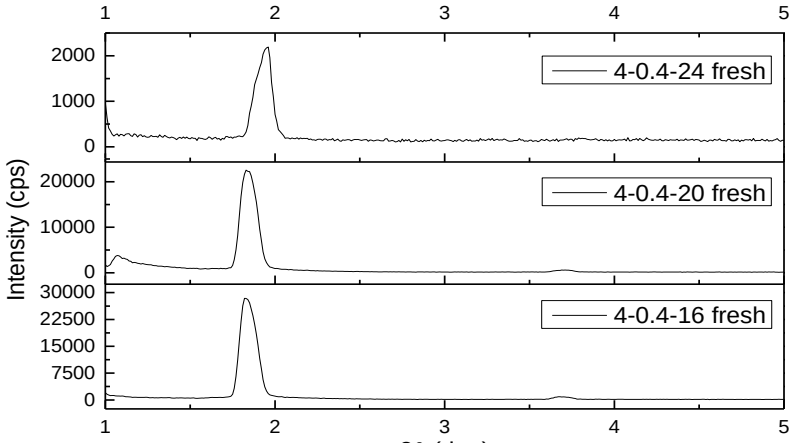

Figure 4.46. The XRD patterns for the fresh 4-0.4 samples with 16, 20, and 24 mole ratios of water.

The ATR-FTIR spectra of the 4-0.4-60 sample were also collected after 24 hours, and then compared with the fresh samples of the other compositions (**Figure 4.47**). It is noticed that after equilibrium of the sample with 60 mole ratio of water is reached, the spectrum is identical to that of the fresh sample of 4-0.4-12 (LiI-I_2-H_2O) ratio. It means that, in the 4-0.4 LiI-I_2 samples, the hydration water amount is approximately 12 per 4 LiI, which is 3 per one LiI salt (see **Figure 4.47**).

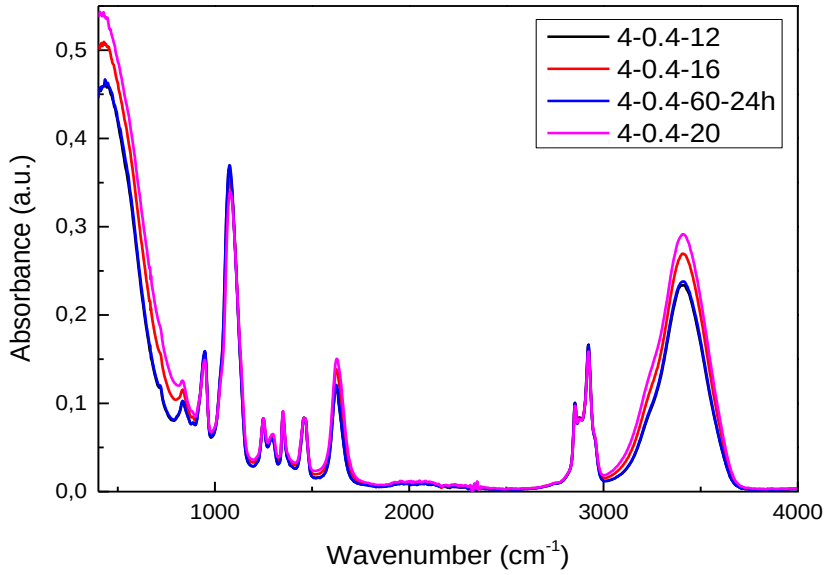

Figure 4.47. The ATR-FTIR spectra for the 4-0.4 LiI-I_2-$C_{12}EO_{10}$ samples with different amount of water.

Finally, the 5-0.5 LiI-I_2-$C_{12}EO_{10}$ samples with various amount of water were also prepared and investigated for the same purpose. However, these samples immediately form the mesocrystals, no hexagonal mesophase was formed; the mesocrystals were observed under the POM (see **Figure 4.48**).

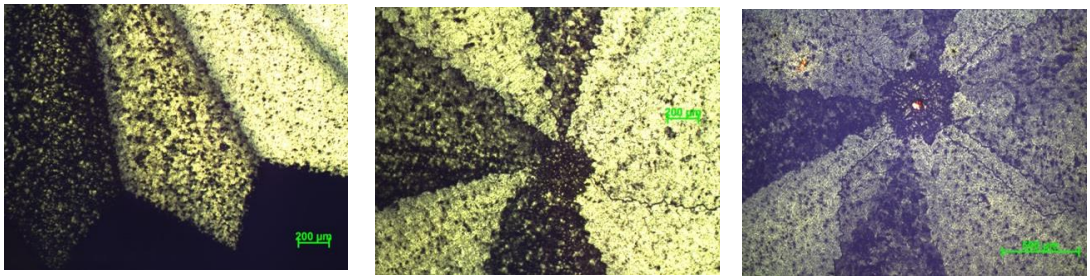

Figure 4.48. POM images of the 5-0.5-60 samples after spin coating and evaporating all excess water.

4.2.1. LiCl – LiBr – $LiNO_3$ Addition to the Redox Couple

The LiI–I_2 mesophases, prepared using non-ionic surfactant and water, have conductivity as low as 0.09-0.10 mS/cm. Because of this, LiCl, LiBr, and $LiNO_3$ were added into the LiI–I_2 samples in different amounts. The 2-0.2 (LiI-I_2 ratio) sample was also prepared using 0.2, 0.4, 0.6, 0.8, and 1.0 mole ratios of the other

lithium salts. The samples were prepared in solution phase, ethanol was used as the volatile solvent, since it was already established that there is no difference between solution phase and gel phase of these samples.

It is clearly observed from **Figure 4.49** to **4.51** that the 2D hexagonal structure of LiI-I_2 samples were preserved with the addition of LiCl, LiBr, and $LiNO_3$ salts. In all ratios (from 0.2 to 1.0), the samples exhibit birefringence with a perfect fan-texture without any phase separation. The samples are all stable, and the LLC mesophase does not change over time.

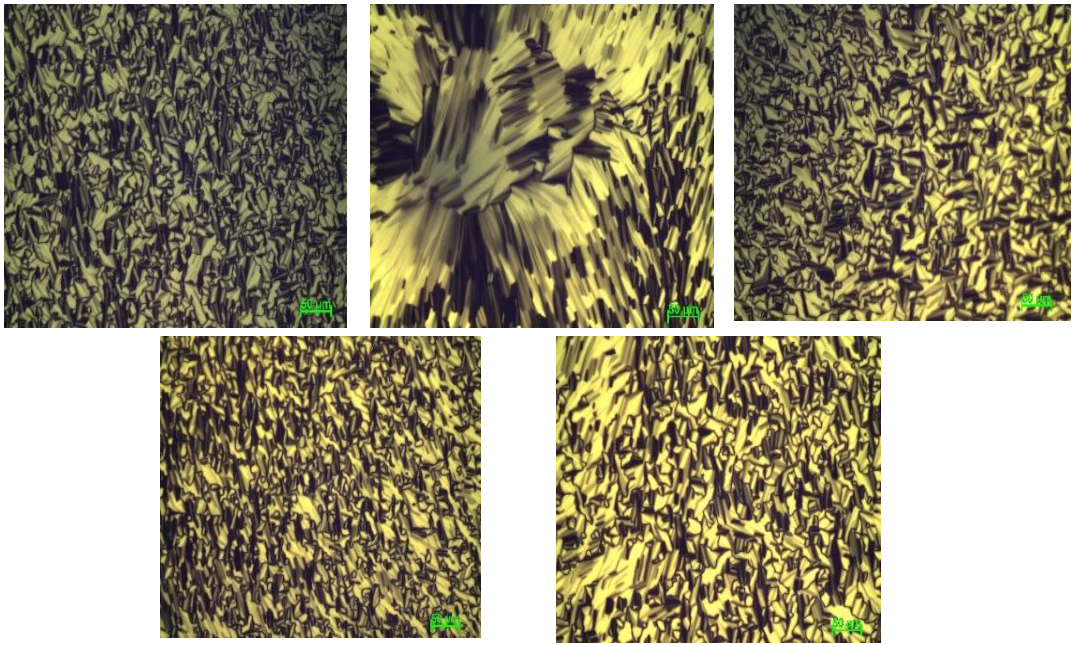

Figure 4.49. The POM images of the samples with 0.2, 0.4, 0.6 (top), 0.8, and 1.0 (bottom) addition of LiCl, respectively, to the 2-0.2 LiI-I_2 sample.

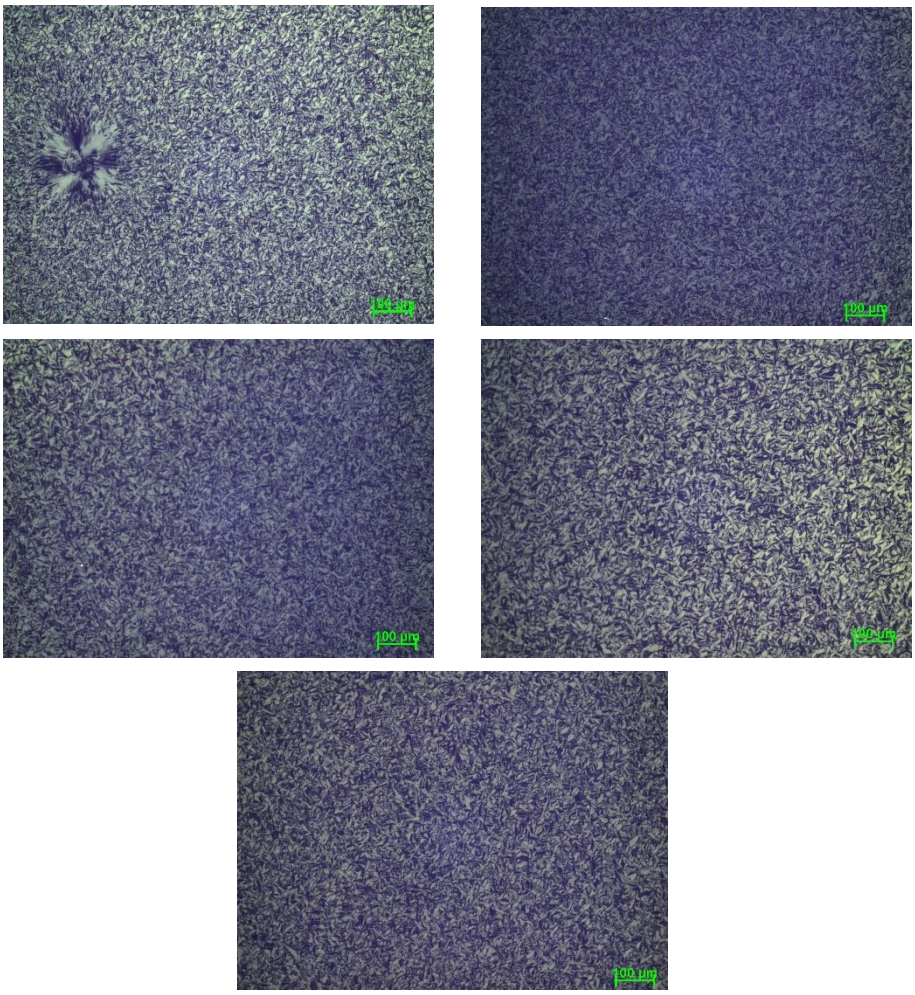

Figure 4.50. The POM images of the samples with 0.2, 0.4 (top), 0.6, 0.8 (middle), and 1.0 (bottom) addition of LiBr, respectively, to the 2-0.2 LiI-I_2 sample.

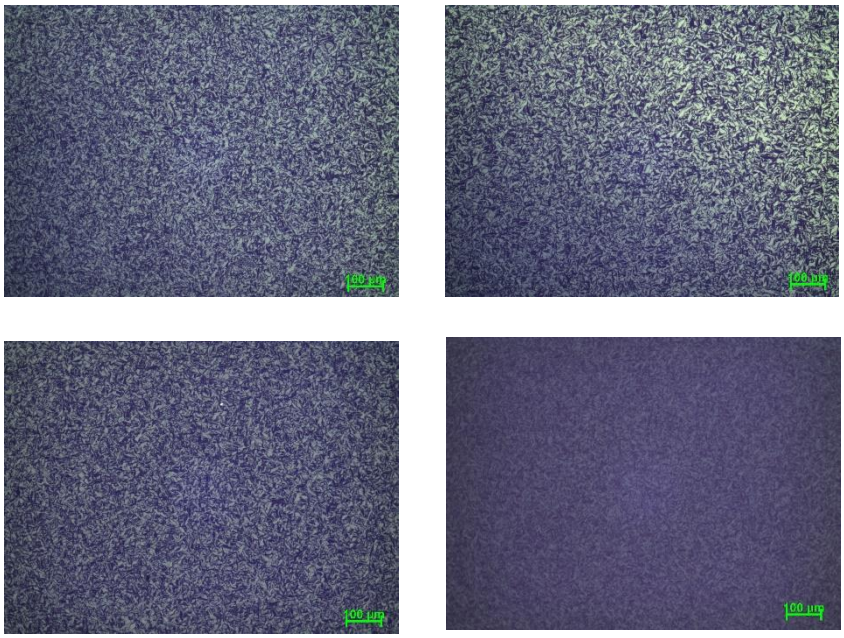

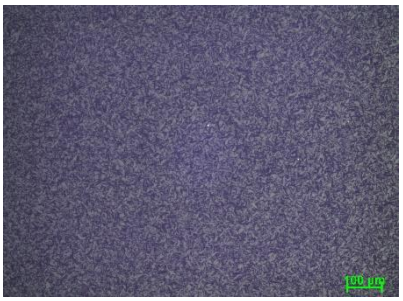

Figure 4.51. The POM images of the samples with 0.2, 0.4 (top), 0.6, 0.8 (middle), and 1.0 (bottom) addition of $LiNO_3$, respectively, to the 2-0.2 LiI-I_2 sample.

To investigate the characteristics of these samples, ATR-FTIR data were also collected. The spectra were normalized with respect to surfactant peak at 1460 cm^{-1}, since the absorbance of that peak does not change with composition. The data of fresh samples were not very reliable, owing to the fact that desorption of ethanol happens too fast, as mentioned in previous parts. While ethanol is released, water is adsorbed from the atmosphere by the sample. After approximately 1 hour, all the samples are stabilized with a fixed water amount.

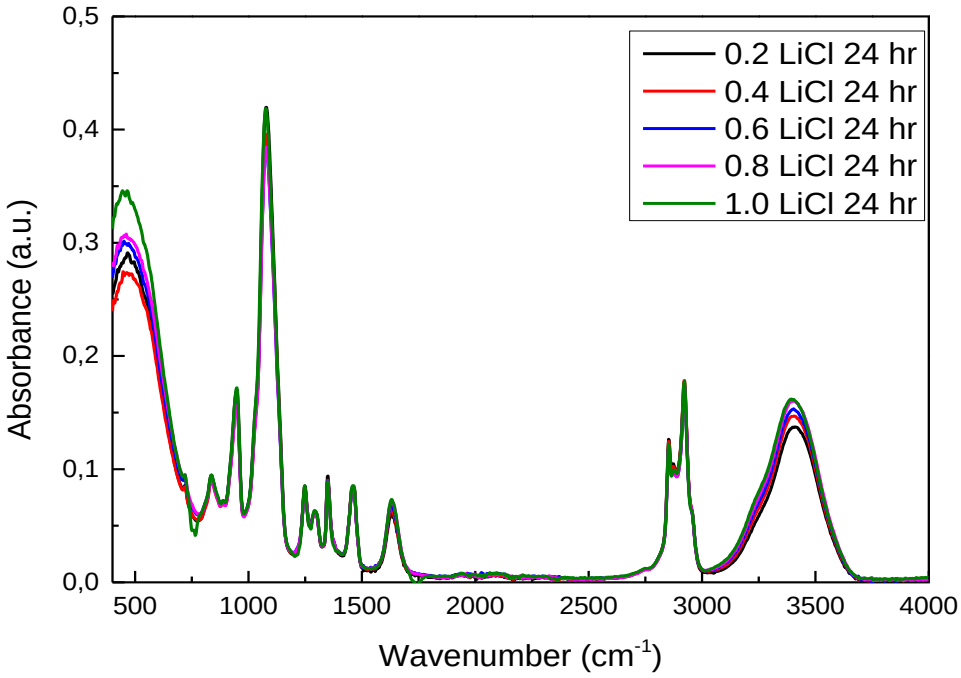

Figure 4.52. The ATR-FTIR spectra of the LiCl-LiI-I_2 samples after 1 day.

From the data in **Figure 4.52** to **Figure 4.54**, it is clear that when the amount of lithium salts, which is added into the redox couple, increases, the hydration water amount in all the samples also increases, regardless of the type of lithium salt.

However, in the case of $LiNO_3$, when 1.0 mole ratio is added into the redox couple, the spectrum changed due to nitrate signals in the 1300-1400 cm^{-1} region (see **Figure 4.54**).

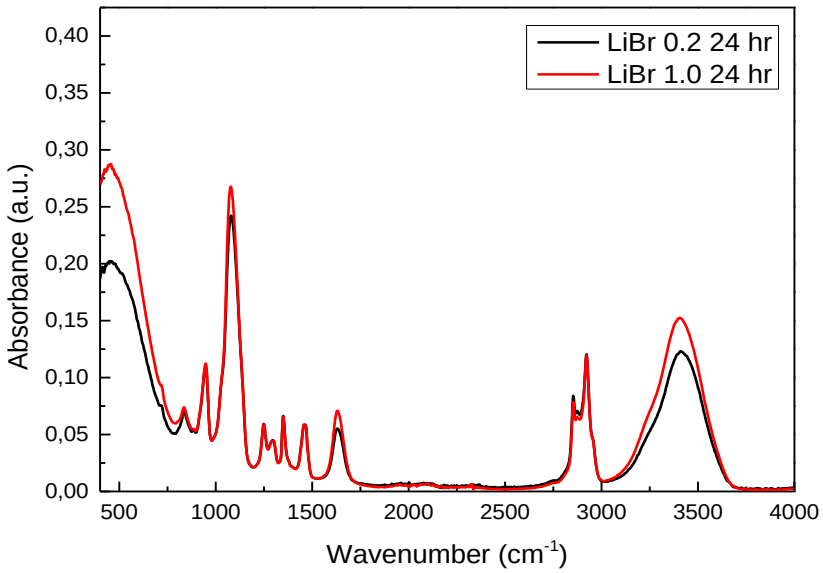

Figure 4.53. The ATR-FTIR spectra of the LiBr addition to the 2-0.2 LiI-I_2 samples after 1 day.

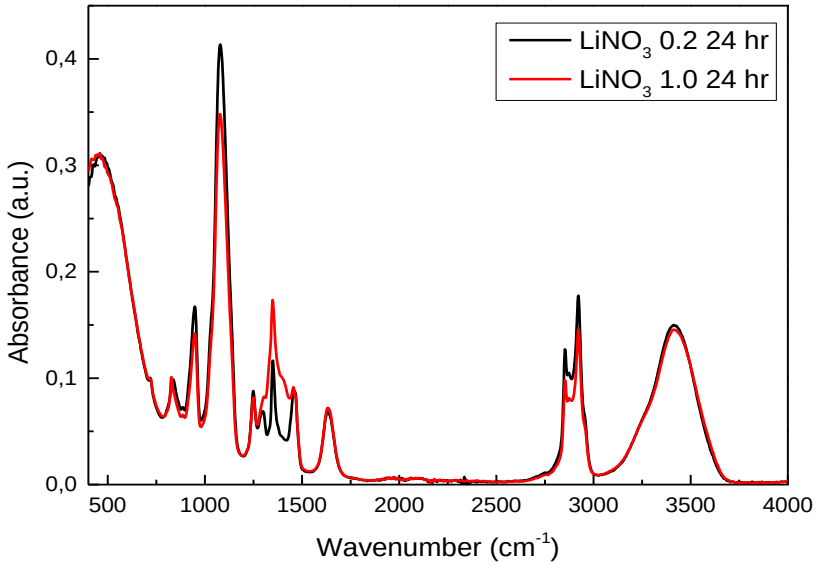

Figure 4.54. The ATR-FTIR spectra of the $LiNO_3$ addition to the 2-0.2 LiI-I_2 samples after 1 day.

To investigate the differences in different lithium salts, the ATR-FTIR spectra of three different lithium salts with the same mole ratio were also collected, see **Figure 4.55**. The spectra were normalized with respect to the surfactant peak at

1460 cm^{-1} (see **Figure 4.55**). It is clear that the LiBr-LiI-I_2 sample keeps more water after 1 day than the LiCl-LiI-I_2 and $LiNO_3$-LiI-I_2 samples. In other words, the hydration water amount has an order of LiBr > $LiNO_3$ ~ LiCl. In this system, they all peak at around 1631 cm^{-1}. When LiCl and $LiNO_3$ are measured in the salt-surfactant system, it is known that they peak at around 1645 cm^{-1} as free water. In the case of LiBr, water peak appears at around 1632 cm^{-1}. However, here all water molecules in the same structure when they are added to the redox couple. It means that the structure of water in LiCl and $LiNO_3$ added samples are changed from free water to hydration water, but it remains same in the LiBr added sample. It seems like LiI determines the nature of water in all samples. The reason for Cl^- ion to keep the less amount of water can be its place in the Hofmeister series. The Cl^- is placed on the left of Br^- ion in the series. Thus, the hydrophobic interaction is increased in the case of Cl^- ion, and that's why it keeps the least amount of water as hydration water.

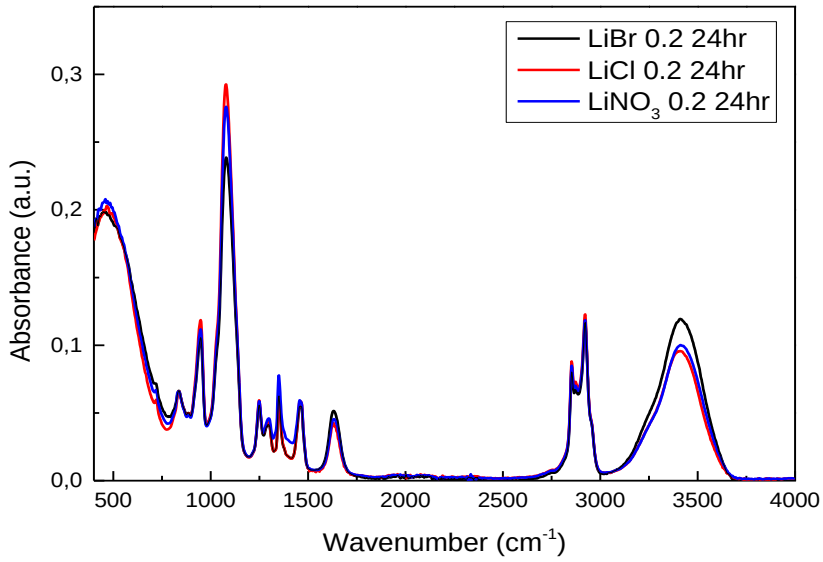

Figure 4.55. The ATR-FTIR spectra of 0.2 mole ratio of LiBr, LiCl, and $LiNO_3$ added samples after 1 day.

Besides the ATR-FTIR measurements, the conductivity measurements were also performed using the same samples. Since the conductivity of LiI-I_2 samples were too low, and to improve the conductivity, the LiCl, LiBr, and $LiNO_3$ salts were separately added to the LiI-I_2 mesophases, see **Table 4.2**. It is also clear from the trends that these lithium salts have a positive effect on conductivity when they are added to the redox couple. The lower amounts of these lithium salts increased the

conductivity slightly, whereas the higher amounts increased the conductivity excessively. In lower amounts of lithium salts, the conductivity order is LiBr > $LiNO_3$ > LiCl; however in higher amounts of salts, the conductivity of $LiNO_3$ and LiBr switch places. 0.6 mole ratio of LiX addition seems to be almost the same in all lithium salts, where the conductivity is approximately 0.38 mS/cm (see **Table 4.2**). The reason for an increase in the conductivity is the extra lithium salts in the samples. Note also that the conductivity increases in water. The highest conductivity was observed from the sample, which has extra 1.0 mole ratio of $LiNO_3$ in addition to the redox couple; however, the ATR-FTIR spectra show the following water trend LiBr > $LiNO_3$ > LiCl. The conductivity order is the same at low concentrations but at higher concentrations the order is $LiNO_3$ > LiBr > LiCl. At high LiBr case, one may expect to form BrI_2^- ions, analog of the I_3^- ion in the media. It is also important to evaluate how these ions interact with the Li^+ ion in such high concentrations to fully elucidate the effect of various ions to ionic conductivity.

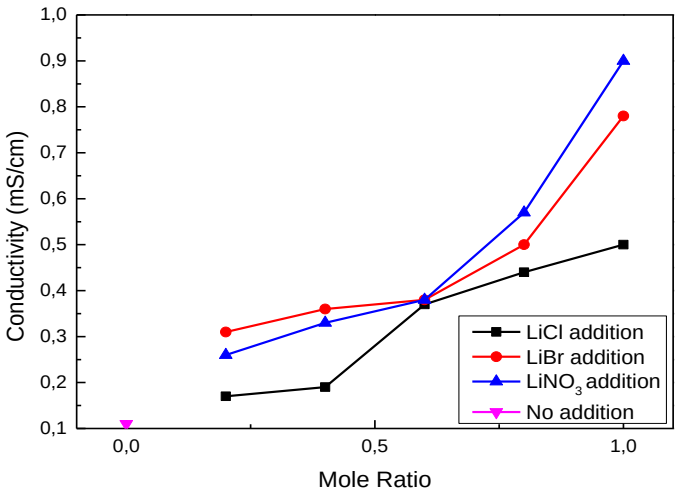

Figure 4.56. The ionic conductivity data of the LiCl, LiBr, and $LiNO_3$ additions to the LiI-I_2 samples, and the sample with no additions.

Mole Ratio	LiCl	LiBr	$LiNO_3$
0.2	0.17 mS/cm	0.31 mS/cm	0.26 mS/cm
0.4	0.19 mS/cm	0.36 mS/cm	0.33 mS/cm
0.6	0.37 mS/cm	0.38 mS/cm	0.38 mS/cm
0.8	0.44 mS/cm	0.50 mS/cm	0.57 mS/cm
1.0	0.50 mS/cm	0.78 mS/cm	0.90 mS/cm

Table 4.2. The conductivity results for LiCl, LiBr, and $LiNO_3$ additions to the LiI-I_2 samples.

In the LiI-I_2 systems as gel-electrolytes and/or redox couple in solar cells, the main problem is the formation of I_2 because of the presence of water, which enforces I_3^- and I_2 equilibrium to favor the formation of I_2 in the media. I_2 formation is not desired that I_2 decreases the efficiency of the solar cells (see latter). All I_2 must be converted to I_3^- for the DSSC to work efficiently. Thus, we also checked the presence of I_2 in the samples using UV-vis absorption spectroscopy (see **Figure 4.57**). The peaks at around 264 and 363 nm belong to the triiodide ion, and the spectra completely overlap regardless of the type of lithium salts. I_2 has an absorption peak at around 520 nm,[128] however in these samples there is no iodine formation due to the fact that there are no peaks at around 520 nm. It is clear from the spectra that all iodine transforms into triiodide as needed.

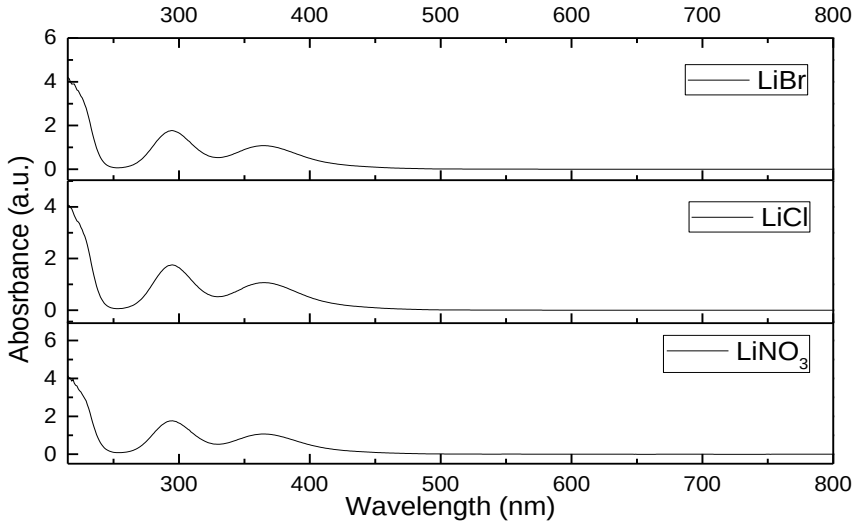

Figure 4.57. The UV-vis absorption spectra of the LiI-I_2 samples upon addition of the other lithium salts.

To summarize; the LiCl, LiBr, and $LiNO_3$ additions to the LiI-I_2 samples are apparent to be a good way to increase conductivity for applications. There is no evidence for the presence of I_2 in the LLC media or destruction of the structure of the LLC 2D hexagonal mesophase upon addition of LiCl, LiBr, and $LiNO_3$. Hence, they can also be used as electrolytes in DSSCs due to these properties.

4.2.2. Summary of LiI – I_2 – $C_{12}EO_{10}$ – Water Systems

To sum up these results, the sample with 1-0.1 (LiI-I_2) mole ratio exhibits isotropic bicontinuous cubic phase, whereas the samples with 2-0.2, 3-0.3, and 4-

0.4 (LiI-I_2) mole ratio per 1 surfactant form 2D hexagonal mesophase and display perfect fan-textures. The XRD patterns of all fresh and aged samples display a single line at small angles. They are all stable for a long time. The amount of hydration water is between 2 and 3 mole ratio of water per LiI salt. This proves that, water is not a problem as long as it is in the structure of these mesophases. To be more specific, this little amount of water is needed for the mesostructure to form. Therefore, these samples can be used as electrolytes in various applications. Dye sensitized solar cell can be a nice application, where the mesophases can be used as the gel-electrolytes. However, there is a diffusion problem for the gel phase when they are employed as electrolytes in the DSSCs (see latter). Besides from that, the gel phase is hard to be characterized and prepared. Thus, because of all these reasons, it is better to prepare the samples in the solution phase. Note also that there is no difference between solution phase and gel phase, upon evaporation the excess solvent. Therefore, the samples were prepared and used in the solution phases as the electrolytes and redox couples in the DSSCs.

4.3. LLC Mesophases as Electrolytes in DSSCs & I-V Curves

The unique properties of the LLC mesophase of the LiI-I_2 samples make them useful in DSSCs as gel electrolytes. Notice also that the LiI-I_2 redox couple has been one of the most widely used electrolytes and redox couple in the DSSCs. Usually, the acetonitrile solutions of the redox couple have been investigated in the DSSCs due to the easy use and better performance. However, acetonitrile is volatile; the solutions are not stable over time, as explained in **Chapter 2**.

The major reason of the use of acetonitrile is that it prevents I_2 formation, which has negative effect on the efficiency of the DSSCs. Water as a solvent has disadvantage in this context, since I_2 is formed in water media. Nevertheless, the water, which causes problem is the free water, as mentioned before. When the water molecules are in the LLC media, they do not cause any problem. Therefore, the water-based salt-surfactant mesophases have been investigated to overcome the problems that other solvents can cause.

The DSSCs were fabricated as explained in **Section 3.3**. The LLC samples with LiI-I_2 redox couple were used as electrolytes. The anode, working electrode,

is FTO glass that is coated with a 20-25 nm TiO_2 particles over a protecting layer, which is also thin layer of TiO_2. Protecting layer is coated onto the FTO glass, to prevent the shortcuts by the contact of the electrolyte to FTO. The cathode is a Pt coated FTO glass, where Pt nanoparticles are used as catalyst for the electron transfer from cathode to the redox couple. On cathode, the I_3^- ion is converted to $3I^-$ ions that supply the electron(s) back to the oxidized dye molecules to regenerate them.

At the beginning of this investigation, the gel phase of the 2-0.2 LiI-I_2 samples has been used, where the efficiency of the DSSC was as low as 0.2 %. Fill factor (FF) of the cells was also low when the gel phases of the electrolytes were employed. This is because of the fact that the gel samples are problematic in terms of the diffusion into the pores of TiO_2 layer. Thus, the solutions of the electrolytes with very similar compositions were prepared in excess water at first. The characterization of the solutions prove that the evaporation of the excess water gives the LLC mesophases with a very similar structure and compositions to that of the samples prepared in the gel-phase. Hence, the solutions were used in the DSSCs as gel electrolytes upon evaporation of the excess water.

The TiO_2 electrode is sensitized upon dipping it into the dye solution for overnight, then the LLC electrolyte solution is spread over the dye adsorbed TiO_2 working electrode, and aged until all the excess water evaporates. Finally, the counter electrode is covered on top and assembled together with two clips. The I-V curve of this sample is obtained by photovoltaic measurement with a solar simulator under 1 sun illumination (see **Figure 4.58**). This cell works with an efficiency of 1.00 % with a fill factor of 0.55.

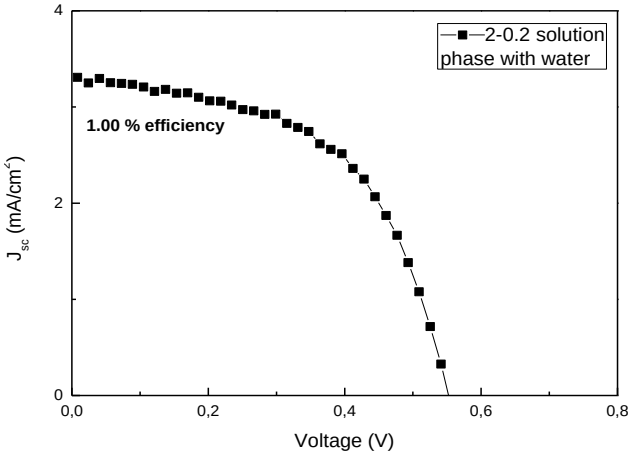

Figure 4.58. The I-V curve of the 2-0.2 LiI-I_2 sample prepared with an excess water.

As a result, the efficiency is increased by using the electrolyte in the solution phase. Notice that the electrolyte was prepared using excess water and dropped over the anode electrode surface, where some of the dye molecules are leached out by the excess water through ligand exchange mechanism. Note that removing the dye molecules decreases the current collected from the DSSC, as a result the efficiency also drops. The 2-0.2 LLC sample was prepared in gel phase as usual and dissolved in excess amount of ethanol and also used as the electrolyte in the DSSC. The results were quite promising that an efficiency of 1.59 % and a FF of 0.60 were recorded from this cell (see **Figure 4.59**).

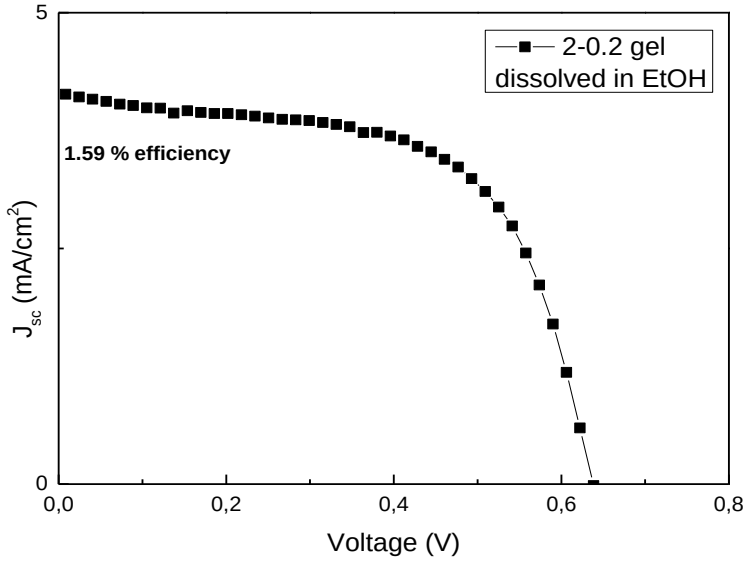

Figure 4.59. The I-V curve of 2-0.2 gel dissolved in excess ethanol.

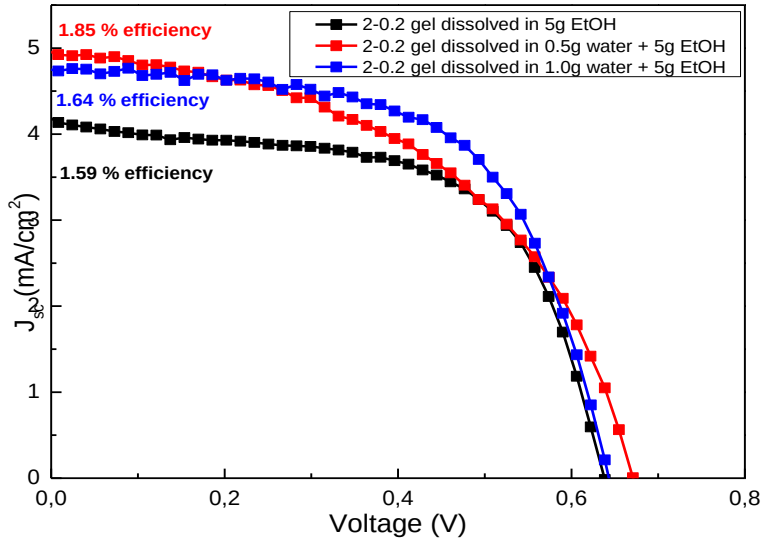

Figure 4.60. The comparison of I-V curves of 2-0.2 gel samples dissolved in excess ethanol, and the effect of water on it.

Figure 4.60 clearly shows that there is an increase in efficiency under different conditions. The excess water is problematic such that it causes the dye molecules to leach out from the surface of titania nanoparticles; however, a trace amount of water in the electrolyte increased the open circuit voltage. If we compare the DSSCs with and without water in the electrolyte, it is obvious that the addition of water increase the short circuit current value with a similar V_{oc} values. However, further increasing the water amount also increases the V_{oc} value. That is why the efficiency increases up to 1.85 %.

Dissolving the gel in ethanol increased the efficiency, but there is still room for enhancements. Thus, the electrolyte was prepared in a solution phase to overcome the diffusion problems and water was replaced with ethanol. Also a small amount of water was added into the solution, to evaluate if there is an effect on the efficiency, like in the case of gel dissolving in ethanol-water mixture. **Figure 4.61** shows the I-V curves of the DSSCs with different electrolytes in solution phase. The electrolyte with just ethanol is the least efficient one, however when a 0.5 grams of water is added into it, the efficiency is increased up to 2.20 %. Besides from the effect on efficiency, somehow water has also a crucial role in FF. The FF is recorded to be 0.51 if the cell with the electrolyte that has no water, whereas it increases up to 0.61 if some water is added to the electrolyte solution.

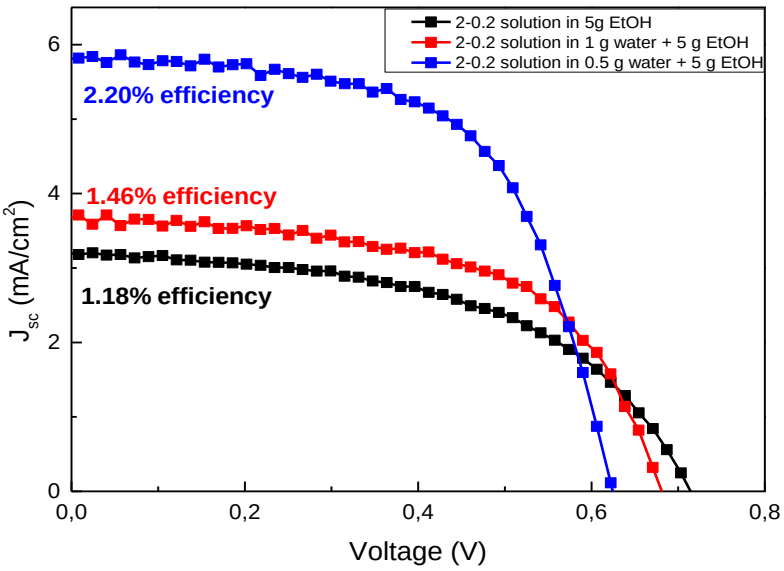

Figure 4.61. The I-V curves of DSSCs with 2-0.2 samples prepared as solution, and the effect of water on efficiencies.

To enhance the efficiency further and improve the fill factor values, many different procedures, for the preparation of TiO_2 paste, has been tested. The old procedure produces a liquid TiO_2 suspension; thus the TiO_2 layer are thinner. A new procedure that uses acetic acid, triton X100, water, ethanol, and TiO_2 nanoparticles has been employed to test the role of the preparation of the anode. Acetic acid is used to prevent aggregation, and triton X100 is used to disperse the particles. The new procedure produces a viscous mixture of TiO_2, and the TiO_2 layer coated over FTO is much thicker. The thicker TiO_2 layer simply means more dye molecules. Hence, the photo-current density should be increased. Indeed, from the **Figure 4.62**, a positive impact, upon changing the procedure, is clearly visible. Furthermore, the addition of 4TBP also increases the efficiency, compare the I-V curves obtained from the cells with and without 4TBP. By comparing all the data, it could be concluded that, besides from the new procedure for TiO_2, there is also an effect of how the electrolyte solution was prepared. For instance if the 4TBP is added to the electrolyte solution after 4 days of stirring, the efficiency is 2.46 %; however when the electrolyte solution is prepared with 4TBP from the start, the efficiency is 3.33 %. This is the highest efficiency that has been achieved so far.

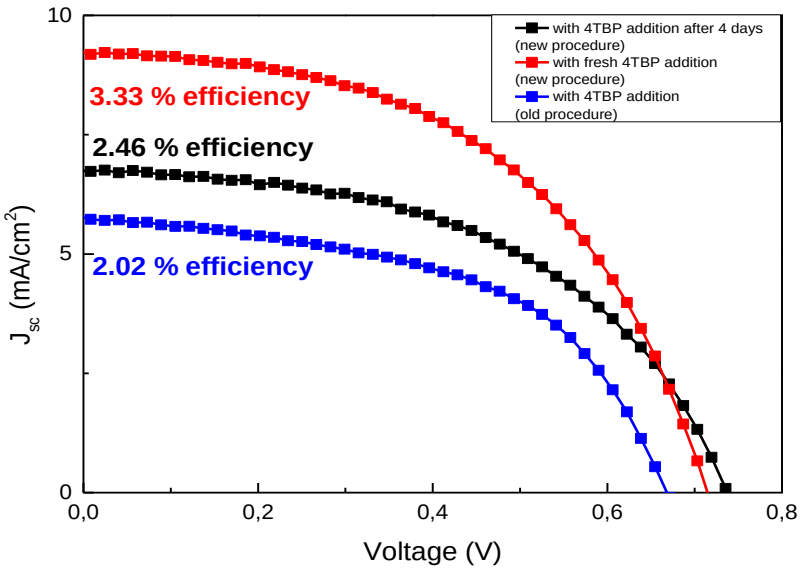

Figure 4.62. The I-V curves of DSSCs with different procedures of TiO_2 layers

Besides from these results, the LiCl, LiBr, and $LiNO_3$ added electrolytes were also tested in the solar cell measurements. The ionic conductivities were enhanced by adding these lithium salts to the LiI-I_2 redox couple, as mentioned above. This is why they were expected to increase the efficiency of DSSCs.

However, they all decrease the efficiencies in compare to the electrolyte without any additions (see **Figure 4.63**).

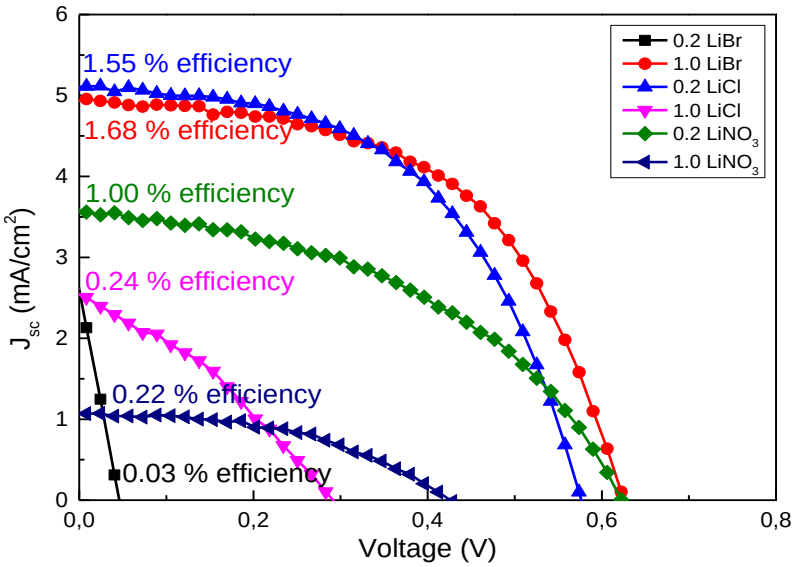

Figure 4.63. The I-V curves of the 2-0.2 (LiI-I_2) samples with LiCl, LiBr, and $LiNO_3$ additions.

It is clear from the I-V curve in **Figure 4.63** that the lithium nitrate has the most negative effect on the efficiency of the DSSC. In the case of LiBr addition, 1.0 mole ratio is more efficient than the 0.2 mole ratio; and in the case of LiCl addition, it is the opposite, where the 0.2 mole ratio is more efficient than 1.0 mole ratio. Since less water is kept in the LiCl mesophases, it is expected to be less efficient than LiBr containing mesophase. In the case of $LiNO_3$ addition, 0.2 mole ratio is more effective than 1.0 mole ratio. This is probably because of the ionic conductivity of $LiNO_3$ added samples, since the one with 1.0 mole ratio of $LiNO_3$ is more conductive. However, when the other lithium salts are considered, it can be concluded that the efficiency is not just about the ionic conductivity, it also depends on the other parameters.

To understand the negative effect of the salts on DSSCs, another experiment was conducted. The working electrodes were prepared and dipped into the dye solutions. After that, the electrolytes were spread over these electrodes and allowed to be in the gel form before further assembly. Then, the working electrodes were washed in an ethanol solution separately to dissolve the electrolytes. Finally, the absorption spectra of the collected solutions were measured using a UV-Vis spectrometer (see **Figure 4.64**). It is clear from the spectra that all the electrolytes

with the addition of LiBr, LiCl, and $LiNO_3$ detach some dye molecules. That is why the current of the cells are decreased. The N719 dye has an absorption peak at around 550 nm. The intensity of this peak is the highest in case of $LiNO_3$, and then LiCl came, followed by LiBr which has the lowest intensity. This correlates well with the efficiency of the cells.

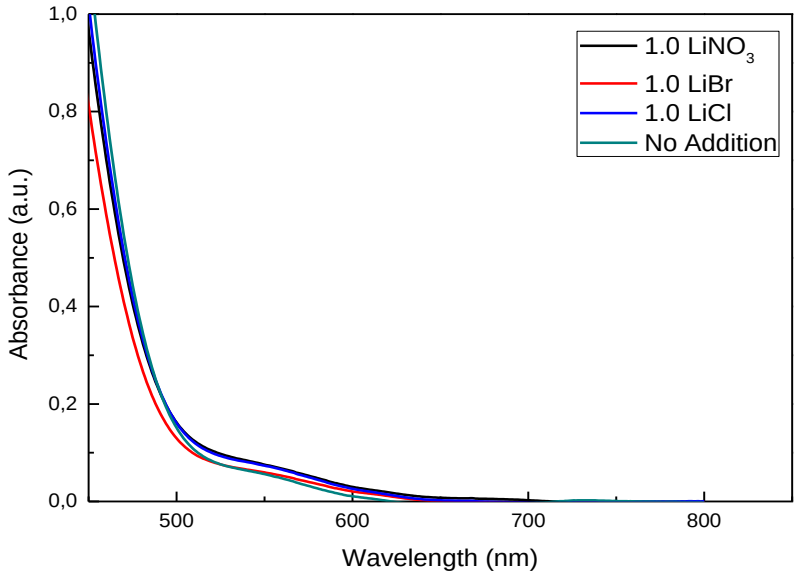

Figure 4.64. The UV-Vis absorption spectra of the LiI-I_2 electrolytes with and without $LiNO_3$, LiCl, and LiBr added upon dissolving from the electrodes.

4.3.1. Summary of DSSCs

Electrolyte	V_{oc} (V)	J_{sc} (mA/cm^2)	Efficiency	Fill Factor
In water	0.56	3.37	1.00 %	0.55
Gel dissolved in 5 g EtOH	0.64	4.16	1.59 %	0.60
Gel dissolved in 0.5 g water + 5 g EtOH	0.68	4.93	1.85 %	0.61
Gel dissolved in 1.0 g water + 5 g EtOH	0.64	4.75	1.64 %	0.49
Solution in 5 g EtOH	0.72	3.17	1.18 %	0.51
Solution in 0.5 g water + 5 g EtOH	0.63	5.86	2.20 %	0.60
Solution in 1.0 g water + 5 g EtOH	0.68	3.73	1.46 %	0.59
Solution with 4TBP (old procedure)	0.75	6.74	2.46 %	0.50

Solution with 4TBP (new procedure)	0.72	9.26	3.33 %	0.50
0.2 mole ratio of LiCl added	0.58	5.13	1.55 %	0.52
1.0 mole ratio of LiCl added	0.29	2.55	0.24 %	0.33
0.2 mole ratio of LiBr added	0.05	2.58	0.03 %	0.25
1.0 mole ratio of LiBr added	0.63	4.95	1.68 %	0.54
0.2 mole ratio of $LiNO_3$ added	0.62	3.55	1.00 %	0.46
1.0 mole ratio of $LiNO_3$ added	0.40	1.11	0.21 %	0.47

Table 4.3. The photovoltaic characteristics of DSSCs with different electrolytes.

Table 4.3 summarizes the V_{oc}, J_{sc}, power conversion efficiency, and fill factor values of the DSSCs, which were measured using the LLC electrolytes. The best efficiency so far is 3.33 %. In the literature, this value is around 4 % in the most efficient DSSC among water-based electrolytes. In this investigation, many promising results were obtained. Because of the presence of water, V_{oc} values had been always lower than the DSSCs with acetonitrile based liquid electrolytes. The 0.8 V is the highest open circuit voltage value, obtained from the liquid electrolytes; and in the water-based systems, this value is around 0.5-0.6 V, at most. However, in this investigation, it is clear that the V_{oc} can be increased up to 0.75 V. This is very important and shows that there is a room for improvement in the LLC gel electrolytes for the DSSCs. Notice also that the highest FF value, recorded so far, is around 0.61 and there is also room for the improvement on the FF values of the LLC based gel electrolytes for DSSCs. One of the disadvantages of gel electrolytes is their high resistances or low conductivities.

Despite the fact that free water molecules detach the dye molecules, and decrease the current; however if there is a trace amount of water, it increases the V_{oc} value of the cells.

Other lithium salts were examined by adding them into the LiI-I_2 redox couple, as mentioned above to improve the conductivity of the gels. However, almost no improvement was recorded for all lithium salts tested in this thesis. Moreover, these extra lithium salt gels were also characterized by using ATR-FTIR spectroscopy and found out that that the samples with LiBr keeps the highest

amount of water in mesostructure among these three lithium salts. That is why, it has the highest efficiency among them. However, they still decrease the V_{oc}, J_{sc} values, efficiencies, and fill factors in compare to the electrolyte without any additions of extra lithium salt.

CHAPTER 5

5. FUTURE WORK

In this study, LLC mesophases of LiCl and LiI with non-ionic surfactant were prepared and characterized. The role of the water in the mesophases was evaluated, and the hydration water amount was determined. Also the LLC mesophases of the LiI-I_2 redox couple were prepared, and characterized by using ATR, Raman, XRD, and POM. The solutions of these samples were also prepared, where the difficulties of the gel form was overcome by using the solution phases in the DSSCs. The efficiency of the cells was improved by using the electrolytes in their solution phase, and by changing the preparation procedure of the TiO_2 paste. We believe that these efficiencies can be further enhanced by improving the conductivity of the gel electrolytes. That's why more investigation in this subject needs to be done. Some of the parameters that change the efficiencies were investigated; however all other parameters will be studied further, such as resistance of electrolyte, increasing the conductivity of it, and so on. Different kinds of electrodes will be tried, such as graphene coated counter electrode instead of Pt, or additives for TiO_2 mixture preparation, or additives for the electrolyte etc. It is known that all of these affect the efficiencies of the DSSCs, and they will be further investigated in the future.

CHAPTER 6

6. CONCLUSIONS

In this investigation, the LLC mesophases of the lithium salts in surfactant-water system and the LLC mesophases of the LiI-I_2 redox couple were prepared and characterized; in addition to fabrication of dye sensitized solar cells in which these samples were used as electrolytes.

In the first part of the thesis, the LiCl and LiI salts were used as the salts, $C_{12}EO_{10}$ was used as non- ionic surfactant, and their LLC mesophases were prepared and characterized in the presence of very little amount of water. The characterization results show that the presence of water in the LLC media is inevitable, and truly it is needed for mesostructure to form. This little amount of water is the hydration water. The rest of the water is called free water, and it can be problematic in various applications of the mesophases. However, the excess water desorbs quickly to the atmosphere and the gel samples become stable after approximately 4-5 hours. This specific amount of water that the sample can keep is around 3 H_2O per 1 lithium salt, in both LiCl and LiI mesophases. The mesophases form perfect 2D hexagonal mesostructures, and they are stable for very long time.

In the second part of the thesis, the LiI-I_2 redox couple was used to form the LLC mesophases with $C_{12}EO_{10}$ in the presence of water. Different mole ratios of this redox couple, and different amount of water were tested and the samples were characterized both in gel and solution phases. It was determined that there is no difference between the gel phase and solution phase upon evaporation of the excess solvent. The samples prepared as a solution released their excess water to the atmosphere and become stable for very long time. Additionally, the gels were hard to prepare and characterize. Therefore, the solution phase of the compositions were prepared and used in the DSSCs. It is also noticed that the 1-0.1 (LiI-I_2) ratio is in the bicontinuous cubic phase, while the samples with 2-0.2 to 4-0.4 mole ratios are in the 2D hexagonal phase, and the 5-0.5 mole ratio exhibits mesophase by forming the mesocrystals. The hydration water amount per lithium salt of these samples lies between 2 and 3, regardless of the mole ratio of LiI-I_2. Besides from these, other lithium salts were added into these samples to increase the conductivity; it is found

out that the 2D hexagonal structure is preserved and the conductivity is improved upon the addition of those salts.

In the third part of the thesis, the LLC mesophases of the LiI-I_2 redox couple were employed as the gel electrolytes in the DSSCs. However, if the gels were used directly, the efficiency of the cells were very low. Thus, they were prepared and used in solution form. Both water and ethanol were tested as solvents. After evaporation of the solvent the samples become gel, and this helps to overcome the diffusion problem of the gels into the pores of the anode electrode. Dissolving the gel form of the sample in both water and ethanol increased the efficiency of the DSSCs; however the best efficiencies were achieved in the ethanol case with small amount of water. The best results were obtained from the cells that are constructed using a thicker TiO_2 layer and also by the addition of 4TBP into the electrolyte solution. As a result of all these changes, the efficiency of the DSSC is enhanced up to 3.33%.

In conclusion, the efficiencies were increased from 0.2 to 3.33 % with approximately 1665 % by optimizing how to prepare the electrodes and electrolytes in the DSSCs. These results are quite promising for the water-based DSSCs. We believe that these efficiencies can be further improved with more optimizations and improving the conductivity of the gel electrolytes.

BIBLIOGRAPHY

[1] C. Albayrak, G. Barim, and Ö. Dag, “Effect of Hygroscopicity of Salts on the Formation of Lyotropic Liquid Crystalline Mesophases,” *J. Colloid Interface Sci.*, vol. 4, pp. 23–25, 2014.

[2] H. An, B. Xue, D. Li, H. Li, Q. Meng, L. Guo, and L. Chen, “Environmentally friendly LiI/ethanol based gel electrolyte for dye-sensitized solar cells,” *Electrochem. commun.*, vol. 8, no. 1, pp. 170–172, 2006.

[3] F. Reinitzer, “Beiträge zur Kenntniss des Cholesterins,” *Monatshefte für Chemie und verwandte Teile anderer Wissenschaften*, vol. 9, no. 1, pp. 421–441, 1888.

[4] S. Hudson and P. Maitlis, “Calamitic metallomesogens: metal-containing liquid crystals with rodlike shapes,” *Chem. Rev.*, vol. 93, no. 3, pp. 861–885, 1993.

[5] E. Bartholin, “Experimenta Crystalli Islandici,” in *Priestley’s Optics*, 1669, p. 550.

[6] P. G. Gennes and J. Prost, *The Physics of Liquid Crystals*. Oxford Science Publications, 1993.

[7] P. J. Collings and M. Hird, *Introduction to Liquid Crystals: Chemistry and Physics*. Taylor & Francis, 1997.

[8] D. Demus, “Plenary Lecture: One Hundred Years of Liquid-Crystal Chemistry: Thermotropic liquid crystals with conventional and unconventional molecular structure,” *Liq. Cryst. I*, vol. 5, no. 1, pp. 75–110, 1989.

[9] Y. Shao and T. W. Zerda, “Phase Transitions of Liquid Crystal PAA in Confined Geometries,” *J. Phys. Chem. B*, vol. 5647, no. 97, pp. 3387–3394, 1998.

[10] M. S. Bakshi, “Micelle Formation,” vol. 89, no. 24, pp. 4323–4326, 1993.

[11] J. W. McBain, “Mobility of Highly-Charged Micelles,” *Trans. Faraday Soc.*, vol. 9, pp. 99–101, 1913.

[12] K. Tsujii, *Surface Activity: principles, phenomena, and applications*. San Diego: Academic Press, 1998.

[13] R. Nagarajan and C. C. Wang, “Theory of surfactant aggregation in water/ethylene glycol mixed solvents,” *Langmuir*, vol. 16, no. 12, pp. 5242–5251, 2000.

[14] P. Somasundaran and L. Huang, “Adsorption/aggregation of surfactants and their mixtures at solid-liquid interfaces,” *Adv. Colloid Interface Sci.*, vol. 88, no. 1–2, pp. 179–208, 2000.

[15] T. Wärnheim, “Aggregation of surfactants in nonaqueous, polar solvents,” *Curr. Opin. Colloid Interface Sci.*, vol. 2, no. 5, pp. 472–477, 1997.

[16] T. Warnheim and A. Jonsson, “Phase Diagrams of Alkyltrimethylammonium Surfactants in Some Polar Solvents,” *J. Colloid Interface Sci.*, vol. 125, pp. 627–633, 1988.

[17] P. D. Sawant, B. K. Mishra, and C. Manohar, “Surface Chemistry in Monoethylene Glycol: Aggregation Behavior of Sodium Dodecyl Sulfate,” *Langmuir*, vol. 10, no. 3, pp. 3485–3487, 1994.

[18] M. Emo, M.-J. Stébé, J.-L. Blin, and A. Pasc, “Metastable micelles and true liquid crystal behaviour of newly designed ‘cataniomeric’ surfactants,” *Soft Matter*, vol. 9, no. 9, p. 2760, 2013.

[19] C. Eaborn, *Handbook of Liquid Crystals*, vol. 214, no. 1. 1981.

[20] M. G. Friedel, “No Title,” *Ann. Phys.*, vol. 18, no. 273, 1922.

[21] S. T. Hyde, “Identification of Lyotropic Liquid Crystalline Mesophases,” in *Handbook of Applied Surface and Colloid Chemistry*, 2001, pp. 299–332.

[22] D. Blunk, P. Bierganns, N. Bongartz, R. Tessendorf, and C. Stubenrauch, “New speciality surfactants with natural structural motifs,” *New J. Chem.*, vol. 30, no. 12, p. 1705, 2006.

[23] B. J. Forrest and L. W. Reeves, “New lyotropic liquid crystals composed of finite nonspherical micelles,” *Chem. Rev.*, vol. 81, no. 1, pp. 1–14, 1981.

[24] S. Hyde, B. W. Ninham, S. Andersson, K. Larsson, T. Landh, Z. Blum, and S. Lidin, “Chapter 4: Beyond Flatland: The Geometric Forms due to Self-Assembly,” in *The Language of Shape*, 1999, pp. 141–197.

[25] D. A. Frankel and D. F. O’Brien, “Supramolecular Assemblies of Diacetylenic Aldonamides,” *J. Am. Chem. Soc.*, vol. 113, pp. 7436–7437, 1991.

[26] V. Luzzatti, H. Mustacchi, A. E. Skoulios, and F. Husson, “No Title,” *Acta Crystallogr.*, vol. 13, p. 660, 1960.

[27] J. W. Goodby, V. Görtz, S. J. Cowling, G. Mackenzie, P. Martin, D. Plusquellec, T. Benvegnu, P. Boullanger, D. Lafont, Y. Queneau, S. Chambert, and J. Fitremann, “Thermotropic liquid crystalline glycolipids.,” *Chem. Soc. Rev.*, vol. 36, no. 12, pp. 1971–2032, 2007.

[28] P. R. Cullis and B. de Kruijff, “Lipid polymorphism and the functional roles of lipids in biological membranes.,” *Biochim. Biophys. Acta*, vol. 559, no. 4, pp. 399–420, 1979.

[29] H.-J. Butt, K. Graf, and M. Kappl, *Physics and Chemistry of Interfaces*. 2003.

[30] E. S. J. Rudolph, J. H. Langeveld, T. W. De Loos, and J. D. S. Arons, "Phase behaviour of water + nonionic surfactant systems : experiments and modelling applying the Peng – Robinson equation of state with the Wong – Sandler mixing rules and the UNIQUAC g E -model," *Fluid Phase Equilibra*, vol. 173, pp. 81–96, 2000.

[31] B. M. Kahlweit and R. Strey, "Phase Behavior of Ternary Systems of the Type H2O-Oil-Nonionic Amphiphile (Microemulsions)," *Angew. Chem. Int. Ed.*, vol. 24, no. 2, pp. 654–668, 1985.

[32] Y. Nibu and T. Inoue, "Phase Behavior of Aqueous Mixtures of Some Polyethylene Glycol Decyl Ethers Revealed by DSC and FT-IR Measurements.," *J. Colloid Interface Sci.*, vol. 205, no. 2, pp. 305–315, 1998.

[33] K. Kratzat and H. Finkelmann, "Asymmetrically Branched Nonionic Oligooxyethylene Va, -Surfactants : Effect of Molecular Geometry on Liquid-Crystalline Phase Behavior," *J. Colloid Interface Sci.*, vol. 550, pp. 542–550, 1996.

[34] H. Kunieda, K. Shigeta, K. Ozawa, and M. Suzuki, "Self-Organizing Structures in Poly(oxyethylene) Oleyl Ether-Water System," *J. Phys. Chem. B*, vol. 101, no. 5, pp. 7952–7957, 1997.

[35] W. Kunz, J. Henle, and B. W. Ninham, "'Zur Lehre von der Wirkung der Salze' (about the science of the effect of salts): Franz Hofmeister's historical papers," *Curr. Opin. Colloid Interface Sci.*, vol. 9, no. 1–2, pp. 19–37, 2004.

[36] Z. Yang, "Hofmeister effects: an explanation for the impact of ionic liquids on biocatalysis," *J. Biotechnol.*, vol. 144, no. 1, pp. 12–22, 2009.

[37] Y. Zhang and P. S. Cremer, "Interactions between macromolecules and ions: the Hofmeister series," *Curr. Opin. Chem. Biol.*, vol. 10, no. 6, pp. 658–663, 2006.

[38] L. Q. Zheng, H. Minamikawa, K. Harada, T. Inoue, and G. G. Chernik, "Effect of inorganic salts on the phase behavior of an aqueous mixture of heptaethylene glycol dodecyl ether," *Langmuir*, vol. 19, no. 25, pp. 10487–10494, 2003.

[39] K. S. Sharma, S. R. Patil, and A. K. Rakshit, "Study of the cloud point of C12En nonionic surfactants: Effect of additives," *Colloids Surfaces A Physicochem. Eng. Asp.*, vol. 219, no. 1–3, pp. 67–74, 2003.

[40] T. Inoue, Y. Yokoyama, and L. Q. Zheng, "Hofmeister anion effect on aqueous phase behavior of heptaethylene glycol dodecyl ether," *J. Colloid Interface Sci.*, vol. 274, no. 1, pp. 349–353, 2004.

[41] G. S. Attard, "Mesoporous Platinum Films from Lyotropic Liquid Crystalline Phases," *Science (80-.).*, vol. 278, no. 5339, pp. 838–840, 1997.

[42] P. V. Braun, P. Osenar, and S. I. Stupp, “Semiconducting superlattices templated by molecular assemblies,” *Nature*, vol. 380, no. 6572. pp. 325–328, 1996.

[43] B. P. Osenar, P. L. Braun, and S. I. Stupp, “Lamellar Semiconductor-Organic Nanostructures from Self-Assembled Templates,” *Adv. Mater.*, no. 12, pp. 1022–1025, 1996.

[44] P. T. Tanev and T. J. Pinnavaia, “Mesoporous Silica Molecular Sieves Prepared by Ionic and Neutral Surfactant Templating: A Comparison of Physical Properties,” *Chem. Mater.*, vol. 8, no. 8, pp. 2068–2079, 1996.

[45] O. Celik and Ö. Dag, “A new lyotropic liquid crystalline system:oligo(ethylene oxide) surfactants with $[M(H_2O)_n]X_m$ Transition metal complexes,” *Angew. Chem. Int. Ed.*, no. 40, pp. 3800–3803, 2001.

[46] Ö. Dag, S. Alayoğlu, and İ. Uysal, “Effects of Ions on the Liquid Crystalline Mesophase of Transition-Metal Salt:Surfactant (C_nEO_m),” *J. Phys. Chem. B*, vol. 108, no. 24, pp. 8439–8446, 2004.

[47] F. Demirörs, B. E. Eser, and Ö. Dag, “Liquid crystalline mesophases of pluronics (L64, P65, and P123) and transition metal nitrate salts ($[M(H_2O)_6](NO_3)_2$),” *Langmuir*, vol. 21, no. 9, pp. 4156–4162, 2005.

[48] C. Albayrak, A. M. Soylu, and Ö. Dag, “Lyotropic Liquid-Crystalline Mesophases of $[Zn(H_2O)_6](NO_3)_2$ - $C_{12}EO_{10}$ - CTAB - H_2O and $[Zn(H_2O)_6](NO_3)_2$ - $C_{12}EO_{10}$ - SDS - H_2O Systems,” *Langmuir*, no. 3, pp. 10592–10595, 2008.

[49] C. Albayrak, N. Özkan, and Ö. Dag, “Origin of lyotropic liquid crystalline mesophase formation and liquid crystalline to mesostructured solid transformation in the metal nitrate salt-surfactant systems,” *Langmuir*, vol. 27, no. 3, pp. 870–873, 2011.

[50] C. Albayrak, A. Cihaner, and Ö. Dag, “A new, highly conductive, lithium salt/nonionic surfactant, lyotropic liquid-crystalline mesophase and its application,” *Chem. Eur. J.*, vol. 18, no. 14, pp. 4190–4194, 2012.

[51] G. Barım, C. Albayrak, E. Yılmaz, and Ö. Dag, “Highly conducting lyotropic liquid crystalline mesophases of pluronics (P65, P85, P103, and P123) and hydrated lithium salts (LiCl and $LiNO_3$),” *Langmuir*, vol. 30, no. 23, pp. 6938–6945, 2014.

[52] P. Chi, Z. Wang, B. Li, and A. C. Shi, “Soft confinement-induced morphologies of diblock copolymers,” *Langmuir*, vol. 27, no. 18, pp. 11683–11689, 2011.

[53] K. Binder, J. Horbach, R. Vink, and A. De Virgiliis, “Confinement effects on phase behavior of soft matter systems,” *Soft Matter*, vol. 4, no. 8, p. 1555, 2008.

[54] F. He, L. M. Wang, and R. Richert, “Dynamics of supercooled liquids in the vicinity of soft and hard interfaces,” *Phys. Rev. B - Condens. Matter Mater. Phys.*, vol. 71, no. 14, pp. 1–10, 2005.

[55] L. M. Wang, F. He, and R. Richert, “Intramicellar glass transition and liquid dynamics in soft confinement,” *Phys. Rev. Lett.*, vol. 92, no. 9, pp. 095701–1, 2004.

[56] F. Kremer and R. Stannarius, “Measurement of orientational order and mobility of a nematic liquid crystal in random nanometer confinement,” *J. Chem. Phys.*, vol. 106, no. 9, pp. 3730–3742, 1997.

[57] M. Ruths, S. Steinberg, and J. N. Israelachvili, “Effects of Confinement and Shear on the Properties of Thin Films of Thermotropic Liquid Crystal,” *Langmuir*, vol. 12, no. 26, pp. 6637–6650, 1996.

[58] A. P. Alivisatos, “Perspectives on the Physical Chemistry of Semiconductor Nanocrystals,” *J. Phys. Chem.*, vol. 100, no. 95, pp. 13226–13239, 1996.

[59] D. D. Awschalom and J. Warnock, “Supercooled Liquids and Solids in Porous Glass,” *Phys. Rev. B Condens. Matter Mater. Phys.*, vol. 35, no. 13, pp. 6779–6785, 1987.

[60] D. D. Awschalom and J. Warnock, “Geometrical Supercooling of Liquids in Porous Glass,” *Phys. Rev. Lett.*, vol. 57, no. 14, pp. 1753–1756, 1986.

[61] H. K. Christenson, “Confinement effects on freezing and melting,” *J. Phys. Condens. Matter*, vol. 13, no. 11, pp. R95–R133, 2001.

[62] A. N. Goldstein, C. M. Echer, and A. P. Alivisatos, “Melting in Semiconductor Nanocrystals,” *Science (80-.).*, vol. 256, p. 1425, 1992.

[63] D. Vargas-Florencia, O. Petrov, and I. Furó, “Inorganic salt hydrates as cryoporometric probe materials to obtain pore size distribution,” *J. Phys. Chem. B*, vol. 110, no. 9, pp. 3867–3870, 2006.

[64] J. Strange, M. Rahman, and E. Smith, “Characterization of porous solids by NMR,” *Phys. Rev. Lett.*, vol. 71, no. 21, pp. 3589–3591, 1993.

[65] M. K. Nazeeruddin, E. Baranoff, and M. Grätzel, “Dye-sensitized solar cells: A brief overview,” *Sol. Energy*, vol. 85, no. 6, pp. 1172–1178, 2011.

[66] D. Martineau, “The assembly guide for making your own solar cells,” *Solaronix*, pp. 3–38, 2012.

[67] L. Analysis, “Part II – Photovoltaic Cell I-V Characterization Theory and LabVIEW Analysis Code - National I ... Page 1 of 4 Part II – Photovoltaic Cell I-V Characterization Theory and LabVIEW Analysis Code Part II – Photovoltaic Cell I-V Characterization Theory and La,” pp. 2012–2015, 2014.

[68] G. Bunea, K. Wilson, Y. Meydbray, M. Campbell, and D. De Ceuster, "Low light performance of mono-crystalline silicon solar cells," *Conf. Rec. IEEE 4th World Conf. Photovolt. Energy Conf.*, pp. 1312–1314, 2006.

[69] N. Sakai, T. Miyasaka, and T. N. Murakami, "Efficiency enhancement of ZnO-based dye-sensitized solar cells by low-temperature $TiCl_4$ treatment and dye optimization," *J. Phys. Chem. C*, vol. 117, no. 21, pp. 10949–10956, 2013.

[70] Z. Wang, X.-F. Qian, J. Yin, and Z.-K. Zhu, "Large-scale fabrication of tower-like, flower-like, and tube-like ZnO arrays by a simple chemical solution route.," *Langmuir*, vol. 20, no. 8, pp. 3441–3448, 2004.

[71] J. H. Lee, N. G. Park, and Y. J. Shin, "Nano-grain SnO_2 electrodes for high conversion efficiency SnO_2 DSSC," *Sol. Energy Mater. Sol. Cells*, vol. 95, no. 1, pp. 179–183, 2011.

[72] K. Sayama, H. Sugihara, and H. Arakawa, "Photoelectrochemical Properties of a Porous Nb_2O_5 Electrode Sensitized by a Ruthenium Dye," *Chem. Mater.*, vol. 100, no. 6, pp. 3825–3832, 1998.

[73] A. Hagfeldt, G. Boschloo, L. Sun, L. Kloo, and H. Pettersson, "Dye-sensitized solar cells.," *Chem. Rev.*, vol. 110, pp. 6595–6663, 2010.

[74] D. Kuciauskas, J. E. Monat, R. Villahermosa, H. B. Gray, N. S. Lewis, and J. K. McCusker, "Transient absorption spectroscopy of ruthenium and osmium polypyridyl complexes adsorbed onto nanocrystalline TiO_2 photoelectrodes," *J. Phys. Chem. B*, vol. 106, no. 36, pp. 9347–9358, 2002.

[75] G. M. M. Hasselmann GJ, "Diffusion-limited interfacial electron transfer with large apparent driving forces," *J. Phys. Chem. B*, vol. 103, no. 36, p. 7675, 1999.

[76] A. Islam, H. Sugihara, K. Hara, L. P. Singh, R. Katoh, Y. Takahashi, S. Murata, H. Arakawa, and G. Fujihashi, "Dye Sensitization of Nanocrystalline Titanium Dioxide with Square Planar Platinum (II) Diimine Dithiolate Complexes Dye Sensitization of Nanocrystalline Titanium Dioxide with Square Planar Platinum (II) Diimine Dithiolate Complexes," *Inorg. Chem.*, vol. 40, pp. 5371–5380, 2001.

[77] J. Baldenebro-Lopez, N. Flores-Holguin, J. Castorena-Gonzalez, J. Almaral-Sanchez, and D. Glossman-Mitnik, "Theoretical study of copper complexes: Molecular structure, properties, and its application to solar cells," *Int. J. Photoenergy*, vol. 2013, 2013.

[78] A. Kay and M. Grätzel, "Low cost photovoltaic modules based on dye sensitized nanocrystalline titanium dioxide and carbon powder," *Sol. Energy Mater. Sol. Cells*, vol. 44, no. 1, pp. 99–117, 1996.

[79] L. Bay, K. West, B. Wintherjensen, and T. Jacobsen, "Electrochemical reaction rates in a dye-sensitised solar cell—the iodide/tri-iodide redox system," *Sol. Energy Mater. Sol. Cells*, vol. 90, no. 3, pp. 341–351, 2006.

[80] M. Wang, A. M. Anghel, B. Marsan, N. L. C. Ha, N. Pootrakulchote, S. M. Zakeeruddin, and M. Grätzel, "CoS supersedes Pt as efficient electrocatalyst for triiodide reduction in dye-sensitized solar cells," *J. Am. Chem. Soc.*, vol. 131, no. 44, pp. 15976–15977, 2009.

[81] E. V. a. Premalal, N. Dematage, and A. Konno, "Carbon Black Paste Combined with Conductivity-enhanced CuSCN for Improved Performance in Quasi-solid-state Dye-sensitized Solar Cells," *Chem. Lett.*, vol. 41, no. 5, pp. 510–512, 2012.

[82] O. a. Ileperuma, G. R. Asoka Kumara, H. S. Yang, and K. Murakami, "Quasi-solid electrolyte based on polyacrylonitrile for dye-sensitized solar cells," *J. Photochem. Photobiol. A*, vol. 217, no. 2–3, pp. 308–312, 2011.

[83] W. Zhang, R. Zhu, F. Li, Q. Wang, and B. Liu, "High-performance solid-state organic dye sensitized solar cells with P3HT as hole transporter," *J. Phys. Chem. C*, vol. 115, no. 14, pp. 7038–7043, 2011.

[84] W. Kubo, K. Murakoshi, T. Kitamura, S. Yoshida, M. Haruki, K. Hanabusa, H. Shirai, Y. Wada, and S. Yanagida, "Quasi-solid-state dye-sensitized TiO_2 solar cells: Effective charge transport in mesoporous space filled with gel electrolytes containing iodide and iodine," *J. Phys. Chem. B*, vol. 105, no. 51, pp. 12809–12815, 2001.

[85] C. Lee, P. Chen, and K. Ho, "Ionic Liquid Based Electrolytes for Dye-Sensitized Solar Cells," in *Ionic Liquids: Theory, Properties, New Approaches*, 2011, pp. 631–657.

[86] K. Tennakone, G. R. R. A. Kumara, A. R. Kumarasinghe, K. G. U. Wijayantha, and P. M. Sirimanne, "A dye-sensitized nano-porous solid-state photovoltaic cell," *Semicond. Sci. Technol.*, vol. 10, pp. 1689–1693, 1995.

[87] K. Murakoshi, R. Kogure, Y. Wada, and S. Yanagida, "Solid State Dye-Sensitized TiO_2 Solar Cell with Polypyrrole as Hole Transport Layer.," *Chemistry Letters*, no. 5. pp. 471–472, 1997.

[88] M. Grätzel, "Photoelectrochemical cells.," *Nature*, vol. 414, no. 6861, pp. 338–344, 2001.

[89] U. Bach, D. Lupo, P. Comte, J. E. Moser, F. Weissörtel, J. Salbeck, H. Spreitzer, and M. Grätzel, "Solid-state dye-sensitized mesoporous TiO_2 solar cells with high photon-to-electron conversion efficiencies," *Nature*, vol. 395, no. 6702, pp. 583–585, 1998.

[90] M. Grätzel, "Recent advances in sensitized mesoscopic solar cells," *Acc. Chem. Res.*, vol. 42, no. 11, pp. 1788–1798, 2009.

[91] I. Chung, B. Lee, J. He, R. P. H. Chang, and M. G. Kanatzidis, “All-solid-state dye-sensitized solar cells with high efficiency,” *Nature*, vol. 485, no. 7399, pp. 486–489, 2012.

[92] I. Y. Song, S.-H. Park, J. Lim, Y. S. Kwon, and T. Park, “A novel hole transport material for iodine-free solid state dye-sensitized solar cells.,” *Chem. Commun. (Camb).*, vol. 47, no. 37, pp. 10395–10397, 2011.

[93] J. Burschka, N. Pellet, S.-J. Moon, R. Humphry-Baker, P. Gao, M. K. Nazeeruddin, and M. Grätzel, “Sequential deposition as a route to high-performance perovskite-sensitized solar cells.,” *Nature*, vol. 499, no. 7458, pp. 316–9, 2013.

[94] G. L. Boschloo J Magnusson, E Holmberg, A Hagfeldt, A, “Optimization of dye-sensitized solar cells prepared by compression method,” *J. Photochem. Photobiol. A Chemistry*, vol. 148, no. 1–3, p. 15, 2002.

[95] S. Control and O. F. Visual, “Porphyrin-Sensitized Solar Cells with Cobalt (II/III)–Based Redox Electrolyte Exceed 12 Percent Efficiency,” *Science (80-.).*, vol. 12, no. 5, pp. 360–366, 2001.

[96] S. Feldt, *Alternative Redox Couples for Dye-Sensitized Solar Cells*. 2013.

[97] A. Fukui, R. Komiya, R. Yamanaka, A. Islam, and L. Han, “Effect of a redox electrolyte in mixed solvents on the photovoltaic performance of a dye-sensitized solar cell,” *Sol. Energy Mater. Sol. Cells*, vol. 90, no. 5, pp. 649–658, 2006.

[98] Y. Liu, A. Hagfeldt, X.-R. Xiao, and S.-E. Lindquist, “Investigation of influence of redox species on the interfacial energetics of a dye-sensitized nanoporous TiO_2 solar cell,” *Sol. Energy Mater. Sol. Cells*, vol. 55, no. 3, pp. 267–281, 1998.

[99] K. Hara, T. Horiguchi, T. Kinoshita, and K. Sayama, “Influence of electrolytes on the photovoltaic performance of organic dye-sensitized nanocrystalline TiO_2 Solar cells,” *Sol. Energy Mater.*, vol. 70, no. Solar Energy Materials, pp. 151–161, 2001.

[100] J. Wu, Z. Lan, J. Lin, M. Huang, and P. Li, “Effect of solvents in liquid electrolyte on the photovoltaic performance of dye-sensitized solar cells,” *J. Power Sources*, vol. 173, no. 1, pp. 585–591, 2007.

[101] B. Enright, C. Redmond, and D. Fitzmaurice, “Spectroscopic Determination of Flatband Potentials for Polycrystalline TiO_2 Electrodes in Mixed Solvent Systems,” *J. Phys. Chem.*, vol. 98, pp. 6195–6200, 1994.

[102] L. a Lyon and J. T. Hupp, “Energetics of Semiconductor Electrode Solution Interfaces - Eqcm Evidence for Charge-Compensating Cation Adsorption and Intercalation during Accumulation Layer Formation in the Titanium-Dioxide Acetonitrile System,” *J. Phys. Chem.*, vol. 99, no. 43, pp. 15718–15720, 1995.

[103] G. Redmond and D. Fitzmaurice, “Spectroscopic determination of flatband potentials for polycrystalline titania electrodes in nonaqueous solvents,” *J. Phys. Chem.*, vol. 97, no. 7, pp. 1426–1430, 1993.

[104] J. Wu, Z. Lan, S. Hao, P. Li, J. Lin, M. Huang, L. Fang, and Y. Huang, “Progress on the electrolytes for dye-sensitized solar cells,” *Pure Appl. Chem.*, vol. 80, no. 11, pp. 2241–2258, 2008.

[105] W. Kubo, S. Kambe, S. Nakade, T. Kitamura, K. Hanabusa, Y. Wada, and S. Yanagida, “Photocurrent-Determining Processes in Quasi-Solid-State Dye-Sensitized Solar Cells Using Ionic Gel Electrolytes,” *J. Phys. Chem. B*, vol. 107, no. 18, pp. 4374–4381, 2003.

[106] S. Kambe, S. Nakade, T. Kitamura, Y. Wada, and S. Yanagida, “Influence of the Electrolytes on Electron Transport in Mesoporous TiO_2 −Electrolyte Systems,” *J. Phys. Chem. B*, vol. 106, no. 11, pp. 2967–2972, 2002.

[107] W. Kubo, Y. Makimoto, T. Kitamura, Y. Wada, and S. Yanagida, “Quasi-Solid-State Dye-Sensitized Solar Cell with Ionic Polymer Electrolyte,” *Chem. Lett.*, no. 9, pp. 948–949, 2002.

[108] M. Matsumoto, “A dye sensitized TiO_2 photoelectrochemical cell constructed with polymer solid electrolyte,” *Solid State Ionics*, vol. 89, no. 3–4, pp. 263–267, 1996.

[109] F. Cao, G. Oskam, and P. C. Searson, “A Solid State, Dye Sensitized Photoelectrochemical Cell,” *J. Phys. Chem.*, vol. 99, no. 47, pp. 17071–17073, 1995.

[110] K. Tennakone, G. R. R. a Kumara, I. R. M. Kottegoda, K. G. U. Wijayantha, and V. P. S. Perera, “A solid-state photovoltaic cell sensitized with a ruthenium bipyridyl complex,” *J. Phys. D. Appl. Phys.*, vol. 31, no. 12, pp. 1492–1496, 1999.

[111] B. O’Regan and D. T. Schwartz, “Efficient Photo-Hole Injection from Adsorbed Cyanine Dyes into Electrodeposited Copper(I) Thiocyanate Thin Films,” *Chem. Mater.*, vol. 7, no. 1, pp. 1349–1354, 1995.

[112] K. Tennakone, G. K. R. Senadeera, V. P. S. Perera, I. R. M. Kottegoda, and L. a a De Silva, “Dye-sensitized photoelectrochemical cells based on porous SnO_2/ZnO composite and TiO_2 films with a polymer electrolyte,” *Chem. Mater.*, vol. 11, no. 9, pp. 2474–2477, 1999.

[113] G. Boschloo and A. Hagfeldt, “Characteristics of the iodide/triiodide redox mediator in dye-sensitized solar cells,” *Acc. Chem. Res.*, vol. 42, no. 11, pp. 1819–1826, 2009.

[114] M. K. Nazeeruddin, A. Kay, E. Miiller, P. Liska, N. Vlachopoulos, M. Gratzel, C.- Lausanne, and R. April, “Conversion of Light to Electricity by SCN^-) on Nanocrystalline TiO_2 Electrodes,” *J. Am. Chem. Soc.*, vol. 115, no. 4, pp. 6382–6390, 1993.

[115] S. Nakade, T. Kanzaki, W. Kubo, T. Kitamura, Y. Wada, and S. Yanagida, "Role of electrolytes on charge recombination in dye-sensitized TiO_2 solar cell (1): the case of solar cells using the I^-/I_3^- redox couple.," *J. Phys. Chem. B*, vol. 109, no. 8, pp. 3480–3487, 2005.

[116] G. Boschloo, L. Häggman, and A. Hagfeldt, "Quantification of the effect of 4-tert-butylpyridine addition to I^-/I_3^- redox electrolytes in dye-sensitized nanostructured TiO_2 solar cells," *J. Phys. Chem. B*, vol. 110, no. 26, pp. 13144–13150, 2006.

[117] R. Mohammadpour, A. Iraji zad, A. Hagfeldt, and G. Boschloo, "Investigation on the dynamics of electron transport and recombination in TiO_2 nanotube/nanoparticle composite electrodes for dye-sensitized solar cells," *Phys. Chem. Chem. Phys.*, vol. 13, no. 48, p. 21487, 2011.

[118] S. Y. Huang, G. Schlichthorl, a J. Nozik, M. Gratzel, and a J. Frank, "Charge recombination in dye-sensitized nanocrystalline TiO_2 solar cells," *J. Phys. Chem. B*, vol. 101, no. 14, pp. 2576–2582, 1997.

[119] X. Yin, W. Tan, J. Zhang, Y. Weng, X. Xiao, X. Zhou, X. Li, and Y. Lin, "The effect mechanism of 4-ethoxy-2-methylpyridine as an electrolyte additive on the performance of dye-sensitized solar cell," *Colloids Surfaces A Physicochem. Eng. Asp.*, vol. 326, no. 1–2, pp. 42–47, 2008.

[120] H. Kusama and H. Arakawa, "Influence of benzimidazole additives in electrolytic solution on dye-sensitized solar cell performance," *J. Photochem. Photobiol. A Chem.*, vol. 162, no. 2–3, pp. 441–448, 2004.

[121] H. Kusama and H. Arakawa, "Influence of pyrazole derivatives in I^-/I_3^- redox electrolyte solution on Ru(II)-dye-sensitized TiO_2 solar cell performance," *Sol. Energy Mater. Sol. Cells*, vol. 85, no. 3, pp. 333–344, 2005.

[122] H. Kusama and H. Arakawa, "Influence of alkylaminopyridine additives in electrolytes on dye-sensitized solar cell performance," *Sol. Energy Mater. Sol. Cells*, vol. 81, no. 1, pp. 87–99, 2004.

[123] H. Kusama, Y. Konishi, H. Sugihara, and H. Arakawa, "Influence of alkylpyridine additives in electrolyte solution on the performance of dye-sensitized solar cell," *Sol. Energy Mater. Sol. Cells*, vol. 80, no. 2, pp. 167–179, 2003.

[124] N. Kopidakis, N. R. Neale, and A. J. Frank, "Effect of an adsorbent on recombination and band-edge movement in dye-sensitized TiO_2 solar cells: evidence for surface passivation.," *J. Phys. Chem. B*, vol. 110, no. 25, pp. 12485–12489, 2006.

[125] C. Zhang, Y. Huang, Z. Huo, S. Chen, and S. Dai, "Photoelectrochemical effects of guanidinium thiocyanate on dye-sensitized solar cell performance and stability," *J. Phys. Chem. C*, vol. 113, no. 52, pp. 21779–21783, 2009.

[126] K. M. Lee, V. Suryanarayanan, K. C. Ho, K. R. Justin Thomas, and J. T. Lin, “Effects of co-adsorbate and additive on the performance of dye-sensitized solar cells: A photophysical study,” *Sol. Energy Mater. Sol. Cells*, vol. 91, no. 15–16, pp. 1426–1431, 2007.

[127] C. Albayrak, Ş. Barim, and Ö. Dag, “Lyotropic liquid crystal to soft mesocrystal transformation in hydrated salt-surfactant mixtures,” *Chem. - A Eur. J.*, vol. 19, no. 44, pp. 15026–15035, 2013.

[128] L. Andrews, E. S. Prochaska, and A. Loewenschuss, “Resonance Raman and ultraviolet absorption spectra of the triiodide ion produced by alkali iodide-iodine argon matrix reactions,” *Inorg. Chem.*, vol. 19, no. 2, pp. 463–465, 1980.